

METHODOLOGICAL CONSIDERATIONS IN THE
CALCULATION OF EFFECTIVE DISCHARGE: APPLICATION
FOR THE TRINITY AND BRAZOS RIVERS

A Thesis

Presented to

the Faculty of the Department of Civil and Environmental Engineering

University of Houston

In Partial Fulfillment

of the Requirements for the Degree

Master of Science

in Civil Engineering

by

S.M. Hossein Hosseiny

May 2015

METHODOLOGICAL CONSIDERATIONS IN THE
CALCULATION OF EFFECTIVE DISCHARGE: APPLICATION
FOR THE TRINITY AND BRAZOS RIVERS

S.M. Hossein Hosseiny

Approved:

Chair of the Committee
Kyle Strom, Associate Professor,
Civil and Environmental Engineering

Committee Members:

Keh-Han Wang, Professor,
Civil and Environmental Engineering

Julia Smith Wellner, Assistant Professor,
Earth and Atmospheric Sciences

Suresh K. Khator, Associate Dean,
Cullen College of Engineering

Roberto Ballarini, Professor and Chair,
Civil and Environmental Engineering

Acknowledgements

First and foremost, I would like to thank my advisor, Dr. Kyle Strom, for his excellent supervision and support for this research. It was under his supervision that I learned how to approach and deal with a problem scientifically. I would like to appreciate him for providing me the chance to study and to do research which helped me to be able to couple science with engineering problems.

I would like to thank Texas Water Development Board for funding this project. Particularly I would like to appreciate Nolan Raphelt for his cooperation and guidance and support for the project.

I would like to appreciate all the graduate and undergraduate students who helped me through hard work to collect field data. Specifically, I would like to appreciate Mohammad Rouhnia, Jose Mendiola, Jaxon, Jassim Jaf, Mohmmad Hanfzadeh, Duc Tran, and Chengzhao Zhang for their great effort and help in field trips.

Finally I would like to appreciate my family who helped me to study abroad by being patient while I am far from home. Particularly I want to acknowledge my mother for her patience and kindness and hope to be satisfied by this work.

METHODOLOGICAL CONSIDERATIONS IN THE
CALCULATION OF EFFECTIVE DISCHARGE: APPLICATION
FOR THE TRINITY AND BRAZOS RIVERS

An Abstract
of a
Thesis
Presented to
the Faculty of the Department of Civil and Environmental Engineering
University of Houston

In Partial Fulfillment
of the Requirements for the Degree
Master of Science
in Civil Engineering

by
S.M. Hossein Hosseiny

May 2015

Abstract

Effective discharge (Q_e) is defined as the discharge responsible for carrying the most amount of sediment over two or three decades. The first objective of this thesis is to calculate Q_e for the middle Trinity River in Texas. The historic discharge data from four gaging stations is used to develop flow probability density functions for the analysis. Suspended sediment rating curves are developed using measured concentration while bedload rating curves are calculated. The second objective of this study is to use collected data to explore how calculations of Q_e can be made when measurements are not feasible. Results show that effective discharge for the middle Trinity River varies from 11,000 cfs to 20,000 cfs, which is significantly smaller than $Q_{1.5}$ and the bankfull discharge. Further analysis shows that historic flow data is sufficient for a reasonable estimate of Q_e and that measurements of river geometry, suspended sediment concentration, and bed sediment samples do not change the calculated Q_e .

Table of Contents

Acknowledgements	iv
Abstract	vi
Table of Contents	vii
List of Figures	ix
List of Tables	xiii
Chapter 1. Introduction	1
1.1 Alluvial Channel Adjustment and the Concept of Grade	1
1.2 Channel-Forming Discharge	2
1.3 Calculating Effective Discharge	3
1.4 Study Objectives	7
Chapter 2. Methods	9
2.1 Overview	9
2.2 Study Site	9
2.3 Data Collection Method	11
2.3.1 Historic Flow Discharges and Flow Statistics	12
2.3.2 Suspended Sediment Concentration and Washload	12
2.3.3 Bed Sediment and Cross Sections	15
2.4 Analysis Methods	15
2.4.1 Methods for Objective 1	15
2.4.2 Methods for Objective 2	17
Chapter 3. Data	20
3.1 Trinity River	20
3.1.1 Summary of Flow Conditions Captured	20
3.1.2 Comparison to Historic Sources	29
3.2 Brazos River	30

Chapter 4. Effective Discharge Estimates for the Trinity River . . .	36
4.1 Sediment Rating Curves and Transport Calculations	36
4.2 Development of the Daily Flow PDF	42
4.3 Sediment Transport Effectiveness Distributions	43
4.4 Effective Discharge Values	45
Chapter 5. Analysis of Effective Discharge Calculations Methods . .	47
5.1 Overview	47
5.2 The Impact of the Method Used to Develop the Flow PDF and the Amount of Field Measured Data on the Calculation of Effective Discharge	48
5.3 Sensitivity of Effective Discharge Calculations	56
5.3.1 Channel Geometry	56
5.3.2 Sediment Grain Size Distribution	59
5.3.3 Slope	61
Chapter 6. Discussion	64
6.1 Comparison of Effective Discharge to the Half-Load Discharge and Pure Flow Metrics	64
6.2 Recommendations for the Calculation of Effective Discharge	67
Chapter 7. Summary and Conclusions	71
References	74
Appendix A. Data for the Brazos River	79

List of Figures

Figure 1.1	Example of a (A)flow duration histogram and (B)sediment load histogram.	5
Figure 2.1	Trinity watershed with USGS gauge stations used in the study listed.	10
Figure 2.2	Brazos watershed with USGS gauge stations used in the study listed.	11
Figure 2.3	Primary sampling equipment. (A) US DH-2TM bag-type sampler suspended from the sampling crane; (B) US BMH-60 bed material sampler; and (C) sounding weight.	14
Figure 3.1	Summary of collected data at Rosser (USGS gage 08062500). . . .	23
Figure 3.2	Summary of collected data at Trinidad (USGS gage 08062700). . .	24
Figure 3.3	Summary of collected data at Oakwood (USGS gage 08065000). . .	25
Figure 3.4	Summary of collected data at Crockett (USGS gage 08065350). . .	26
Figure 3.5	Downstream trends in major steam properties.	27
Figure 3.6	Comparison of UH and USGS data at the Rosser station.	30
Figure 3.7	Comparison of UH and USGS data at the Trinidad station.	31
Figure 3.8	Comparison of UH and USGS data at the Oakwood station.	32
Figure 3.9	Comparison of UH and USGS data at the Crockett station.	33
Figure 3.10	Downstream trends in major steam properties- borrowed from Strom and Rouhnia (2013).	34
Figure 4.1	Rating curves.	39
Figure 4.2	Flow duration curves for Trinity River generated by 25 evenly spaced bins.	43
Figure 4.3	Sediment transport effectiveness distributions for Rosser and Trinidad using both the manual and kernel density estimate derived daily flow PDFs.	45

Figure 4.4	Sediment transport effectiveness distributions for Oakwood and Crockett using both the manual and kernel density estimate derived daily flow PDFs.	46
Figure 5.1	Effective discharge calculations for each for the four scenarios using each of the four different methods for generating the flow PDF on the Trinity River.	49
Figure 5.2	Comparison of the sediment effectiveness histograms of the High-bank station calculated by 100 bins and kernel density estimate.	50
Figure 5.3	Variability of the effective discharge of the Brazos River due to different flow-frequency analysis and amount of measured data used in calculations.	50
Figure 5.4	Spike in initial bin of sediment effectiveness histogram for Rosser gauge station at Trinity.	51
Figure 5.5	Smoothed curves fit to total bed material load of Trinity River.	53
Figure 5.6	Variability of the effective discharge of the Trinity River after applying smoothing technique due to different flow-frequency analysis and amount of measured data used in calculations.	54
Figure 5.7	Variability of the effective discharge of the Brazos River after applying smoothing technique due to different flow-frequency analysis and amount of measured data used in calculations.	55
Figure 5.8	Gravel and sand grain size distribution used in analysis of geometry effect on β value.	57
Figure 5.9	Synthetic grain size distributions used in analysis of the variability of the β due to change in grain size distribution.	59

Figure 6.1	Summary plots showing the cumulative fraction of flow and sediment moved as a function of discharge, the flow non-exceedance curve, the sediment effective and half-load discharges for Rosser and Trinidad using the manual and kernel density estimate derived daily flow pdfs.	67
Figure 6.2	Summary plots showing the cumulative fraction of flow and sediment moved as a function of discharge, the flow non-exceedance curve, the sediment effective and half-load discharges for Oakwood and Crocket using the manual and kernel density estimate derived daily flow pdfs.	68
Figure A.1	Summary of collected data at Waco (USGS gage 0809650)- borrowed from Strom and Rouhnia (2013).	79
Figure A.2	Summary of collected data at Highbank (USGS gage 08098290).	80
Figure A.3	Summary of collected data at Bryan (USGS gage 08108700).	81
Figure A.4	Summary of collected data at Hempstead (USGS gage 08111500).	82
Figure A.5	Summary of collected data at Richmond (USGS gage 08114000).	83
Figure A.6	Summary of collected data at Rosharon (USGS gage 08116650).	84
Figure A.7	Sediment transport effectiveness distributions for Waco, Highbank, and Bryan using both the manual and kernel density estimate derived daily flow pdfs.	85
Figure A.8	Sediment transport effectiveness distributions for Hempstead, Richmond, and Rosharon using both the manual and kernel density estimate derived daily flow pdfs.	86

Figure A.9	Summary plots showing the cumulative fraction of flow and sediment moved as a function of discharge, the flow non-exceedance curve, the sediment effective and half-load discharges for Waco, Highbank, and Bryan using the manual and kernel density estimate derived daily flow pdfs.	87
Figure A.10	Summary plots showing the cumulative fraction of flow and sediment moved as a function of discharge, the flow non-exceedance curve, the sediment effective and half-load discharges for Hempstead, Richmond, and Rosharon using the manual and kernel density estimate derived daily flow pdfs.	88

List of Tables

Table 2.1	Discharge statistics for the percent of time exceeded ($Q_{90\%}$, $Q_{50\%}$, and $Q_{20\%}$) for the Trinity River along with the 1.5, 2, and 10 year return period flows calculated by ranking and linear interpolation using available USGS data.	13
Table 2.2	Sampling conditions indicating six measurements per station. . . .	13
Table 3.1	Summary of measured data. Bold text highlights the highest measured concentrations at that site, and the <i>italics</i> highlights the highest daily main discharge during the sampling at the site. For the <i>bold italics</i> , the two maximums coincided.	28
Table 3.2	Discharge statistics for the percent of time exceeded ($Q_{90\%}$, $Q_{50\%}$, and $Q_{20\%}$) along with the 1.5, 2, and 10 year return period flows calculated by ranking and linear interpolation using available USGS data. Table borrowed from Strom and Rouhnia (2013).	32
Table 3.3	Summary of measured data for Brazos River. Bold text highlights the highest measured concentrations at that site, and the <i>italics</i> highlights the highest daily main discharge during the sampling at the site. For the <i>bold italics</i> , the two maximums coincided. *Wash load values used in the development of the sediment rating curves. From Strom and Rouhnia (2013).	35
Table 4.1	Rating curve coefficient values and correlation coefficients. *Rating curves developed using all of the historic USGS data at the site along with the additional data collected by UH. Rating curves have the form of $Q_i = \alpha Q^\beta$ where i is the transport mode.	40

Table 4.2	Summary of sediment transport calculations. ${}^1h_{ss90}$ is the predicted distance above the bed for which 90% of the total suspended sand load passes beneath; the calculate is based on d_{50} of the bed material. *Wash load values used in the development of the sediment rating curves.	41
Table 4.3	Comparison of calculated effective discharge for total bed material load and suspended bed material load along with calculated Q_e by using USGS historic sediment data.	46
Table 5.1	Slope of the sediment transport rating curves of Trinity River for different scenarios. Bold and <i>Italic</i> numbers show the maximum and minimum values respectively.	52
Table 5.2	Summary of sediment transport equations used in analysis.	56
Table 5.3	Variability of the α and β values by change in side slope of trapezoidal cross sections in different sediment transport formulas	58
Table 5.4	Variability of α and β due to change in grain size distribution using Ackers-White and Yang sediment transport equation	60
Table 5.5	Variability of the effective discharge of the Trinity River due to different sediment transport equations	61
Table 5.6	Variability of effective discharge of total bed material load in a sand bed river due to change in calculated slope	62
Table 5.7	Variability of effective discharge of total bed material load calculated by Yang transport equation in a gravel bed river due to change in calculated slope	63

Table 6.1	Final effective discharge, Q_e , half-load discharges, $Q_{1/2}$, and bankfull discharges, Q_{bf} , at each of the four stations of Trinity River. ¹ Effective and half-load discharges calculated from the total load histogram, $S_h = S_{h:sbm} + S_{h:b}$. ² Effective discharges calculated using the suspended bed material load histogram only, $S_{h:sbm}$	65
Table 6.2	Effective discharge summary table for Trinity River. PT: percentage of time that the effective discharge, Q_e is exceeded. PS: percentage of sediment carried by flows less than the effective discharge. T_R : return period of the effective discharge.	66
Table 6.3	Final effective discharge, Q_e , half-load discharges, $Q_{1/2}$, and bankfull discharges, Q_{bf} , at each of the six stations of Brazos River. Table from Strom and Rouhnia (2013).	69
Table 6.4	Effective discharge summary table for Brazos River. PT: percentage of time that the effective discharge, Q_e is exceeded. PS: percentage of sediment carried by flows less than the effective discharge. T_R : return period of the effective discharge. Table from Strom and Rouhnia (2013).	69

Chapter 1. Introduction

1.1 ALLUVIAL CHANNEL ADJUSTMENT AND THE CONCEPT OF GRADE

Rivers are dynamic parts of natural geomorphic systems that transport sediment to lower lands. The interaction between flow and sediment, along with the bank and bed characteristics of the river, define morphology of the river as well as its mode of stability (Church, 2006). River stability is a morphologic term describing the ability of a river to handle the imposed sediment load and water discharge. The cross section and slope of a stable river are not fixed in time but persist in state of dynamic equilibrium wherein the boundary is modified to accommodate change in upstream conditions. A stable river may experience changes in its boundaries due to a catastrophic flood but it is capable of gaining the initial boundaries again and recover itself before the next flood. Mackin (1948) defined the concept of a graded river as one which could transport all of the imposed sediment load. The qualitative form of the dynamic equilibrium condition, which is presented by Lane (1955), asserts that the product of the water discharge, Q , and slope, S , is proportionally related to the product of the bed material load, Q_S , and median size of the bed material, D_{50} :

$$QS \propto Q_S D_{50}. \quad (1.1)$$

Embedded in equation 1.1, and other similar relationships (e.g., Eaton and Church, 2011), is the idea that a river's slope, bed material, and cross sectional channel geometry respond and adjust to a characteristic, channel-forming discharge.

1.2 CHANNEL-FORMING DISCHARGE

Watershed characteristics impose water and sediment discharge variability in space and time. Over long time scales, a river can experience a range of discharges that forces the river to change its geometry (Ma et al., 2010). The channel-forming (or dominant) discharge refers to a single characteristic discharge associated with the average channel properties such as depth, width and hydraulic roughness (Garcia, 2008). This concept helps engineers in river restoration and environmental management to make designs and plans based off of a single channel-defining discharge rather than a spectrum of discharges (Shields et al., 2003; Ma et al., 2010). Leopold et al. (1964) proposed that the bankfull discharge is equivalent to the channel forming discharge. Bankfull discharge is defined as the discharge corresponding to full hydraulic section or the maximum discharge that can pass through the river cross section without river water spilling out onto the floodplain. The recurrence of bankfull discharge has been examined by many researchers and a return period of 1 to 2 years has been found to be a good estimate based on annual peak discharge series (Wolman and Miller, 1960; Simon et al., 2004; Garcia, 2008; Ma et al., 2010). This gives two approaches toward estimating channel-forming discharge; bankfull condition and 1-2 year return period. Notwithstanding the inconsistencies in the definition of the state of the bankfull, one can claim that this definition is based only on the hydraulics and therefore is missing the key aspect of sediment transport.

Rivers are exposed to a continuous range of discharges with different erosion capabilities over time. The range of imposed discharges cause rivers to adjust themselves with erosion or deposition toward the dynamic equilibrium condition where the form and processes are in balance (Goodwin, 2004). As a result, rivers near the equilibrium condition do not experience significant change in their average slope or average cross-sectional geometries with time.

Discharges fluctuate from very low flows, that occur frequently and transport

little sediment, up to very large floods that have large recurrence intervals but are capable of transporting large quantities of sediment. By assuming that the total geomorphic work in a river is a function of transported sediment, Wolman and Miller (1960) defined the effective discharge as the discharge responsible for carrying the most amount of the sediment over a long time. With this definition, effective discharge is considered the channel forming discharge since morphological work is proportional to the sediment transport.

The concept of the effective discharge has been used for a broad range of issues such as minimum flow requirements for channel stability, river restoration, maintenance and engineering constructions (Roy and Sinha, 2014). For instance, Senate bill 2 established the Texas Instream Flow Program (TIFP) in 2001 to determine the flow condition necessary to maintain healthy ecological conditions in the rivers of Texas (Texas instream flow program and Brazos River authority, 2010). Because a healthy stream ecosystem is dependent on the morphology of the river, the TIFP sought to identify the characteristic, channel-forming discharge at key locations within a spectrum of Texas rivers. For the study, the characteristic, channel-forming discharge was taken to be equal to the effective discharge.

1.3 CALCULATING EFFECTIVE DISCHARGE

Various methods have been used to calculate the conceptualized effective discharge (Wolman and Miller, 1960; Sickingabula, 1999; Crowder and Knapp, 2005; Lenzi et al., 2006; Klonsky and Vogel, 2011). The most often used method is the one proposed by Wolman and Miller (1960), where the probability density function (PDF) or histogram of the daily mean flow is multiplied by the average sediment load to produce a histogram of sediment loads, $S_h = S_h(Q)$, that represents the fraction

of load carried by a given discharge, Q , over the time interval of interest,

$$S_h = Q_s f_Q \quad (1.2)$$

where, $Q_s = Q_s(Q)$ is the daily sediment load (in tons per day) associated with the daily discharge value of Q , and f_Q is the PDF of the daily flow discharges (percent of time that the flow was at a rate of Q). Q_s is the total sediment bed material load and includes contributions from both bed load, Q_b , and suspended bed material load Q_{sbm} . Sediment load histograms of the form of S_h (equation 1.2) can be developed for suspended and bed material load independently and then added together for determination of the effective discharge (Andrews, 1980; Biedenharn et al., 2000), or they can be based solely on suspended material if the transport mode is suspension dominated (Wolman and Miller, 1960; Sickingabula, 1999); often times, the analysis is done using only the suspended load because suspended load is typically the only data easily available (e.g., Klonsky and Vogel, 2011). Typically, in developing the sediment load histogram, S_L , a rating curve that gives the average sediment load as a function of discharge, $Q_s = Q_s(Q)$, is developed from historic or measured data using regression. The sediment load rating curve take the form of:

$$Q_s = \alpha Q^\beta \quad (1.3)$$

where α and β are site-specific coefficients that can be obtained through regression of the Q_s and Q paired data. Once α and β are obtained, the sediment rating equation can be used with the PDF of the daily flow data to produce a histogram that shows the distribution of the percentage of total sediment load as a function of flow rate following equation 1.2 (fig. 1.1). The effective discharge is then selected as the flow rate, Q , associated with the peak in the S_h histogram.

Effective discharge varies from site to site not only due to changes in probability

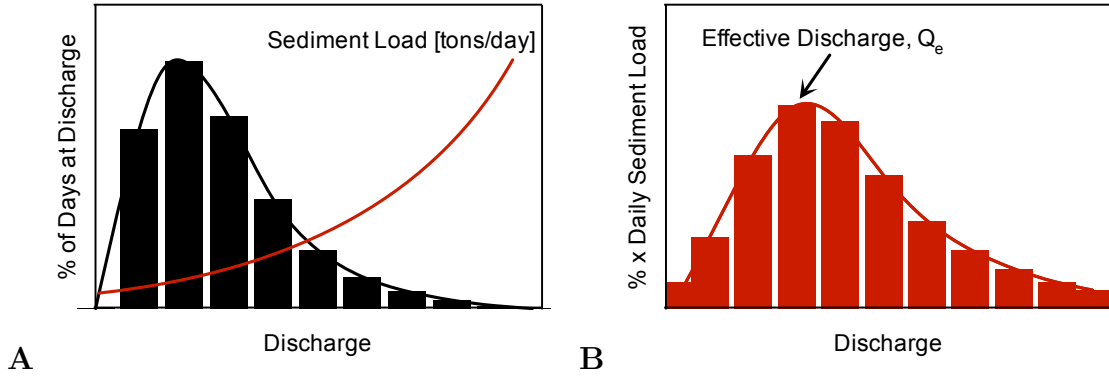


Figure 1.1: Example of a (A)flow duration histogram and (B)sediment load histogram.

distribution of the water discharge and sediment load histograms (Vogel et al., 2003), but also due to inconsistencies in the approach taken in the calculation of the effective discharge (Klonsky and Vogel, 2011). In particular, there is no standard procedure for producing the flow PDF. For example, Biedenharn et al. (2000) suggested 25 evenly spaced bins followed by an iteration toward decreasing the number of the bins in order to get non zero value for all the bins, while Doyle et al. (2005) used 25 logarithmically spaced bins to make the probability density function of the discharge. Ma et al. (2010) used equal arithmetic intervals of the standard deviation for all the discharges. Using a different approach, with the aim of reducing the subjectivity in the frequency analysis, Klonsky and Vogel (2011) applied the kernel density function to calculate the frequencies. While several different approaches for the development of the PDF have been tried, no single method has been recognized as the most appropriate standard. This is true even though the value of the effective discharge resulting from the calculation will depend on the method used to develop the PDF.

Sediment can be carried through a river either mixed up in suspension or traveling down in contact with the bed. The addition of the material moving along the bed plus the material being transported in suspension is known as total bed material load. Calculation of the effective discharge for total bed material load requires that both modes of transport be quantified. Quantification of the sediment load can be

accomplished by measurement or calculation. Depending on the feasibility of the measurements, calculation of the effective discharge may be based on a combination of measured and calculated sediment loads. For example, one might (1) measure both suspended and bedload in the field, (2) measure one mode and calculate of the other, (3) measure one mode of transport and neglect the other, or (4) calculate the load from both bed and suspended load. Because of the importance of sediment transport rates in defining the effective discharge, it is possible that the calculated effective discharge value could vary among these four approaches even for the same site and flow conditions.

Of the four options listed above, it is most common to use option (3), i.e., using measured suspended sediment data while neglecting bedload. This is typically a pragmatic decisions since suspended sediment is typically more available and easier to measure than bedload. For instance, 29 years available records of suspended sediment for 21 sites in Saskatchewan, and 23 years records for Fraser River in Canada helped Ashmore (1988) and Sickingabula (1999) to calculate effective discharge for the two rivers. Similarly, Vogel et al. (2003), Simon et al. (2004), Ma et al. (2010), and more recently, Klonsky and Vogel (2011) used historic suspended sediment records available from approximately two decades to calculate effective discharge for different rivers. Neglect of the bedload may be reasonable for high transport conditions on sand bed rivers since the majority of the sediment likely travels as suspended load. However, not all rivers are suspended load dominated, and it is possible that neglect of the bedload fraction may significantly alter effective discharge calculations. The potential effect of neglecting bedload in effective discharge calculations has not been examined.

Only a handful of studies have directly measured bedload as part of an effective discharge calculation. This is due to the difficulties and cost involved with making bedload measurements. Examples of studies that have measured bedload include

the work of Francalanci et al. (2013) and Bunte et al. (2014). More often than not, bedload formulas are used in lieu of direct measurements to quantify the rate of bedload transport when the fraction is not neglected. These formulas are generally a function of the hydraulic characteristics of the flow such as depth, velocity, and hydraulic radius along with sediment properties such as sediment size. For instance, Pickup and Warner (1976) applied both Meyer-Peter and Müller (1948) and Brown (1950) bedload equations to quantify bedload transport rate based on sediment grain size. In a similar approach, Andrews (1980) and Strom and Rouhnia (2013) applied the Einstein-Brown formula to calculate the bedload rate for Yampa River in Colorado and Wyoming and Brazos River at Texas. In these two latter mentioned works, the calculated bedload rates were based on the measured hydraulic parameters of the flow such as depth and velocity.

It is possible that the calculated effective discharge could vary strongly depending on how much measured field data is used and what type of transport equation is used when calculations are needed. No systematic study exploring the resulting changes in effective discharge with varying amounts of site specific field data has ever been conducted. Additionally, if bedload must be calculated, Bunte et al. (2014) has shown that the steepness of the transport rating curve significantly alters the predicted effective discharge. For steep mountain stream, Bunte et al. (2014) suggest that the steepness was related to the presence of various bedforms. Such an analysis has not been done for low-slope rivers though it is expected that the slope of the rating curve would influence Q_e .

1.4 STUDY OBJECTIVES

The **first objective** of this work is to provide estimates of the effective discharge of the middle Trinity River at four USGS gauging stations as part of the Texas Instream Flow Program. The goal of this program, and the purpose for making the

effective discharge estimates, is to help assess the geomorphic state of the Trinity River to allow for the establish a baseline for future policy decisions.

The **second objective** of the thesis is to use data collected on the Trinity and Brazos rivers to explore general questions related to the calculation of effective discharge. Specifically, the work will examine the following three questions:

1. What is the impact of the method used to develop the flow PDF on calculated effective discharge?
2. What is the impact of the type of measured field data on the calculation of effective discharge?
3. If sediment transport is calculated rather than measured, how does the section of different transport relations impact the effective discharge calculations, and what input parameters in the transport relations most influence the final result?

Following this more general analysis, the thesis will also compare and discuss differences between effective discharge calculations and other measures of the channel forming discharge.

Chapter 2. Methods

2.1 OVERVIEW

The first objective of this study is to calculate the effective discharge for the middle Trinity River at four USGS gauging stations. This chapter contains an overview of the field sites on the Trinity and the data collection methods used for the effective discharge calculations. The chapter also includes an outline of the methods used to address the research questions associated with second study objective pertaining to the general calculation of effective discharge.

2.2 STUDY SITE

The 46,100 km² Trinity River watershed runs from northern Texas to Trinity Bay in southeast Texas just east of the city of Houston, TX (Philips et al., 2005). This study focuses on the middle Trinity River between the cities of Rosser, near Dallas, to Crockett. The four USGS gauges in the middle Trinity River from upstream to downstream are (1) 08062500 - Trinity River near Rosser, Texas; (2) 08062700 - Trinity River near Trinidad, Texas; (3) 08065000 - Trinity River near Oakwood, Texas; and (4) 08065350 - Trinity River near Crockett, Texas.

The Trinity River is a low-slope meandering river with wide floodplains and numerous oxbow lakes (Philips et al., 2005). Flows in the study region are influenced by three major lakes; Cedar Creek Reservoir, Richland Chambers Reservoirs, and Lake Livingston. Cedar Creek Reservoir and Richland Chamber Reservoir are both located on tributaries that feed the Trinity at junctions located 7 miles upstream and 25 miles downstream of the Trinidad gauge station respectively. Lake Livingstone is directly fed by the Trinity River at 32 miles downstream from the Crockett gauge station. Because of its far downstream location, Lake Livingstone is expected not to have effect on the study reach. The sinuosity of the Trinity River through the four

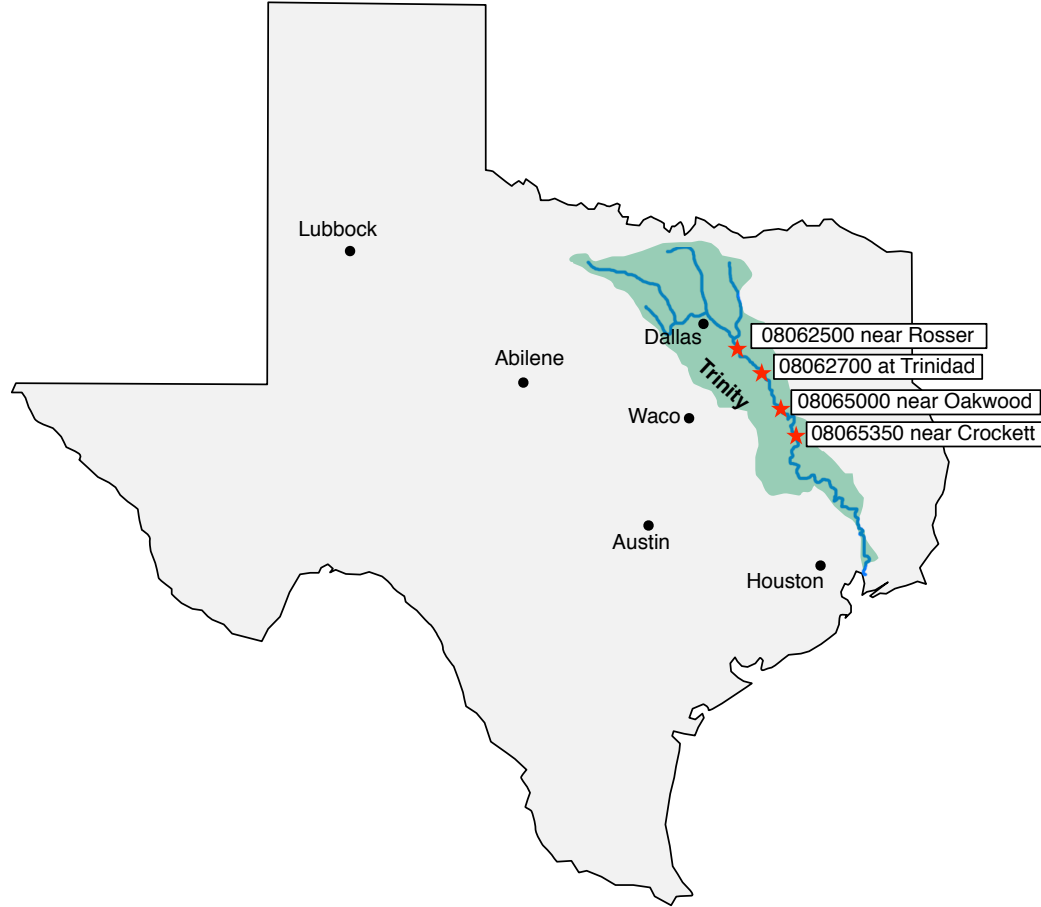


Figure 2.1: Trinity watershed with USGS gauge stations used in the study listed.

gauging stations varies from 1.4 to 2.2 with no real systematic change as one progresses downstream through the study zone. The bankfull width of the river increases in the downstream direction from 40 m at Rosser to 100 m at Crockett. Slope and median bed sediment size follow a decreasing trend in downstream direction.

For the second study objective, data collected on the Trinity was supplemented with data previously collected on the Brazos River and reported in Strom and Rouhnia (2013). The Brazos River watershed is one major river basin to the west of the Trinity (fig. 2.2). Data used in the analysis was collected at six USGS gaging stations. Like the Trinity, the lower Brazos River is a low-slope meandering sand-bed river, but overall the Brazos is larger. Slope along the study sites decreases in the downstream direction varying from 0.0002 to 0.0004. Grain size also decreases in the downstream

direction while width and depth both increase from 250 to 300 feet (width) and from 25 to 45 feet (depth).

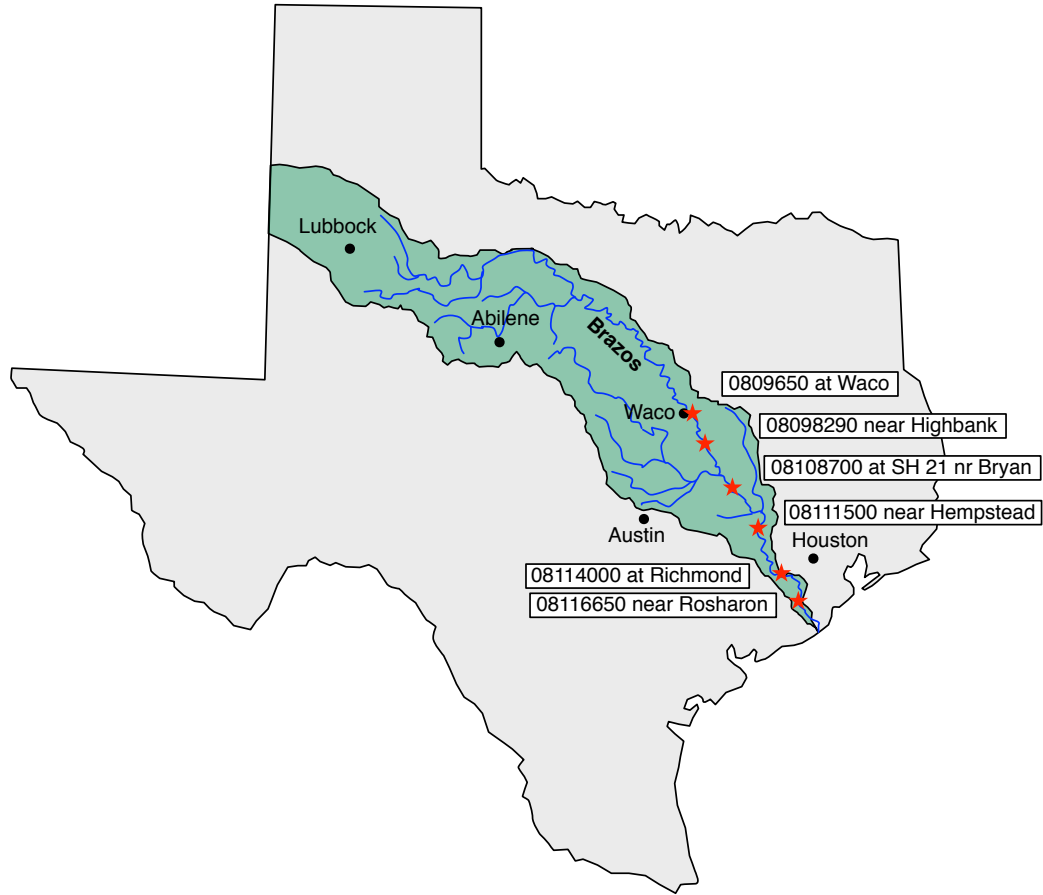


Figure 2.2: Brazos watershed with USGS gauge stations used in the study listed.

2.3 DATA COLLECTION METHOD

Effective discharge calculations need the following types of data: (1) historic discharge data for the development of the probability density functions, and (2) sediment load data for developing sediment rating curves. Q_s in equation 1.3 refers to the total bed material load which includes bedload and bed material load moving in suspension as

$$Q_s = Q_b + Q_{sbm}, \quad (2.1)$$

where Q_b is the volumetric bedload transport rate and Q_{sbm} is the volumetric suspended bed material transport rate. Quantification of the suspended sediment load in equation 2.1 is done on the Trinity by measuring suspended sediment concentration over a range of flow, whereas bedload is calculated using the Einstein-Brown formula similar to the calculations of Strom and Rouhnia (2013) and Andrews (1980). Therefore the primary data collected during each sampling trip to the Trinity included: a cross-sectionally integrated water column sample of the suspended sediment concentration, the grain size distribution of the material in suspension, a bed material sample for characterization of the bed material size distribution, and measurement of the river bathymetry flow cross section properties for calculation of the depth and averaged velocity.

2.3.1 Historic Flow Discharges and Flow Statistics

Historic discharge data was obtained from the USGS National Water Information System (NWIS) from January 1, 1990 to December 31, 2011. These records were initially used to calculate low, moderate, and high flow discharges as follows: a low flow is a discharge that historically 90 percent of the time is exceeded; a moderate flow is a discharge exceeded between 90 and 50 percent of the time and; a high flow is a discharge that has been exceeded just 10 percent of the time. These flows were used for sampling of suspended sediment over low to moderate and high flows. The flow statistics were calculated base on ranking the maximum annual discharges and finding the probability of occurrence of each event by linear interpolation (Bedient et al., 2002).

2.3.2 Suspended Sediment Concentration and Washload

All four of the study gauge stations on the Trinity are located at bridge crossing, and all of the samples were collected from the bridge. For each station, 6 samples

Table 2.1: Discharge statistics for the percent of time exceeded ($Q_{90\%}$, $Q_{50\%}$, and $Q_{20\%}$) for the Trinity River along with the 1.5, 2, and 10 year return period flows calculated by ranking and linear interpolation using available USGS data.

Station	20 Years of Record						All Years of Record		
	Exceedence Value			Return periods			Return periods		
	$Q_{90\%}$ [cfs]	$Q_{50\%}$ [cfs]	$Q_{20\%}$ [cfs]	$Q_{1.5}$ [cfs]	Q_2 [cfs]	Q_{10} [cfs]	$Q_{1.5}$ [cfs]	Q_2 [cfs]	Q_{10} [cfs]
Rosser	800	1,500	7,000	29,543	34,100	78,774	20,800	26,000	58,600
Trinidad	800	1,600	8,500	26,600	37,250	66,974	25,650	32,600	68,004
Oakwood	900	2,200	11,200	28,200	44,052	94,770	22,500	36,100	90,191
Crockett	1,000	2,500	13,600	30,100	38,700	93,348	25,700	32,800	69,000

were collected over a range of flow conditions to allow for the development of sediment rating curves following the form of equation 1.3. The flow conditions sampled for each gage included 2 samples at “high” flow, two at “moderate” flow, and two at “low” flow (Table 2.2).

Table 2.2: Sampling conditions indicating six measurements per station.

Sites	# of Samples	Relative Flow Magnitude	Flow Exceedance Condition
All 4 sites	2	High	Q exceeded $\leq 20\%$
All 4 sites	2	Moderate	$20\% \leq Q$ exceeded $\leq 50\%$
All 4 sites	2	Low	$50\% \leq Q$ exceeded $\leq 90\%$

The water column samples used for determination of the suspended sediment concentration and grain size distribution were obtained using a bucket-on-a-rope method and a Federal Interagency Sedimentation Project (FISP) depth-integrated sampler (US DH-2TM bag-type). With both samplers, the Equivalent Width Increment (EWI) method (Diplas et al., 2008) was used to define cross-section averaged suspended sediment concentration. The US DH-2TM bag-type sampler is designed to collect 1 L isokinetic samples in depths up to 35 ft and velocities in the range of 2.0 to 6.0 ft/sec. The sampler was lowered and raised using a three-wheel USGS Type A crane truck with a B-56M sounding reel (fig. 2.3A). Nozzles of differing inner diameter (3/16”, 1/4”, and 5/16”) were used to optimize the sampler for the flow

conditions present at the time of sample collection, while keeping the sampler transit rate through the vertical limited to 40% of the mean channel velocity (Edwards and Glysson, 1999; Davis, 2005). All water samples from individual vertical transits were combined to build integrated samples for the cross sections following the EWI method. In general, velocities on the Trinity were too slow during the “low” flow conditions to use the depth-integrated sampler. When deployed during these periods of low velocity, the sampler simply would not fill with water. Therefore, for the low flow conditions, data from the bucket sampler was used. Interestingly, for all flow conditions sampled with both methods, it was found that both the concentration and suspended grain size distribution were approximately equivalent in samples from the two sampling methods.



Figure 2.3: Primary sampling equipment. (A) US DH-2TM bag-type sampler suspended from the sampling crane; (B) US BMH-60 bed material sampler; and (C) sounding weight.

Field samples of suspended sediment were processed in the laboratory to obtain the average suspended sediment concentration, C , associated with each particular flow discharge. Measurements of the total suspended sediment concentration were obtained through filtering for the lower concentration samples following the ASTM standards outlined in ASTM D3977 - 97(2007) (ASTM, 2007). For higher concentrations, the entire water and sediment mixture was placed in pre-weighed pans. The pans were then placed in an oven at low temperatures to evaporate all of the water and dry the sediment out. Following several days in the oven, the pans were reweighed to allow for calculation of the total suspended sediment mass.

Washload percentage was determined by from the grain size distribution of the sediment in suspension. The grain size distribution of the sediment in suspension was measured by running small, well-mixed water column samplers through a Malvern Mastersizer capable of measuring particle sizes in the range of 0.05 μm to 0.9 mm. By this way, the washload percentage associated by each discharge is quantified as the percentage (by volume) of the grains below 63 microns.

2.3.3 Bed Sediment and Cross Sections

A US BMH-60 FISP scoop-type bed material sampler (fig. 2.3B) was used to collect samples of the bed material at each measurement increment across the channel. All samples were combined in a bucket to provide a single representative bed material sample for the cross section. Cross-sectional geometry data was obtained using a sounding weight dropped from the bridge deck using the sampling crane (fig. 2.3B). At each increment across the width, the distance to the bed and water surface from the bridge railing was recorded. For consistency, the sampling increments across the bridge were setup from the same starting point on each repeated visit. During most of the high flow conditions, fluid drag on the sounding weight and the bed material sampler was great enough to prevent data from being obtained with the sounding weight and bed material sampler.

2.4 ANALYSIS METHODS

2.4.1 Methods for Objective 1

Estimation of the effective discharge for the middle Trinity River (objective 1), needs quantification of both bedload and suspended bed material load. Suspended bed material rating curves were developed based on measured suspended sediment concentrations while bedload rating curves were calculated using the Einstein-Brown equation.

Bedload Quantification

The Einstein-Brown equation uses the original dimensionless parameters defined by Einstein (1942) with the two-part power-law curves of Brown (1950):

$$q_b^* = \begin{cases} 40F(\tau^*)^3 & \text{for } \tau^* \geq 0.182 \\ 2.15F e^{-0.391/\tau^*} & \text{for } \tau^* < 0.182. \end{cases} \quad (2.2)$$

Here, q_b^* and τ^* are the dimensionless bedload transport rate and dimensionless bed shear stress respectively:

$$q_b^* = \frac{q_{bv}}{\sqrt{R_s g d_{50}^3}}, \quad \tau^* = \frac{\tau_B}{R_s \gamma d_{50}}. \quad (2.3)$$

In these definitions, q_{bv} is volumetric bedload transport rate per unit width, τ_B is the bed shear stress, $R_s = (\rho_s - \rho)/\rho$ is the submerged specific gravity, and d_{50} is the sediment size for which 50% of the material is finer than by weight. F in equation 2.2 is the Rubey (1933) settling velocity factor:

$$F = \left[\frac{2}{3} + \frac{36\nu^2}{gd^3 R_s} \right]^{1/2} - \left[\frac{36\nu^2}{gd^3 R_s} \right]^{1/2}. \quad (2.4)$$

In the Einstein-Brown equation, the stress driving transport is the stress associated with only the skin friction component of stress. Hence, $\tau_B = \tau'_B$ with,

$$\tau'_B = \gamma R' S = \rho u_*'^2, \quad (2.5)$$

where u_*' is the friction velocity associated with the skin friction and R' is the hydraulic radius associated with skin friction. In this framework, the total hydraulic radius is a summation of the skin and form roughness associated hydraulic radii, $R = R' + R''$ where R'' is due to form roughness. The transport equation is solved using the Einstein

skin friction resistance relation:

$$\frac{U}{u'_*} = 5.74 \log \left(12.27 \frac{R'}{d_{65}} \right). \quad (2.6)$$

The depth and geometric properties of the cross section were measured at each site at the time of sampling. Therefore, if S is known, and uniform flow is assumed (i.e., eq. 2.5 is valid), then R' and τ'_B can be calculated using equations 2.5 and 2.6 with U defined from continuity. This procedure for calculating τ'_B was used, and the skin friction component of the bed shear stress was used in the bedload transport calculations with equation 2.2. However, following through with the entire effective discharge analysis using the skin friction shear stress values resulted in very steep bedload rating curves. In turn, the steep rating curves pushed the effective discharge estimates to the very largest flows observed during the period of record. The reason for this is that the shear stress partitioning method produced a difference between the total and skin shear stress that increased with a reduction in mean channel velocity. This amplified the difference in transport capacity between low and high flows. To avoid having the effective discharge land in the largest flow bin, we used the bed shear stress obtained from the total hydraulic radius in all bedload calculations.

2.4.2 Methods for Objective 2

The second objective of this thesis is to use data collected on the Trinity and Brazos rivers to answer the three research questions regarding effective discharge calculations in general. These three questions are stated at the end of the Introduction. The first two questions deal with how the calculated effective discharge varies as a function of the method used in the development of the flow PDF and the amount of on-site data used in the overall analysis. These two questions are investigated in an integrated way by calculating the effective discharge using four different scenarios of

decreasing amounts of on-site measured data. These four scenarios are listed below:

Scenario 1: In this scenario, which is mainly based on measurements, the measured hydraulic characteristics of the flow along with the measured sediment size are used for calculation of the bedload rating curve. Measured sand concentrations at different condition of discharges are used to develop suspended bed material rating curves.

Scenario 2: In this scenario, the measured hydraulic characteristics of the flow such as depth and velocity and measured sediment size are used along with SAMwin to calculate the total bed material load rating curves which means that measured suspended sediment is substituted with calculated suspended sediment.

Scenario 3: This scenario is quite similar to scenario 2 with this difference that hydraulic characteristics of the flow are calculated by SAMwin. This means that just measured cross section and sediment size distribution along with SAMwin produces sediment rating curves.

Scenario 4: This scenario is defined to use relatively minimum measured data which includes the width of the river and sediment size distribution. The river is assumed to be rectangular with the width of the river estimated from Google Earth images. Then the hydraulic and sediment transport calculations are done by SAMwin.

For each scenario, the effective discharge is calculated at each of the four Trinity stations and at each of the six stations along the Brazos using four different methods for obtaining the flow PDF. These four different methods of obtaining the flow frequency include using (1) equal arithmetic intervals with bin numbers of 25, 50 and 100, and (2) the kernel density estimate method as proposed by Klonsky and Vogel (2011) on

20 year records of flow obtained from the USGS National Water Information System website. Again, the data from Brazos river comes the study of Strom and Rouhnia (2013), and contains information similar to that obtained for the Trinity. The data at each site includes: mean daily flow discharge, measured suspended sediment concentration over a range of flow conditions, bed sediment samples, and cross sectional geometry.

For the analysis, the bedload rating curves are developed based on bed sediment samples and the Einstein-Brown formula. The SAMwin package (developed under a cooperative research and development agreement between Ayres Associates and the US Army Corps of Engineers) is also used to calculate total bed sediment load. SAMwin is capable of calculating the sediment transport rate based on either its own hydraulic calculations or direct input of hydraulic data such as velocity and depth by the user. Therefore input for the SAMwin model preliminary includes channel geometry, sediment size, slope, roughness coefficient and/or depth and velocity. Except for the Crockett station, slopes for all the sites were obtained from a USGS database computed for Texas gauging stations. Roughness values evaluated by the Manning equation vary from 0.03 to 0.04.

The third research question aims to show the effect of different sediment transport equations and input parameters on the steepness of the calculated total bed material load rating curves and associated effective discharges. To do that, transport rates were quantified by several sediment transport equations with change in input parameters of (1) cross section, (2) grain size distribution, and (3) river slope through SAMwin model. Then the transport rating curves were used along with Trinity flow PDFs to analyze the variability of the effective discharge.

Chapter 3. Data

3.1 TRINITY RIVER

3.1.1 Summary of Flow Conditions Captured

Twenty three of the planned twenty four samples were collected on the Trinity River (table 2.2). One high flow sample at Rosser was not collected due to difficulty in getting to the station in time to capture the peak flow. The largest flow event to occur during the sampling period took place during the last week of November 2013. However, while the discharge during this event still did not reach the 1.5 year return period flow for any of the stations (table 2.1).

Figures 3.1-3.4 show a summary of collected data for all gauge stations. All collected data is listed in table 3.1. Discharges shown in the figures and tables are the 15-minute USGS instantaneous discharges. The actual discharge at the time of measurement was typically slightly different than the mean daily value. However, mean daily discharge are used in developing flow duration curves.

Two types of concentrations and suspended sediment discharges are reported. The first is the total suspended sediment load, Q_{ss} [tons/day], which contains both suspended bed material and suspended wash load; suspended bed material was defined as material coarser than 0.062 mm. Q_{ss} is calculated using the total concentration measurement from the sampler multiplied by the volume of flow passing the station in one day,

$$Q_{ss} = (1.1 \times 10^{-6})C_{ss}V_{24hr}, \quad (3.1)$$

where C_{ss} is the concentration in g/m^3 (which is equivalent to the concentration in mg/l), V_{24hr} is the volume of water in m^3 passing the station per day, and 1.1×10^{-6} is a factor used to convert from grams to US short tons so that the units on Q_{ss} work out to be tons/day. The second type of suspended sediment load shown in the

figures and tables and used in the analysis is the suspended bed material load, Q_{sbm} , computed as

$$Q_{sbm} = \left(\frac{100 - \%WL}{100} \right) Q_{ss}, \quad (3.2)$$

where, $\%WL$ is the wash load percentage, defined as the percent by volume of the material traveling in suspension that is less than 0.062 mm. $\%WL$ was calculated using the Malvern measured suspended sediment grain size distributions. For sampling dates without Malvern measurements of the suspended sediment, $\%WL$ values for flows that most closely matched the missing data were used (table 3.1).

In general, suspended sediment discharge increased with stream discharge. However, for some cases, the largest measured total suspended concentrations (bed material + wash load) occurred at moderate discharges. For example, at Oakwood, the maximum measured suspended sediment concentration was 2.7 g/l and this was associated with a moderate discharge of 5,010 cfs on 5/18/13. Comparatively, concentrations were 1.1 g/l during the time of measurement on 10/31/13 when flows reached 18,100 cfs (table 3.1). Such differences are likely reflective of sampling variability or differences in wash load produced by variations in location of rainfall, vegetation cover, or land use. Maximum observed suspended sediment concentrations per site are marked in table 3.1 with bold text, and the maximum daily discharge for the sampling days is highlighted with italics. Bolded italics are used when the two maximums coincide. This occurred at Rosser and Crockett (table 3.1).

An unusual occurrence in the dataset for the suspended sediment is that the overall largest grain size distributions for each site were associated with low and moderate flow events. While no strong trend in size was present with discharge, suspended sediment samples taken during the high flow conditions did consistently produce some of the finest observed suspended sediment grain size distributions (figures 3.1-3.4).

Channel cross sectional geometry measurements are expected to be the most accurate during the low flow conditions. During high flow, it is possible that drag on

the sounding weight made the cross section appear to be “deeper” than it actually was due to the angled line-of-fall of the weight. Therefore, all cross sectional data presented was collected at low or the lower end of the moderate flow condition. Some data was collected during higher flows, but this data is not presented because of the significant drag observed on the sounding weight.

Figure 3.5 shows the overall downstream trends for drainage area, slope (discussed in detail in the next section), active channel width, bankfull depth, return period flows at 1.5, 2, and 10 years, and the average bed material grain size statistics. As expected, channel width and depth both slightly increase in the downstream direction. The bankfull width of the river increases in the downstream direction from 40 m at Rosser to 100 m at Crockett. Also, on average, discharge increases and grain size decreases moving down from Rosser to Crockett.

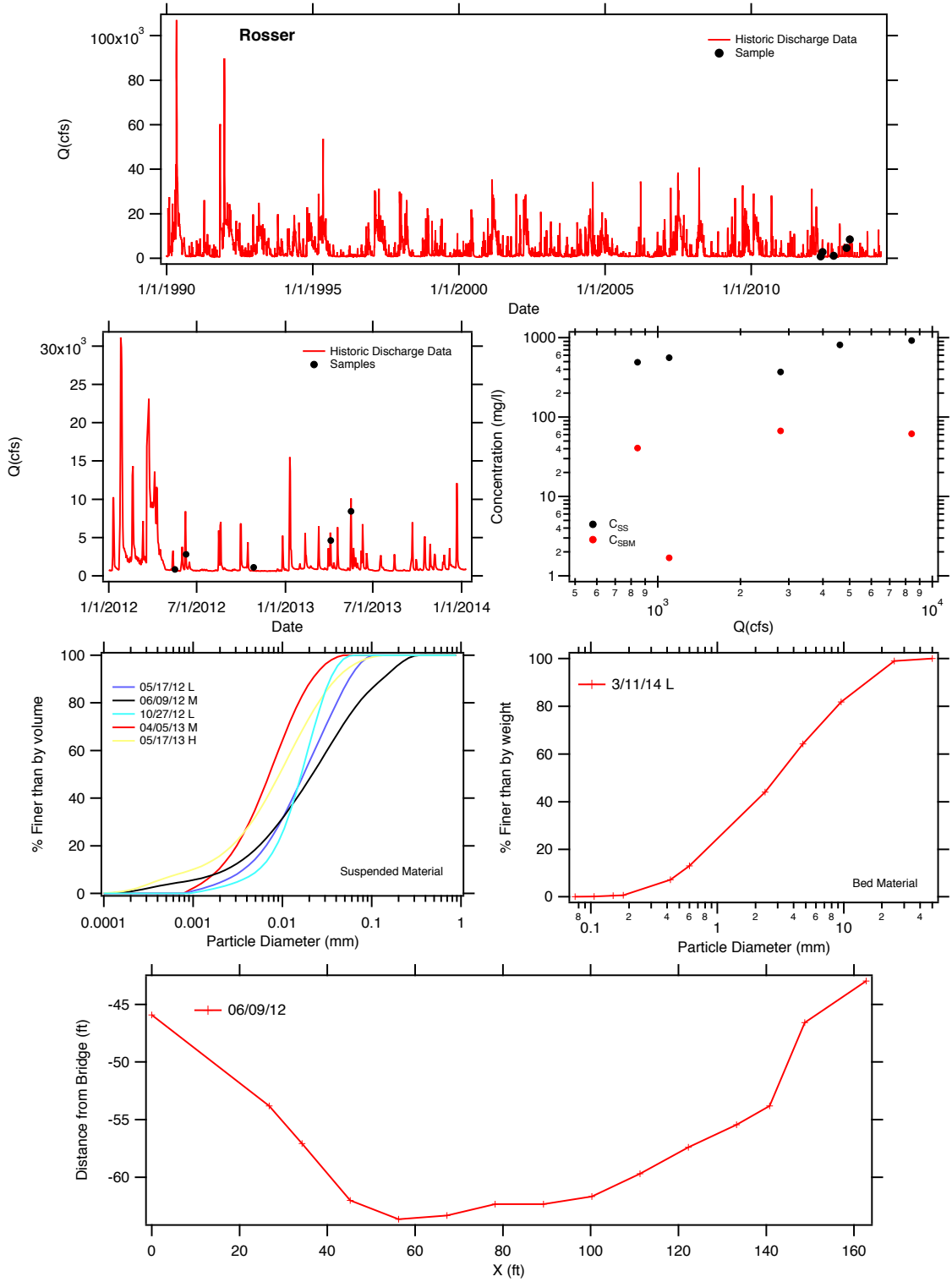


Figure 3.1: Summary of collected data at Rosser (USGS gage 08062500).

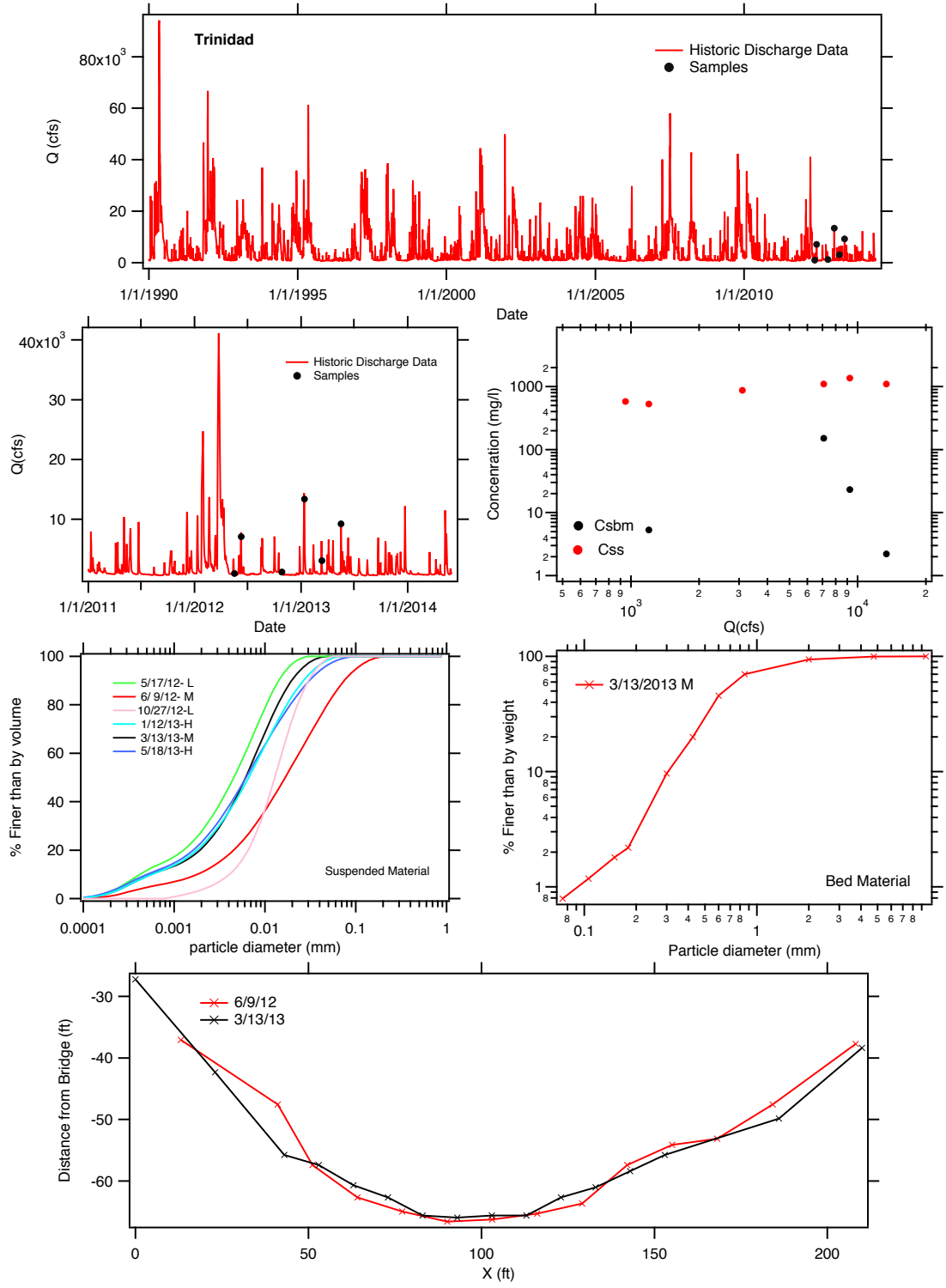


Figure 3.2: Summary of collected data at Trinidad (USGS gage 08062700).

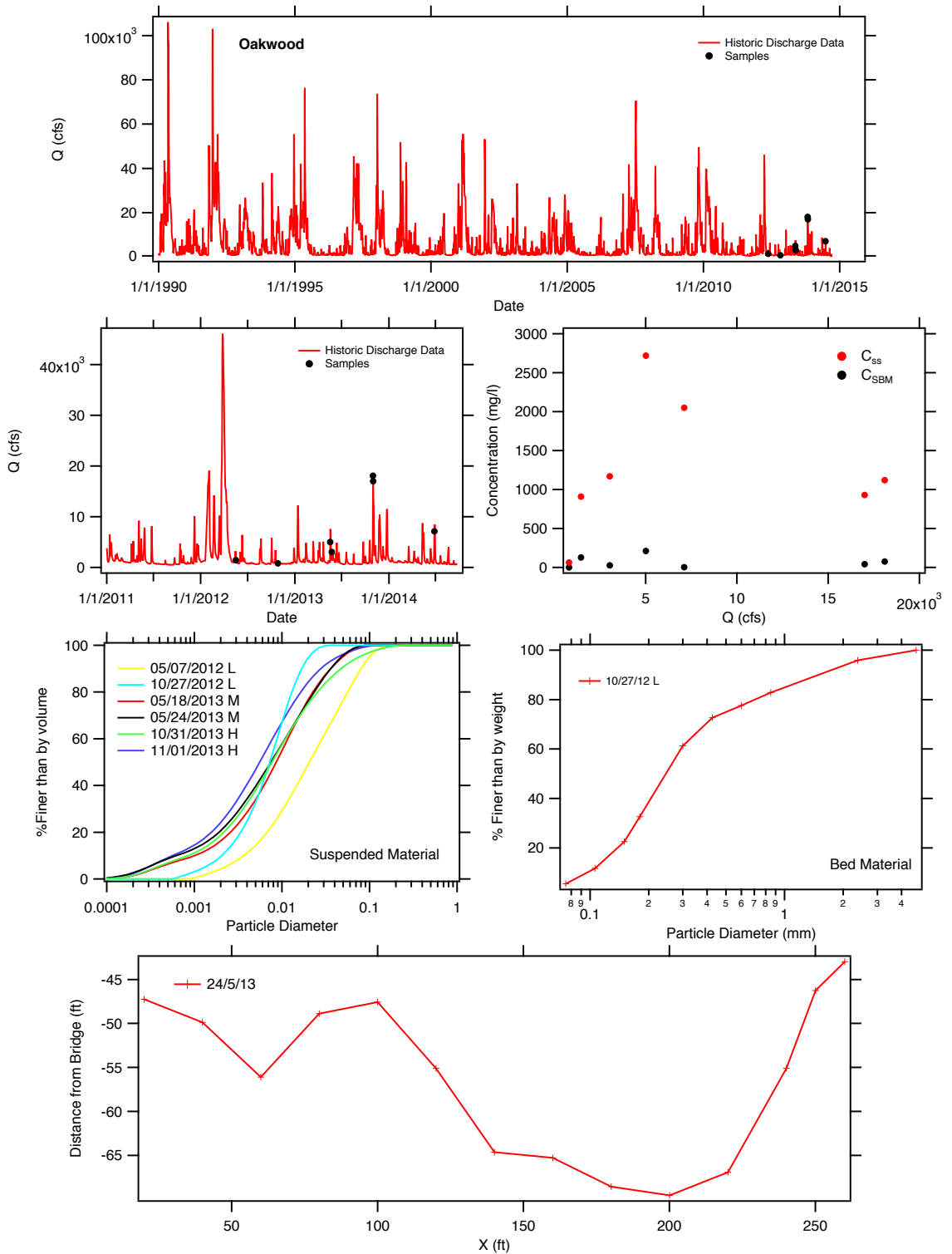


Figure 3.3: Summary of collected data at Oakwood (USGS gage 08065000).

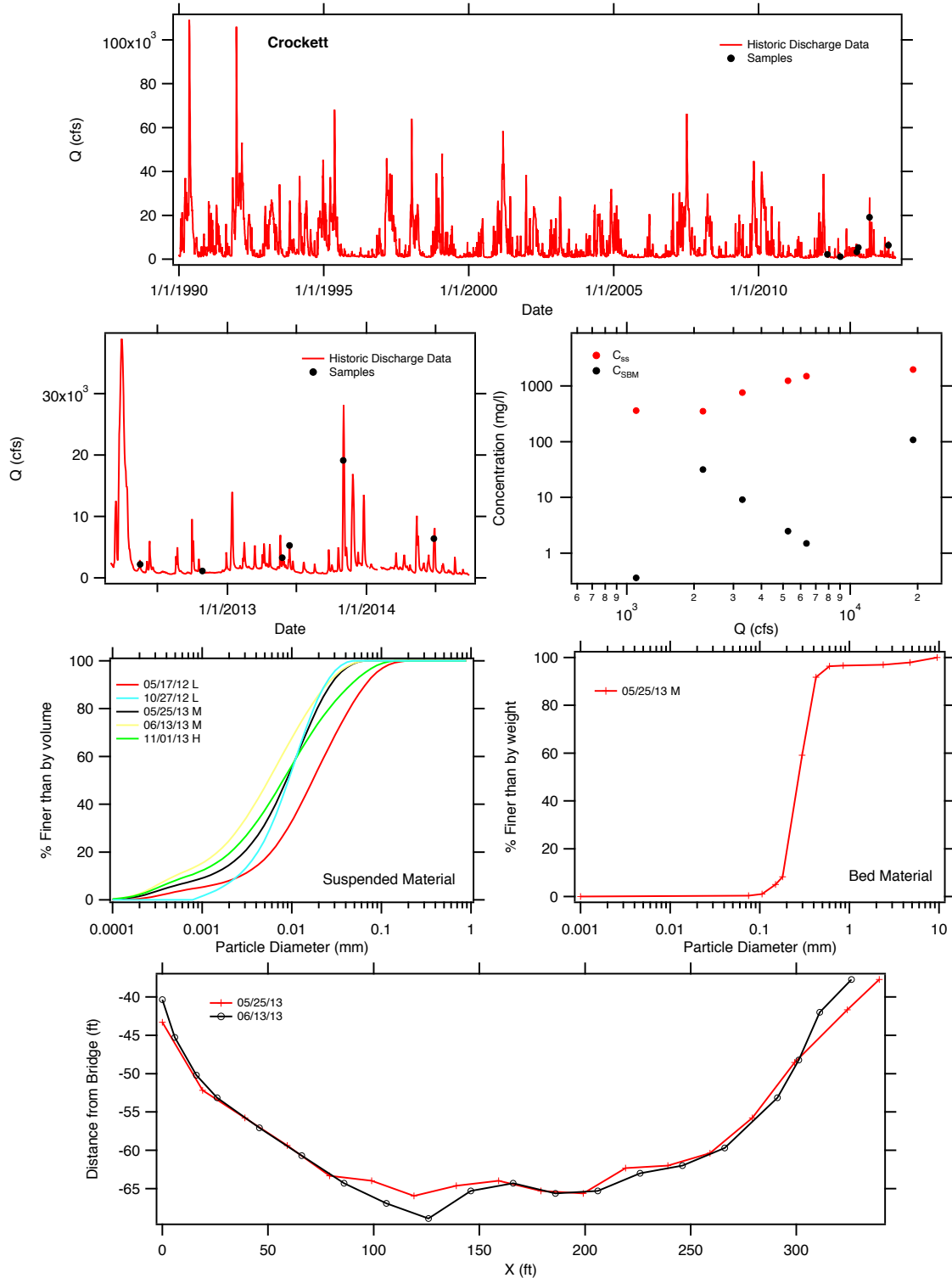


Figure 3.4: Summary of collected data at Crockett (USGS gage 08065350).

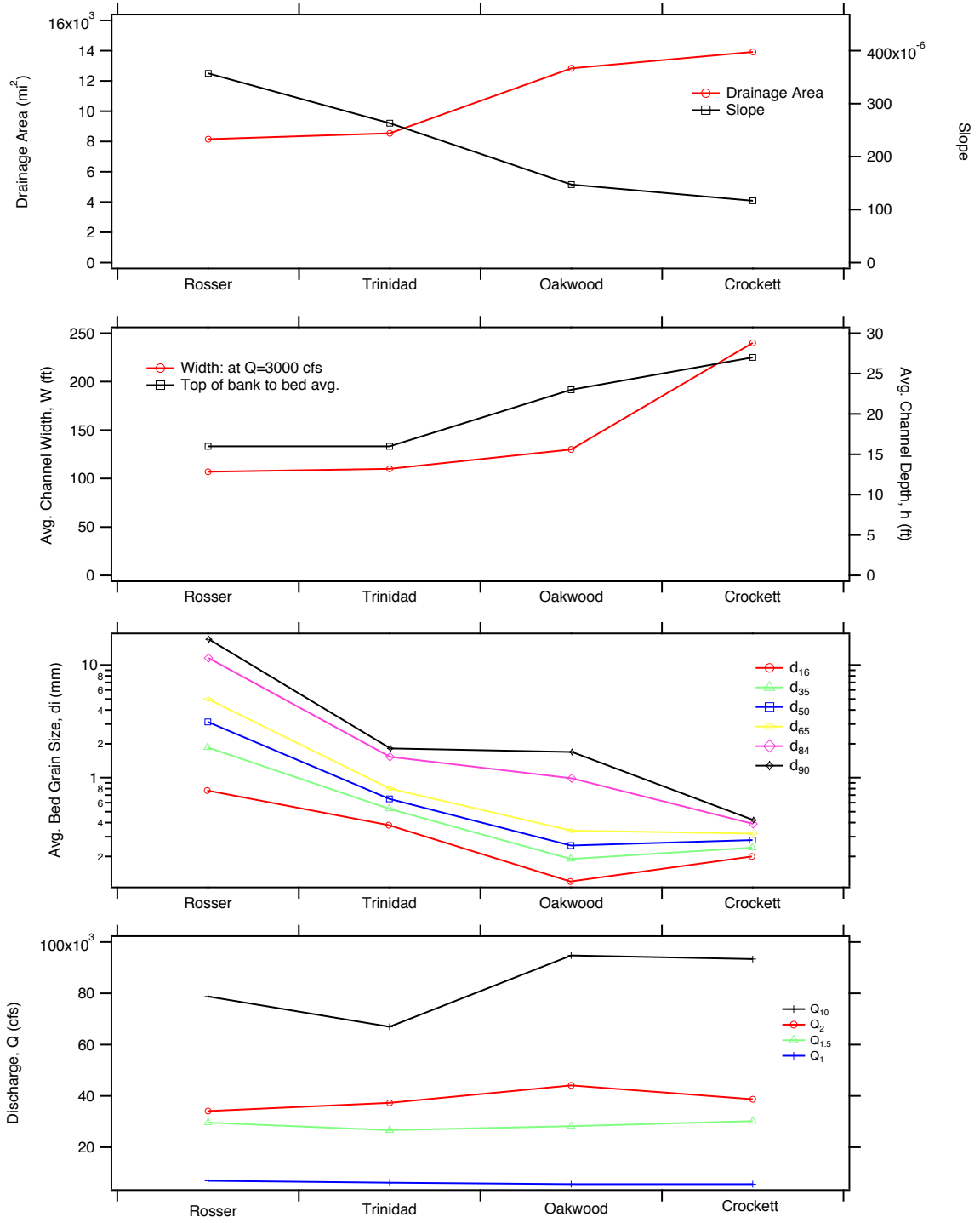


Figure 3.5: Downstream trends in major stream properties.

Table 3.1: Summary of measured data. **Bold** text highlights the highest measured concentrations at that site, and the *italics* highlights the highest daily main discharge during the sampling at the site. For the **bold italics**, the two maximums coincided.

Site	Date	Condition	Location on Hydrograph	SS Sample Method	Bed Size Measured? (Used)	SS Size Measured? (Used)	Q [cfs]	R _h [ft]	U [ft/s]	Bed Material				Wash		Total SSC [mg/l]
										d ₁₆ [mm]	d ₅₀ [mm]	d ₈₄ [mm]	d ₉₀ [mm]	Load [%]		
Rosser	5/17/12	Low	Base	Bucket	No (3/11/14)	Yes	844	4.3	2	0.77	3.13	11.52	16.91	16.91	91.7	490
Rosser	6/9/12	Moderate	Falling	DIS	No (3/11/14)	Yes	2800	6.2	3.8	0.77	3.13	11.52	16.91	16.91	81.9	370
Rosser	10/27/12	Low	Base	Bucket	No (3/11/14)	Yes	1100	4.5	2.5	0.77	3.13	11.52	16.91	16.91	99.7	560
Rosser	4/5/13	Moderate	Falling	DIS	No (3/11/14)	Yes	4610	7.1	5.4	0.77	3.13	11.52	16.91	16.91	99.9	810
Rosser	5/17/13	High	Peak	DIS	No (3/11/14)	Yes	8410	11.2	5.3	0.77	3.13	11.52	16.91	16.91	93.3	920
Rosser	3/11/14	Low	Base	Bucket	Yes	No (5/7/12)	718	4.1	1.9	0.77	3.13	11.52	16.91	16.91	91.7	490
Trinidad	5/17/12	Low	Base	Bucket	No (3/13/13)	Yes	946	4.2	2.8	0.38	0.65	1.53	1.82	1.82	99.9	580
Trinidad	6/9/12	Moderate	Falling	DIS	No (3/13/13)	Yes	7080	10.5	4.1	0.38	0.65	1.53	1.82	1.82	86.3	1100
Trinidad	10/27/12	Low	Base	Bucket	No (3/13/13)	Yes	1200	4.8	2.9	0.38	0.65	1.53	1.82	1.82	99	530
Trinidad	1/12/13	High	Peak	DIS	No (3/13/13)	Yes	<i>13400</i>	14	4.3	0.38	0.65	1.53	1.82	1.82	99.8	1100
Trinidad	3/13/13	Moderate	Falling	DIS	Yes	Yes	3100	6	4.5	0.38	0.65	1.53	1.82	1.82	99.9	870
Trinidad	5/18/13	High	Peak	DIS	No (3/13/13)	Yes	9240	12.6	4.1	0.38	0.65	1.53	1.82	1.82	98.3	1360
Oakwood	5/17/12	Low	Falling	Bucket	No (10/27/12)	Yes	1460	7.5	1.7	0.12	0.25	0.99	1.69	1.69	86.1	910
Oakwood	10/27/12	Low	Base	Bucket	Yes	Yes	800	5.8	1.3	0.12	0.25	0.99	1.69	1.69	99.9	62
Oakwood	5/18/13	Moderate	Rising	DIS	No (10/27/12)	Yes	5010	11.6	3	0.12	0.25	0.99	1.69	1.69	92.2	2720
Oakwood	5/24/13	Moderate	Rising	DIS	No (10/27/12)	Yes	3030	9.4	2.6	0.12	0.25	0.99	1.69	1.69	97.7	1170
Oakwood	10/31/13	High	Rising	DIS	No (10/27/12)	Yes	<i>18100</i>	17.9	3.3	0.12	0.25	0.99	1.69	1.69	93.3	1119
Oakwood	11/1/13	High	Falling	DIS	No (10/27/12)	Yes	17000	17.1	3.3	0.12	0.25	0.99	1.69	1.69	95.5	930
Oakwood	6/27/14	Moderate	Rising	DIS	No (10/27/12)	Yes	7110	13.1	3.5	0.12	0.25	0.99	1.69	1.69	99.9	2050
Crockett	5/17/12	Low	Falling	Bucket	No (5/25/13)	Yes	2190	7.4	1.1	0.2	0.28	0.39	0.42	0.42	91	350
Crockett	10/27/12	Low	Base	Bucket	No (5/25/13)	Yes	1100	6.6	0.7	0.2	0.28	0.39	0.42	0.42	99.9	360
Crockett	5/25/13	Moderate	Peak	DIS	Yes	Yes	3290	8	1.6	0.2	0.28	0.39	0.42	0.42	98.8	760
Crockett	6/13/13	Moderate	Peak	DIS	No (5/25/13)	Yes	5260	8.8	2.2	0.2	0.28	0.39	0.42	0.42	99.8	1240
Crockett	11/1/13	High	Rising	DIS	No (5/25/13)	Yes	19100	16.4	3.5	0.2	0.28	0.39	0.42	0.42	94.5	1960
Crockett	6/27/14	Moderate	Rising	DIS	No (5/25/13)	Yes	6370	9.3	2.5	0.2	0.28	0.39	0.42	0.42	99.9	1500

3.1.2 Comparison to Historic Sources

The collected suspended and bed material samples were compared to USGS measured values when available from each of the four gage stations. The USGS dataset for these sites contains spot measurements between 1964 to 1994. The Rosser, Oakwood, and Crockett sites all contain measurements of total suspended sediment concentration, percent wash load, a limited suspended bed material grain size distribution, and bed material size distribution. At Trinidad, only data for total suspended sediment and the percentage of wash load are available. The USGS data for the sites was obtained from the NWIS sites for each gage under the “Water Quality: Field/Lab Sample” section.

Comparisons of the measured concentrations and suspended bed material load with the historic data shows that the newly measured total concentrations fall within the range of those previously observed. But, they are, in general, a bit higher than most of the the historic values. This is especially true for the Trinidad and Crockett sites (figures 3.7 and 3.9). Nevertheless, the measured sand loads from all sites between the UH measurements and the USGS measurements are very comparable for all sites. The newly measured bed material grain size distribution are all comparable to the older USGS values (figures 3.6, 3.8, 3.9).

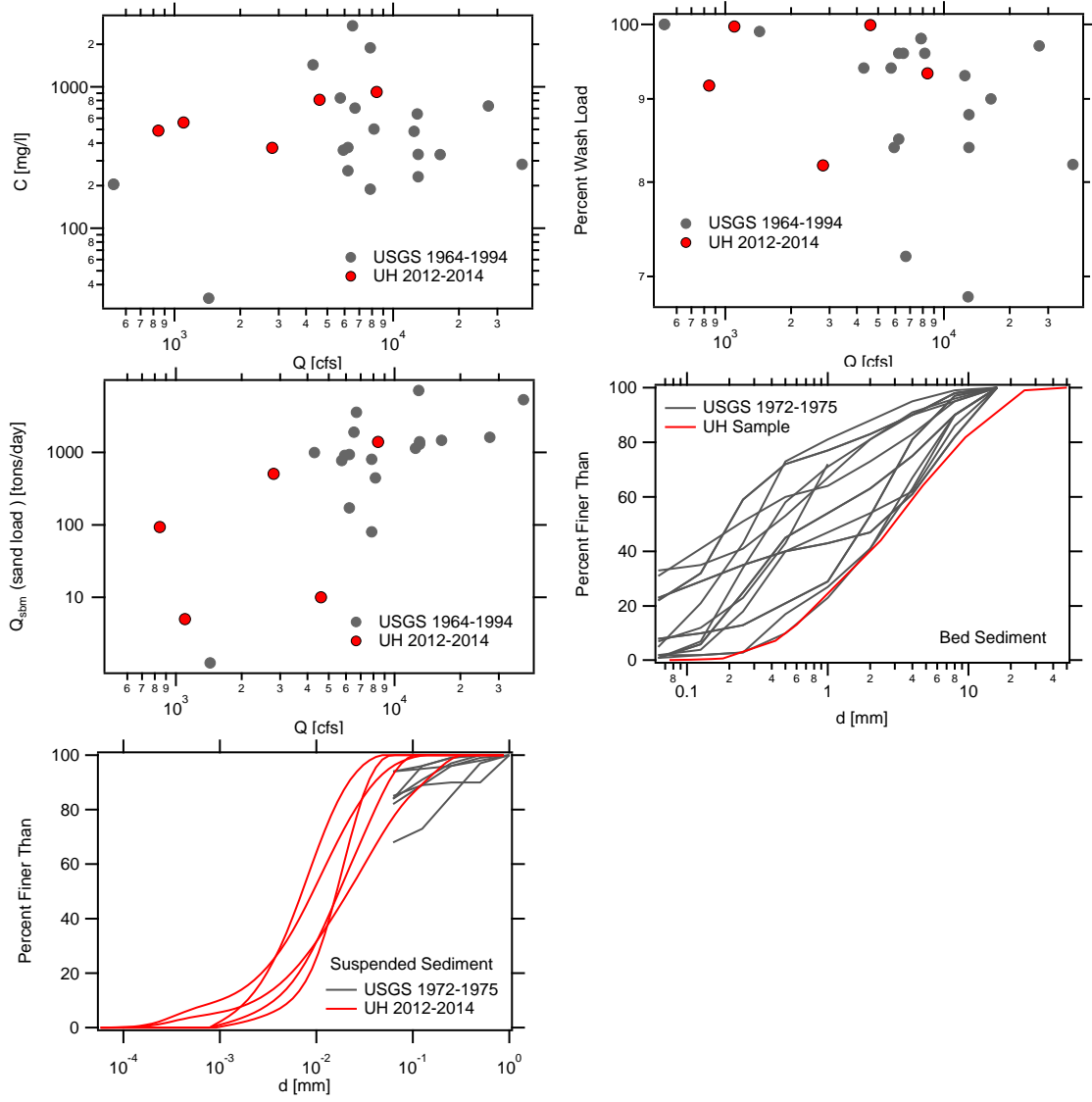


Figure 3.6: Comparison of UH and USGS data at the Rosser station.

3.2 BRAZOS RIVER

Brazos River data are extracted from Strom and Rouhnia (2013). For this river, 33 samples were collected for 6 following USGS gauge stations: (1) 08096500 - Brazos River at Waco, Texas; (2) 08098290 - Brazos River near Highbank, Texas; (3) 08108700 - Brazos River at SH 21 near Bryan, Texas; (4) 08111500 - Brazos River near Hempstead, Texas; (5) 08114000 - Brazos River at Richmond, Texas; and (6) 08116650 - Brazos River near Rosharon, Texas.

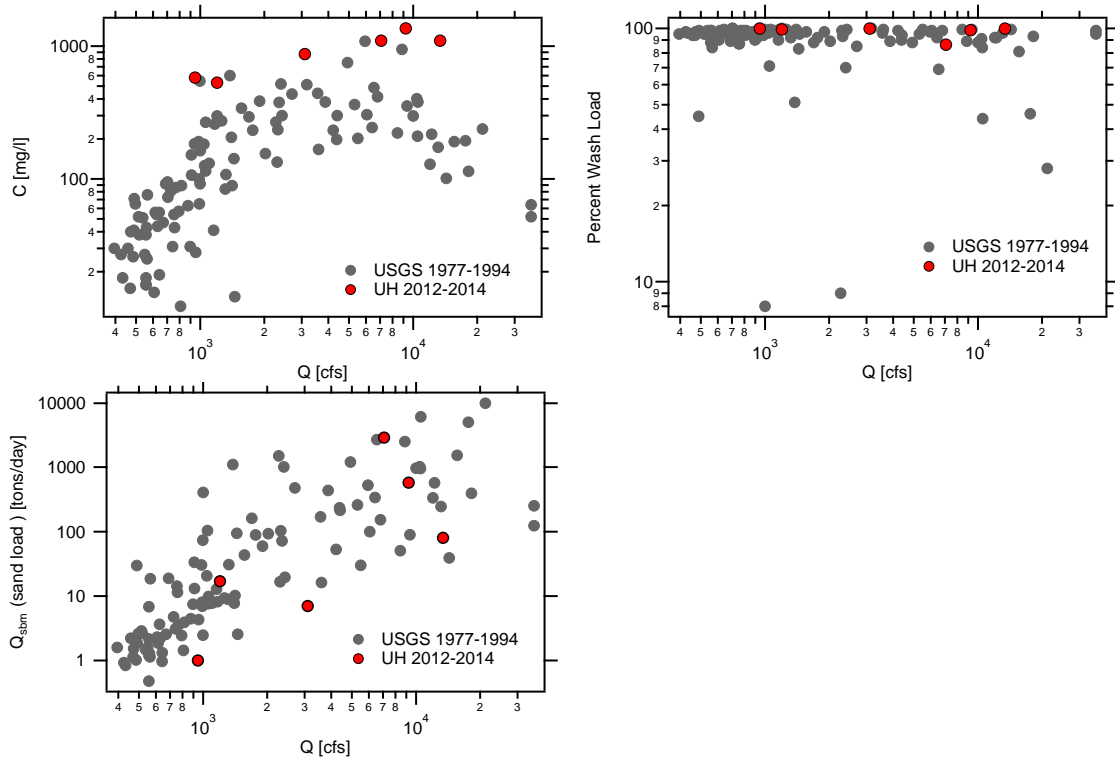


Figure 3.7: Comparison of UH and USGS data at the Trinidad station.

Flow statistics for the Brazos River are presented in table 3.2. Summary figures of collected data for all six stations are presented in Appendix.

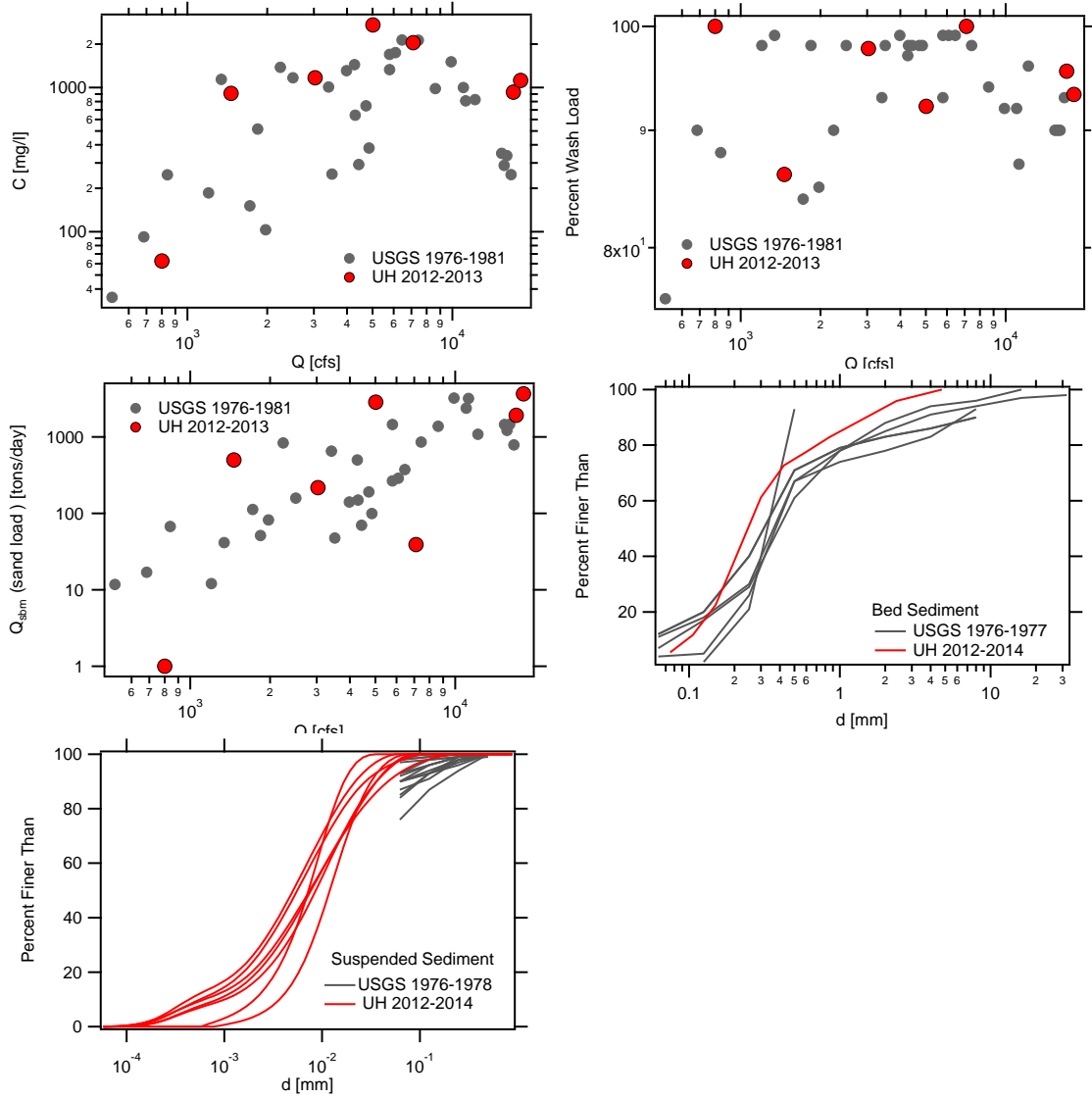


Figure 3.8: Comparison of UH and USGS data at the Oakwood station.

Table 3.2: Discharge statistics for the percent of time exceeded ($Q_{90\%}$, $Q_{50\%}$, and $Q_{20\%}$) along with the 1.5, 2, and 10 year return period flows calculated by ranking and linear interpolation using available USGS data. Table borrowed from Strom and Rouhnia (2013).

	20 Years of Record						All Years of Record		
	Exceedance Values			Return Periods			Return Periods		
	$Q_{90\%}$ [cfs]	$Q_{50\%}$ [cfs]	$Q_{20\%}$ [cfs]	$Q_{1.5}$ [cfs]	Q_2 [cfs]	Q_{10} [cfs]	$Q_{1.5}$ [cfs]	Q_2 [cfs]	Q_{10} [cfs]
Waco - 0809650	90	440	1,290	16,300	20,400	40,800	24,800	33,700	104,929
Highbank - 08098290	140	710	3,000	20,000	29,824	44,300	21,200	29,500	55,491
Bryan - 08098290	195	1,080	4,340	28,800	48,600	79,411	28,800	48,600	79,411
Hempstead - 08111500	550	2,715	10,350	45,900	56,176	105,443	40,700	52,000	102,844
Richmond - 0811400	425	2,665	10,780	51,400	54,438	86,986	44,500	55,800	88,235
Rosharon - 08116650	525	3,370	12,000	46,300	55,257	81,800	44,000	51,600	78,633

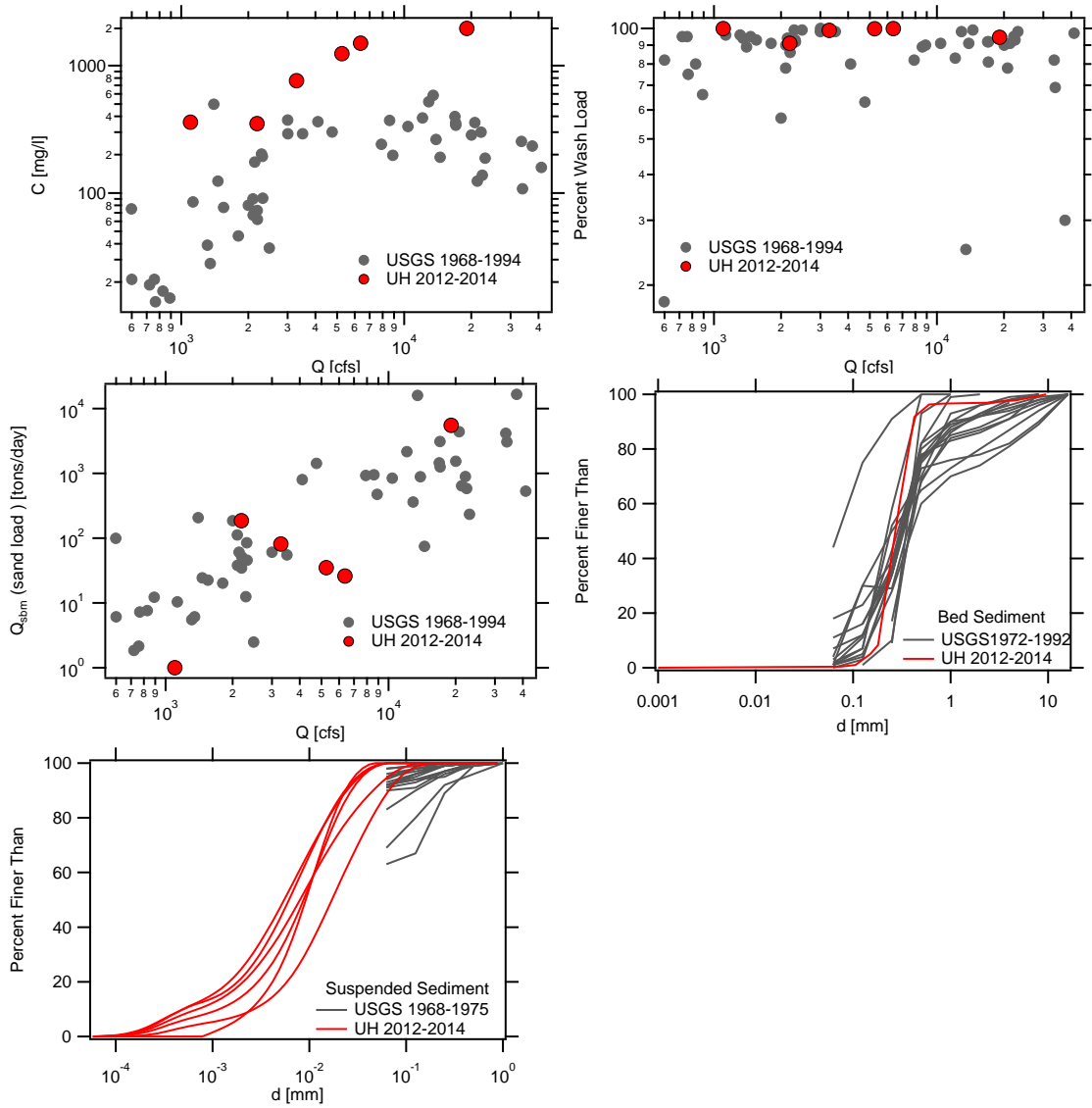


Figure 3.9: Comparison of UH and USGS data at the Crockett station.

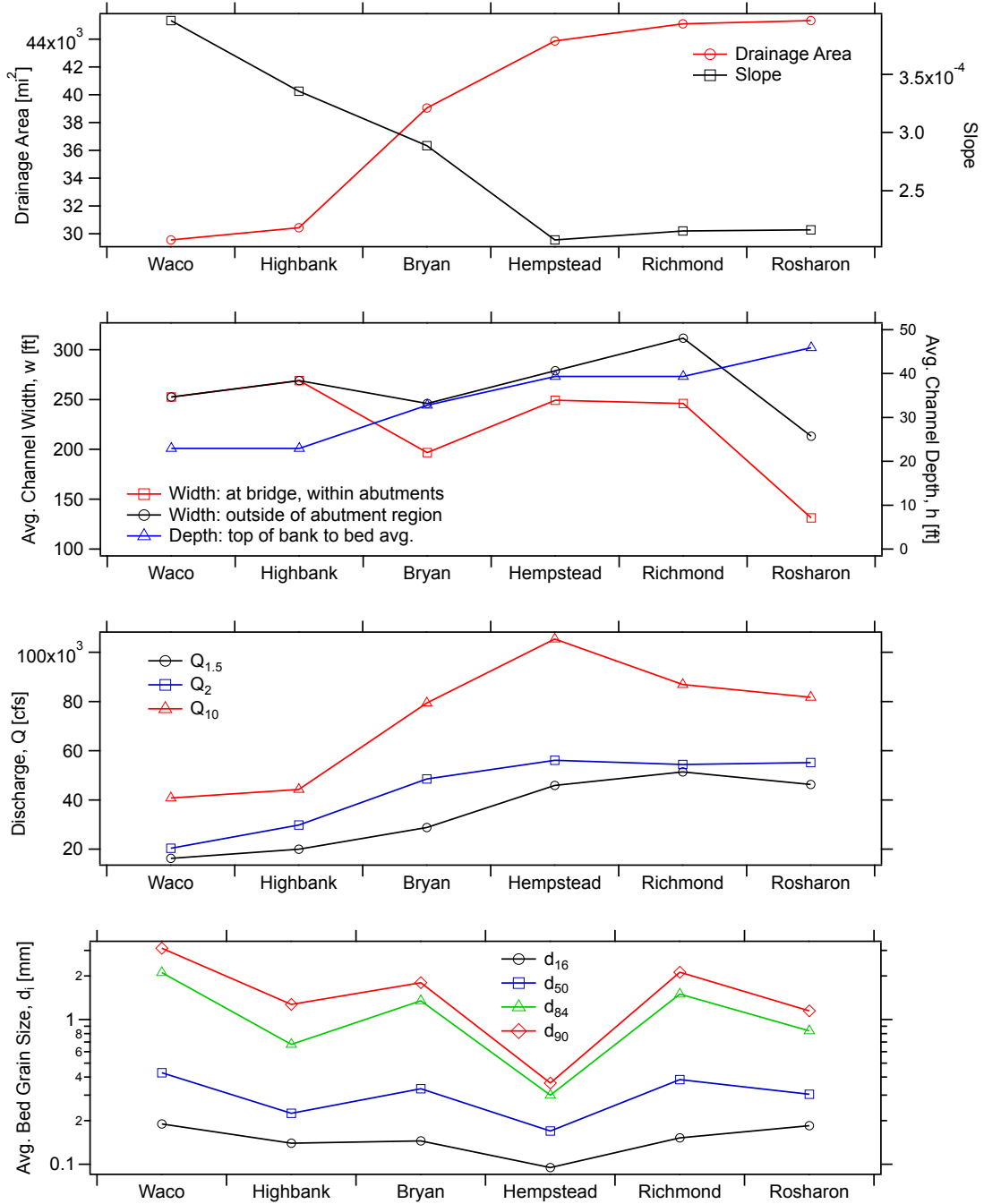


Figure 3.10: Downstream trends in major stream properties- borrowed from Strom and Rouhnia (2013).

Table 3.3: Summary of measured data for Brazos River. **Bold** text highlights the highest measured concentrations at that site, and the *italics* highlights the highest daily main discharge during the sampling at the site. For the ***bold italics***, the two maximums coincided. *Wash load values used in the development of the sediment rating curves. From Strom and Rouhnia (2013).

Site	Date	Condition	Location on Hydrograph	SS Sample Method	Bed Size Measured? (Used)	SS Size Measured? (Used)	Q [cfs]	R _h [ft]	U [ft/s]	Bed Material			Wash Load [%]	Total SSC [mg/l]
										d ₁₆ [mm]	d ₅₀ [mm]	d ₈₄ [mm]		
Waco	06/11/11	Low	Base	Bucket	Yes	Yes	500	3.4	0.5	0.11	0.20	1.50	2.70	51
Waco	12/22/11	Low	Base	Bucket	No (6/11/11)	No (6/11/11)	250	3.0	0.3	0.11	0.20	1.50	2.70	51
Waco	02/19/12	High	Falling	DIS	Yes	Yes	6,000	8.8	2.2	0.22	0.32	0.45	0.55	51*
Waco	03/25/12	High	Falling	DIS	Yes	Yes	<i>13,000</i>	13.4	2.8	0.32	1.00	5.00	6.50	51*
Highbank	06/11/11	Low	Base	Bucket	Yes	Yes	500	0.8	2.5	0.16	0.20	0.40	1.00	100*
Highbank	12/21/11	Moderate	Peak	DIS	No (6/11/11)	Yes	2,200	2.0	4.1	0.16	0.20	0.40	1.00	30
Highbank	01/26/12	High	Peak	DIS	No (6/11/11)	No (12/21/11)	16,500	8.6	4.7	0.16	0.20	0.40	1.00	30
Highbank	03/25/12	High	Falling	DIS	No (6/11/11)	No (12/21/11)	15,500	7.7	4.9	0.16	0.20	0.40	1.00	30
Highbank	07/28/12	Low	Base	Bucket	Yes	Yes	350	0.8	1.7	0.08	0.30	1.50	2.10	100*
Bryan	06/11/11	Low	Base	Bucket	Yes	Yes	600	3.3	0.8	0.09	0.21	0.90	1.30	99
Bryan	10/11/11	Moderate	Peak	DIS	Yes	Yes	3,400	6.4	2.3	0.17	0.26	0.90	1.30	46
Bryan	12/21/11	Low	Base	Bucket	No (6/11/11)	Yes	750	3.3	1.1	0.09	0.21	0.90	1.30	41
Bryan	01/27/12	High	Peak	DIS	Yes	No (06/11/11)	21,200	17.6	3.0	0.12	0.21	0.50	0.70	99*
Bryan	03/24/12	High	Falling	DIS	No (1/27/12)	Yes	<i>30,000</i>	20.4	3.4	0.12	0.21	0.50	0.70	100
Bryan	04/13/12	Moderate	Falling	DIS	Yes	Yes	5,000	9.0	1.6	0.25	0.70	3.50	4.50	100
Hempstead	06/12/11	Low	Base	Bucket	Yes	Yes	700	10.6	0.2	0.11	0.21	0.85	1.20	97
Hempstead	10/13/11	Low	Peak	Bucket	Yes	Yes	2,400	14.3	0.6	0.09	0.22	1.80	2.30	49
Hempstead	01/27/12	High	Rising	DIS	Yes	No (03/24/12)	16,000	21.5	1.8	0.09	0.13	0.25	0.28	97
Hempstead	02/17/12	Moderate	Rising	DIS	Yes	Yes	4,500	15.6	1.1	0.10	0.21	0.35	0.45	100
Hempstead	03/24/12	High	Peak	DIS	No (1/27/12)	Yes	<i>57,500</i>	27.2	2.1	0.09	0.13	0.25	0.28	97
Hempstead	04/13/12	Moderate	Falling	DIS	No (2/17/12)	Yes	7,900	17.9	1.6	0.10	0.21	0.35	0.45	97
Richmond	11/10/10	Low	Base	Bucket	Yes	No (3/26/12)	2,500	10.5	1.0	0.14	0.37	2.00	3.00	90
Richmond	01/09/12	Moderate	Peak	DIS	Yes	No (3/26/12)	7,300	12.9	2.2	0.11	0.22	0.86	1.60	90
Richmond	01/28/12	Moderate	Rising	DIS	Yes	No (3/26/12)	5,800	12.1	1.8	0.11	0.21	1.20	1.70	90
Richmond	01/30/12	High	Peak	DIS	Yes	No (3/26/12)	14,400	15.3	3.2	0.17	0.54	2.00	2.70	90
Richmond	02/02/12	Moderate	Falling	Bucket	Yes	No (3/26/12)	4,300	11.3	1.6	0.16	0.25	0.80	1.40	90
Richmond	03/26/12	High	Peak	DIS	No (1/30/12)	Yes	<i>53,000</i>	25.8	6.0	0.17	0.54	2.00	2.70	90
Rosharon	01/10/12	Moderate	Peak	DIS	yes	Yes	10,500	13.0	3.4	0.29	0.38	0.55	0.61	71
Rosharon	01/28/12	Moderate	Rising	DIS	yes	No (01/10/12)	4,400	8.1	3.1	0.31	0.46	0.72	1.00	71
Rosharon	01/30/12	High	Peak	DIS	yes	No	15,700	15.5	4.0	0.25	0.38	0.77	1.00	100
Rosharon	03/26/12	High	Peak	DIS	No (1/30/12)	Yes	<i>47,600</i>	27.3	5.7	0.25	0.38	0.77	1.00	71*
Rosharon	05/17/12	Low	Falling	Bucket	No (7/12/12)	Yes	2,100	6.6	1.9	0.12	0.23	0.90	1.30	57
Rosharon	07/12/12	Low	Rising	Bucket	yes	Yes	1,500	6.2	1.5	0.12	0.23	0.90	1.30	100

Chapter 4. Effective Discharge Estimates for the Trinity River

4.1 SEDIMENT RATING CURVES AND TRANSPORT CALCULATIONS

Sediment rating curves for the suspended load, Q_{sbm} , and the bedload, Q_b , were developed and used to construct the sediment load histograms for the suspended load and bedload independently. The resulting histograms were then added together to produce the total bed material histograms from which the effective discharge was obtained. The suspended sediment rating curves for Q_{sbm} and Q_{ss} were developed using regression and the measured data (figure 4.1). The bedload rating curves were developed by calculating the total bedload in tons per day associated with the daily discharge data at the time of sampling at each site by Einstein-Brown formula. The paired data was then fit with a power law curve to produce the rating curve. All rating curves retained the power-law functionality of equation 1.3. A list of all coefficients and the correlation coefficient for curve are listed in Table 4.1.

Slope measurements were not made at the time of sampling because the surveying equipment available to us (construction level and tape) was not accurate enough to measure the very small slopes on the Trinity. For this reason, values of S were obtained from a USGS database of computed slopes for Texas gaging stations and some additional analysis.

The USGS computed slope used is referred to as the “main-channel slope” (Asquith and Slade, 1997). The main-channel slope is defined as the change in elevation between the two end points of the main-channel divided by the distance, L (Asquith and Slade, 1997). In the calculation method, L is the longest defined channel shown in a 10-meter digital elevation model (DEM) from the approximate watershed headwaters to the point of interest, and the elevation change between the

two points is extracted directly from the 10-meter DEM. The main-channel slope is therefore more of a watershed slope based on the channel network than it is a local reach slope. Because of its calculation method, we suspect that the main channel slope values will be, on average, slightly higher than the local reach slopes at the stations because the main channel slope by definition incorporate elevation change further up in the watershed where slopes are likely higher. Nevertheless, this definition of slope was very reasonable for all but the Crockett station. For example, the reported main channel slope at each of the four sites was, Rosser $S = 0.00036$, Trinidad $S = 0.00026$, Oakwood $S = 0.00015$, and Crockett $S = 0.000823$. These main channel slopes would mean that the Crockett site had a slope that was over 5 times greater than the nearest upstream station (Oakwood). Since sediment continually fined in the downstream direction and discharge increased, it did not seem reasonable to use the 0.000823 value for the slope at Crockett. Instead, slope was estimated using the measured cross sectional geometry during the time of sampling and the USGS 15-min discharge data. Using this data, a slope was calculated for each flow condition using the Manning equation and assumed n values ranging from 0.03 to 0.04. The average of all back calculated slopes was then taken and used for the slope at Crockett. This analysis yield a slope of $S = 0.00012$, which seemed to be reasonable given that the upstream slope at Oakwood was $S = 0.00015$.

Slope estimates for Crockett were also obtained using the local floodplain elevation and the river length over 10's of kilometers. Doing so produced slopes with an average of 0.0002; a value slightly steeper than the slope used for Oakwood, but much less than the 0.000823 value in the USGS database. Phillips (2008) also tried several methods for estimating slope and water surface slope at Rosser, Trinidad, Oakwood, and Crockett. Similar to our analysis, Phillips reported that the calculated values and trend in slope progressing downstream varied depending on the method used to calculate slope. Sometimes slopes continually decreased. Other times they fluctuated

between increasing and decreasing. For his stream power estimation, Phillips use a decreasing slope going from Oakwood to Crockett as we have done here. The full analysis described below was done using several different slope values for Crockett; some of which were steeper than Oakwood and some that were lower. In the end, the exact slope value did not impact the effective discharge calculation.

A summary of all measured and calculated sediment loads used in development of the rating curves is given in Table 4.2. The table also lists the total calculated sediment according to equation 2.1 which includes the bedload and the suspended load. $Q_{\text{sed-all}}$ in table 4.2 lists all sediment load as

$$Q_{\text{sed-all}} = Q_{ss} + Q_b, \quad (4.1)$$

which includes bedload, suspended load, and wash load; and the SAMwin derived total bed material load Q_u . The SAMwin derived Q_u was developed using the measured cross sectional data and the computer program SAMwin, a Windows version of the SAM Hydraulic Design Package For Channels. The Einstein total load equation was used for calculating the total loads with SAMwin. For most cases, the calculated bedload was greater than the measured suspended bed material load. This can be seen from the rating curves (figure 4.1) and the tabulated values in Table 4.2.

Part of this might be somewhat artificial due to the use of τ_B rather than τ'_B in the bedload calculations. However, a large component is certainly a result of very little sand being physical captured in either the bucket or the depth-integrated sampler during the majority of the sampling trips. Two potential reasons for the low sand content could be, (1) that the sampler wasn't physically capturing sand that was suspended high up in the water column, or (2) very little sand actually made up into the water column past the first few inches from the bed.

To further investigate the lack of sand in the samples, we examine the predicted

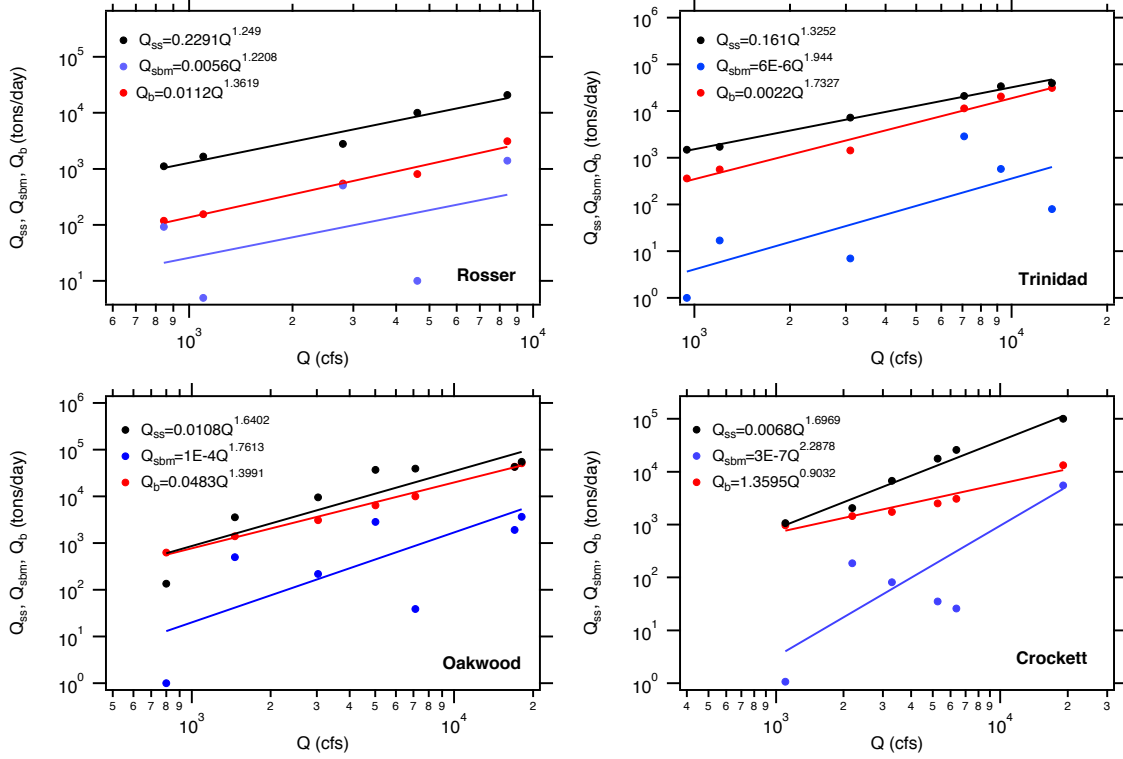


Figure 4.1: Rating curves.

sand concentration profile to see how the bed material d_{50} should theoretically have been distributed in the water column. To do this, we examined the Rouse number,

$$Z^* = \frac{w_s}{\kappa u_*'} \quad (4.2)$$

and the vertical sand flux profile for each sample location and day. In equation 4.2, w_s is the settling velocity of the bed material d_{50} and κ is the von Karman constant ($\kappa = 0.4$). The standard equilibrium Rouse profile with a Schmidt number of 1 without buoyant damping was used to develop $C = C(z)$ at each condition. This was then multiplied with the velocity profile of Wright and Parker (2004) to obtain the suspended sand flux profile. For the Rouse profile calculations, a reference height of $0.05h$ was used along with the reference concentration prediction and shear stress partitioning methods of Wright and Parker (2004). The sand flux profile was then used to locate the height at which 90% of the total suspended sand flow rate is

reached, h_{ss90} . If the total unit width sand flow rate is:

$$q_{ss} = \int_{z=0}^{z=h} uCdz, \quad (4.3)$$

then h_{ss90} is the depth that satisfies the following:

$$0.9q_{ss} = \int_{z=0}^{z=h_{ss90}} uCdz. \quad (4.4)$$

The theoretical calculations showed that the Rouse number ranged from 1 to 5, and that h_{ss90} most often occurred within the first meter from the bed (Table 4.2). In fact, in several cases, 90% of the suspended sand load was predicted to occur within the first 10 cm from the bed. Sampling suspended sand traveling this low is problematic. This is true for the bucket sampler since it collects water and sediment near the free surface. And, it is also an issue for the depth integrated sampler since the US DH-2 cannot sample the first 4 in (10 cm) from the bed due to its physical construction and nozzle location. Unfortunately, no clear h_{ss90} threshold was found from the analysis to predict when the depth-integrated sampler would or would not capture sand. Nevertheless, in a broad generalization, the analysis suggests that the Trinity is bedload dominated and that the majority of suspended sands likely travel very close to the bed.

Table 4.1: Rating curve coefficient values and correlation coefficients. *Rating curves developed using all of the historic USGS data at the site along with the additional data collected by UH. Rating curves have the form of $Q_i = \alpha Q^\beta$ where i is the transport mode.

Site	Q_{sbm} [tons/day]			Q_{ss} [tons/day]			Q_b [tons/day]			Q_{SAM} [tons/day]		
	α	β	R^2	α	β	R^2	α	β	R^2	α	β	R^2
Rosser	0.005	1.220	0.24	0.229	1.249	0.94	0.011	1.362	0.97	3.0E-05	2.065	0.92
Rosser (USGS)*	1E-05	1.992	0.69	0.200	1.209	0.72						
Trinidad	6E-06	1.944	0.57	0.161	1.325	0.99	0.002	1.733	0.97	9.9E-02	1.173	0.90
Trinidad (USGS)*	6E-05	1.715	0.64	0.003	1.594	0.80						
Oakwood	1E-04	1.761	0.50	0.010	1.640	0.79	0.048	1.399	0.99	4.0E-06	2.371	0.97
Oakwood(USGS)*	8E-04	1.520	0.63	0.018	1.538	0.72						
Crockett	3E-07	2.288	0.64	0.006	1.697	0.97	1.360	0.903	0.93	3.0E-07	2.527	0.95
Crockett (USGS)*	1E-04	1.624	0.66	0.004	1.553	0.81						

Table 4.2: Summary of sediment transport calculations. $^1h_{s,90}$ is the predicted distance above the bed for which 90% of the total suspended sand load passes beneath; the calculate is based on d_{50} of the bed material. *Wash load values used in the development of the sediment rating curves.

Site	Date	Condition	S	Q [cfs]	d_{50} [mm]	d_m [mm]	τ^*/τ_{cr}^*	z^*	$h_{s,90}^1$ [m]	$Q_{s,s}$ [T/day]	Wash Load [%]	Q_{sbm} [T/day]	Q_b [T/day]	$Q_{sed-all}$ [T/day]	Q_{tl} [T/day]	SAM Q_{tl} [T/day]
Rosser	5/17/12	Low	0.000357	844	3.13	5.8	2	11.4	0.05	1115	92	93	119	1234	211	33
Rosser	6/9/12	Moderate	0.000357	2800	3.13	5.8	3	7.9	0.10	2794	82	506	544	3338	1050	394
Rosser	10/27/12	Low	0.000357	1100	3.13	5.8	2	10.1	0.05	1661	100	5	155	1816	160	57
Rosser	4/5/13	Moderate	0.000357	4610	3.13	5.8	3	5.4	0.11	10072	100	10	811	10882	821	1103
Rosser	5/17/13	High	0.000357	8410	3.13	5.8	5	5.9	0.17	20869	93	1398	3129	23998	4527	3818
Trinidad	5/17/12	Low	0.00026	946	0.65	0.93	7	4.8	0.06	1480	100	1	361	1841	363	306
Trinidad	6/9/12	Moderate	0.00026	7080	0.65	0.93	17	3.5	0.22	21006	86	2878	11475	32480	14352	3249
Trinidad	10/27/12	Low	0.00026	1200	0.65	0.93	8	4.6	0.07	1715	99	17	560	2275	577	405
Trinidad	1/12/13	High	0.00026	13400	0.65	0.93	22	3.5	0.30	39757	100	80	31111	70868	31190	6866
Trinidad	3/13/13	Moderate	0.00026	3100	0.65	0.93	9	3.0	0.13	7274	100	7	1433	8707	1440	1233
Trinidad	5/18/13	High	0.00026	9240	0.65	0.93	20	3.6	0.27	33894	98	576	20506	54400	21083	4440
Oakwood	5/17/12	Low	0.000147	1460	0.25	0.57	17	2.7	0.21	3584	86	498	1402	4985	1900	127
Oakwood	10/27/12	Low	0.000147	800	0.25	0.57	13	3.7	0.13	135	100	1	626	761	627	31
Oakwood	5/18/13	Moderate	0.000147	5010	0.25	0.57	27	1.4	1.02	36755	92	2850	6433	43188	9283	2368
Oakwood	5/24/13	Moderate	0.000147	3030	0.25	0.57	22	1.8	0.60	9562	98	217	3070	12632	3288	719
Oakwood	10/31/13	High	0.000147	18100	0.25	0.57	41	1.5	1.58	54629	93	3660	51077	105705	54737	49776
Oakwood	11/1/13	High	0.000147	17000	0.25	0.57	39	1.5	1.50	42643	96	1919	43431	86074	45350	42900
Oakwood	6/27/14	Moderate	0.000147	7110	0.25	0.57	30	1.3	1.31	39313	100	39	10000	49313	10039	5431
Crockett	5/17/12	Low	0.00012	2190	0.28	0.47	12	3.3	0.16	2067	91	186	1452	3519	1638	83
Crockett	10/27/12	Low	0.00012	1100	0.28	0.47	11	4.0	0.10	1068	100	1	973	2041	974	15
Crockett	5/25/13	Moderate	0.00012	3290	0.28	0.47	13	3.3	0.17	6744	99	81	1737	8481	1818	232
Crockett	6/13/13	Moderate	0.00012	5260	0.28	0.47	15	2.3	0.35	17592	100	35	2509	20102	2545	759
Crockett	11/1/13	High	0.00012	19100	0.28	0.47	18	1.5	1.37	100972	95	5523	13331	114303	18854	19738
Crockett	6/27/14	Moderate	0.00012	6370	0.28	0.47	15	2.0	0.48	25772	100	26	3087	28858	3112	1231

4.2 DEVELOPMENT OF THE DAILY FLOW PDF

The developed rating curves were used in conjunction with the flow duration histograms (pdf of the daily flow discharge) to build the sediment transport histograms as a function of daily flow levels (fig. 1.1). The flow duration histograms, S_h , were computed two different ways. In the first, the histogram was developed by manually selecting the discharge bin width and sorting the observed daily flow data. In the second, the histogram was generated objectively using the kernel density method of Klonsky and Vogel (2011).

For the manual method, the discharge bin widths were first set to an evenly spaced 25 bins over the range of observed data at each site following the recommendations of Hey (1997), and Biedenharn et al. (2000). Figure 4.2 shows the flow duration curves of Trinity River generated by 25 evenly spaced bins.

However, when doing this, it was most often the case that the first bin in the sediment histogram, S_h , contained the greatest percentage of sediment; this would result in the effective discharge being defined as the discharge equal to the midpoint discharge of the first bin. When this occurred, the number of bins was increased in increments up to a total of 40 or 50 bins in an attempt to produce a smoother histogram.

During this process of manually modifying the discharge bin widths, it was observed that the selection of the bin width greatly impacted the final effective discharge estimates. In an effort to avoid the subjectiveness of the bin width selection, a second, more objective, method for creating the flow duration histogram was used. The method used was the kernel density estimation method as suggested by Klonsky and Vogel (2011).

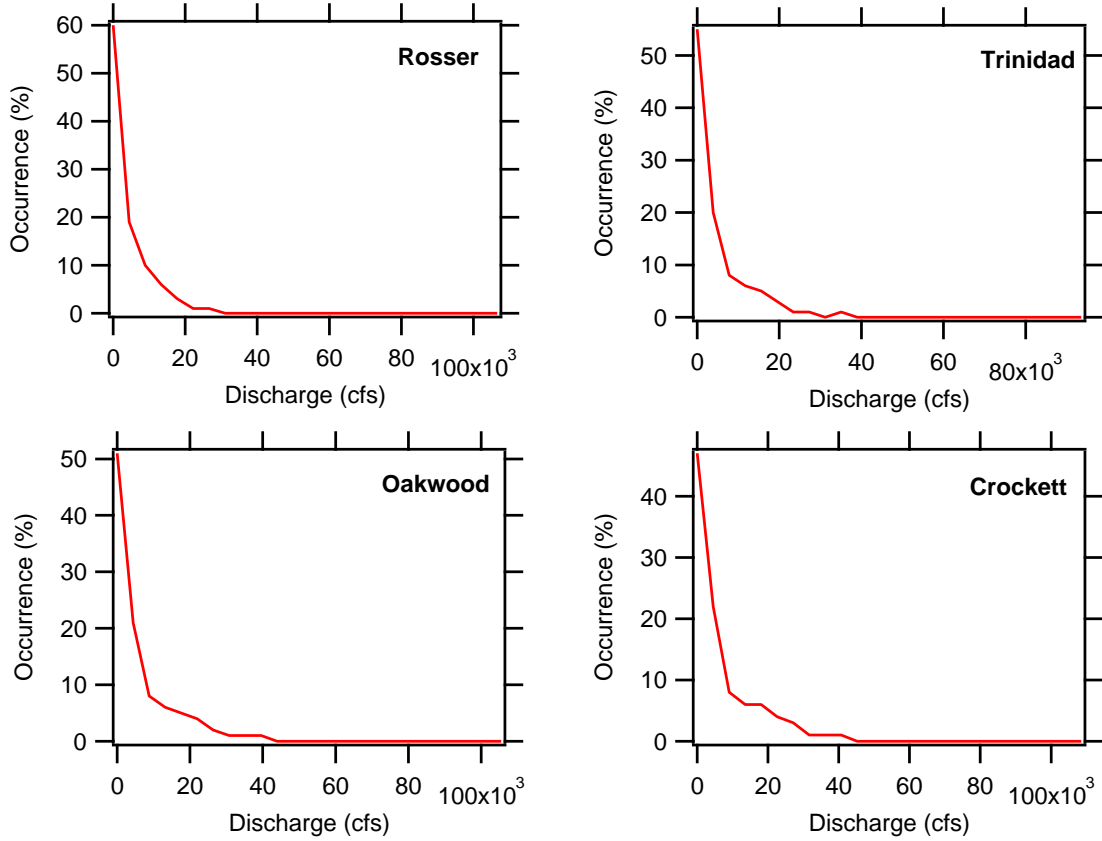


Figure 4.2: Flow duration curves for Trinity River generated by 25 evenly spaced bins.

4.3 SEDIMENT TRANSPORT EFFECTIVENESS DISTRIBUTIONS

Effective discharge estimates, Q_e , were made directly from sediment transport effectiveness histograms, S_h (Wolman and Miller, 1960), that were developed using both the manual and kernel density pdfs of the flow. The S_h distributions were developed by multiplying the load at a particular discharge as estimated by the rating curves with the pdf of the daily flow discharge. This was done independently for the bedload, Q_b , and suspended bed material load, Q_{sbm} as

$$S_{h:sbm} = Q_{sbm} f_Q, \text{ and} \quad (4.5)$$

$$S_{h:b} = Q_b f_Q \quad (4.6)$$

with the total transport effectiveness distribution being the summation of the bed and suspended load,

$$S_h = S_{h:sbm} + S_{h:b}. \quad (4.7)$$

For the manually developed histograms, the discharge at the midpoint of the discharge bin was used to calculate that daily loads from the rating equations. For the kernel density method, the Q values used corresponded with 100 regularly spaced values for which f_Q was calculated. The sediment effectiveness distributions were calculated using the rating curves developed using (1) only data from this study, (2) using all available USGS data plus the data from this study, and (3) using the SAMwin rating curves. Coefficients for all of these rating curves can be found in Table 4.1. Figures 4.3 and 4.4 show these effectiveness distributions developed using the data obtained in this study.

All of the S_h distributions show the dominance of bedload transport over suspended load for the study sites (figures 4.3 and 4.4). This is to be expected from the Rouse numbers and h_{ss90} values (table 4.2) and the developed rating curves (figure 4.1). Because of the dominance of bedload, which was a calculated in our analysis, we also ran the effective discharge calculations using other bedload transport equations. The other equations tested included: the Meyer-Peter and Müller (1948) equation and the standard Einstein bedload formula. Using other bedload formulas did change the magnitude of the calculated bedload, but it did not change the shape of the sediment transport effectiveness histograms. Therefore, the use of different equations did not significantly alter the final effective discharge. Nonetheless, the dominance of bedload in the calculations and lack of physical bedload samples should be considered as a limitation of this study.

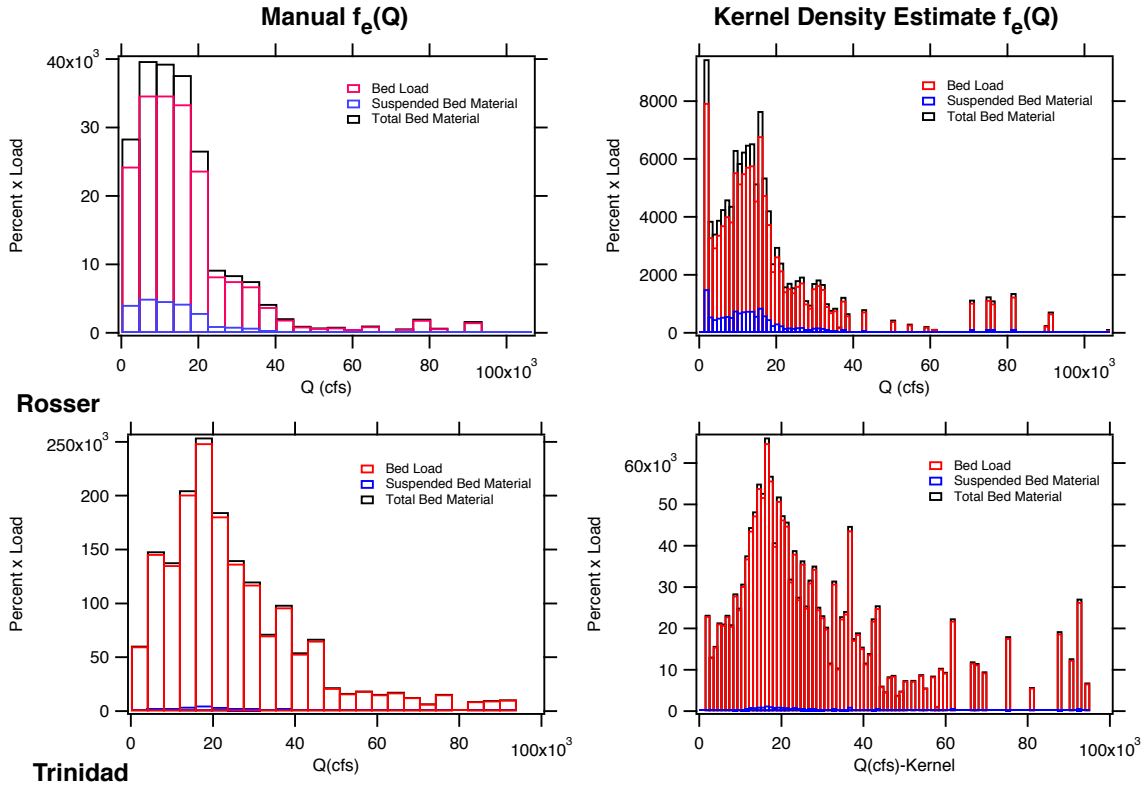


Figure 4.3: Sediment transport effectiveness distributions for Rosser and Trinidad using both the manual and kernel density estimate derived daily flow PDFs.

4.4 EFFECTIVE DISCHARGE VALUES

The effective discharge was selected using the smoothing method (described in section 5.2) from each of the sediment effectiveness histograms generated using (1) only data from this study, (2) using all available USGS data plus the data from this study. For each, the effectiveness histograms were generated with manual method for generating the flow pdf where as the number of the bins is set to 25. The values of effective discharge for Trinity River are given in Table 4.3. Very little difference was found in the computed effective discharge when using the rating curves developed with only the UH measured data for the suspended bed material compared to those developed using the UH plus USGS data (Table 4.3). The only small difference between the USGS+UH and UH only was for the effective discharge estimate at Rosser where the rating curve with the UH only data produced an effective discharge

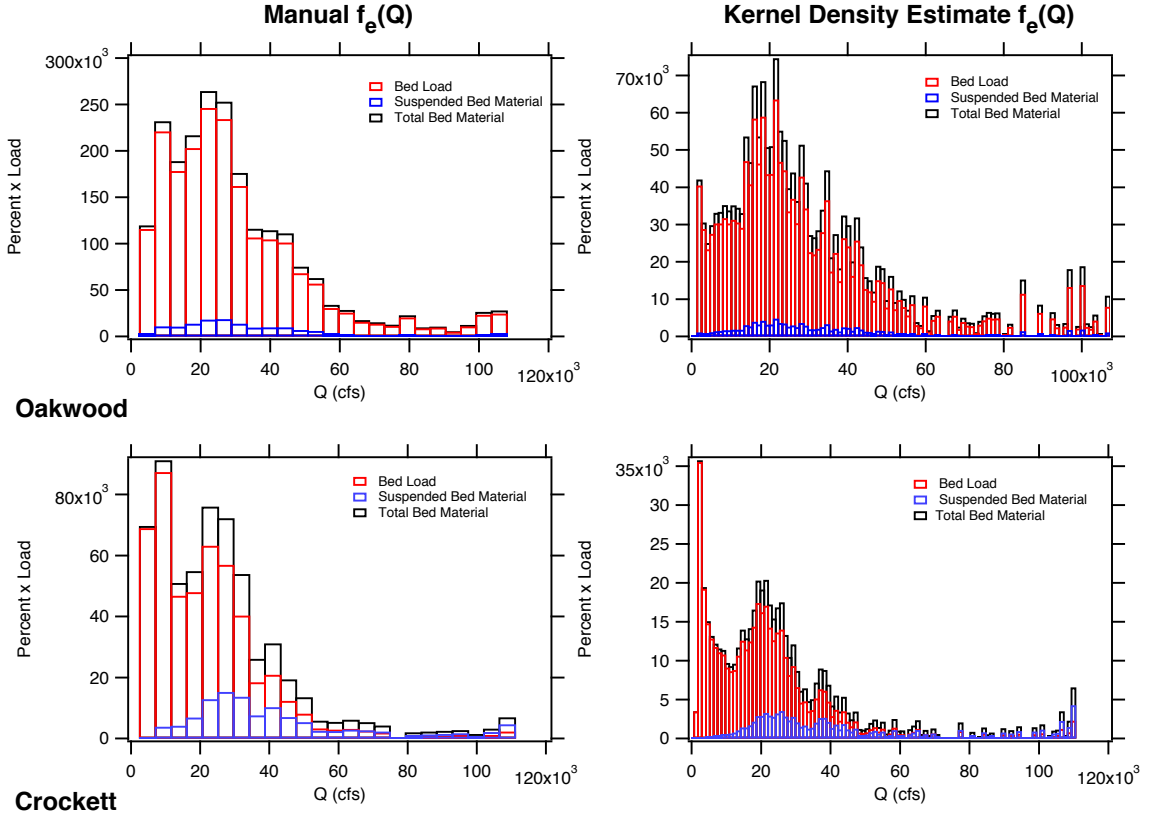


Figure 4.4: Sediment transport effectiveness distributions for Oakwood and Crockett using both the manual and kernel density estimate derived daily flow PDFs.

of 11,102 cfs compared to the 15,543 cfs (one bin to the right) produced with the added USGS data. In the remainder of this work, only the rating curves developed with the measured data from this study are used.

Table 4.3: Comparison of calculated effective discharge for total bed material load and suspended bed material load along with calculated Q_e by using USGS historic sediment data.

Site	Total load Q_e [cfs]	Suspended Bed Material Q_e [cfs]	Different Q_e values by method? UH vs USGS+UH
Rosser	11,102	6,661	yes
Trinidad	17,535	17,535	no
Oakwood	19,781	27,365	no
Crockett	20,345	34,031	no

Chapter 5. Analysis of Effective Discharge Calculations Methods

5.1 OVERVIEW

The process of calculating the effective discharge on the Trinity River raised several questions relevant to the general methodology of such calculations. These questions come out of the fact that choices have to be made regarding how the flow PDF is generated and how much and what type of field data can and should be collected. These two choices are reflected in research questions 1 and 2 in the Introduction. Additionally, in the case when bedload or bed and suspended load can not be collected, one is forced to make calculations of transport rate. Logical followup questions in such cases are, how does the selection of one question over another impact the final resulting effective discharge, and what input parameters to the questions most significantly influence the slope of the rating curve and hence the effective discharge calculations?

In the following section, questions regarding how the method used to develop flow PDF and the amount of on-site data used in the calculations impacts the final effective discharge value are examined together. Following this, the two questions pertaining specifically to the calculation of sediment transport rate are addressed. Data from the Trinity and Brazos rivers are used for the analysis. Both of these rivers are low-slope, Texas rivers. However, the two rivers do present key differences in transport mode since the Trinity is bedload dominated while the Brazos is more strongly influenced by suspended load.

5.2 THE IMPACT OF THE METHOD USED TO DEVELOP THE FLOW PDF AND THE AMOUNT OF FIELD MEASURED DATA ON THE CALCULATION OF EFFECTIVE DISCHARGE

The scenarios listed in section 2.4.2 are defined such that at one end of the spectrum all measured data is used, and at the other end the only on-site data used is the bed material grain size distribution. This approach helps to evaluate the change in effective discharges due to the amount and type of on-site measured data used in the calculations. Scenario 1 uses the most amount of on-site data and scenario four uses the least. For each scenario, the effective discharge is calculated using four different flow PDFs. These flow PDFs are developed using 25, 50, and 100 equally spaced bins and the kernel density estimate method of Klonsky and Vogel (2011). The combination of the four scenarios and the four different flow PDF generation methods results in a total of 16 different Q_e estimates per gaging station.

The resulting effective discharges following this procedure for both the Trinity and Brazos river stations are shown in figure 5.1 and 5.3. The results show that the effective discharge values can be quite sensitive to both the frequency analysis method and the amount of on-site data used.

On the Brazos, the effective discharge at Rosharon and Waco (figure 5.3) do not vary much among the 16 different calculations. However, for the other stations on the Brazos, the effective discharge does vary significantly with changes in the amount of data used in calculations. In the case of the frequency analysis, change in the number of the bins substantially changes the magnitude of the effective discharges. For instance, at the Oakwood station on Trinity River, changing the number of the bins from 25 to 50, causes the effective discharge to drop down from 20,000 cfs to 3,000 cfs. The reason for this is that by reducing the number of bins, and thereby increasing the width of each bin, the frequency of the lowest bin increases substantially and forces the effective discharge to technically be located in the first bin.

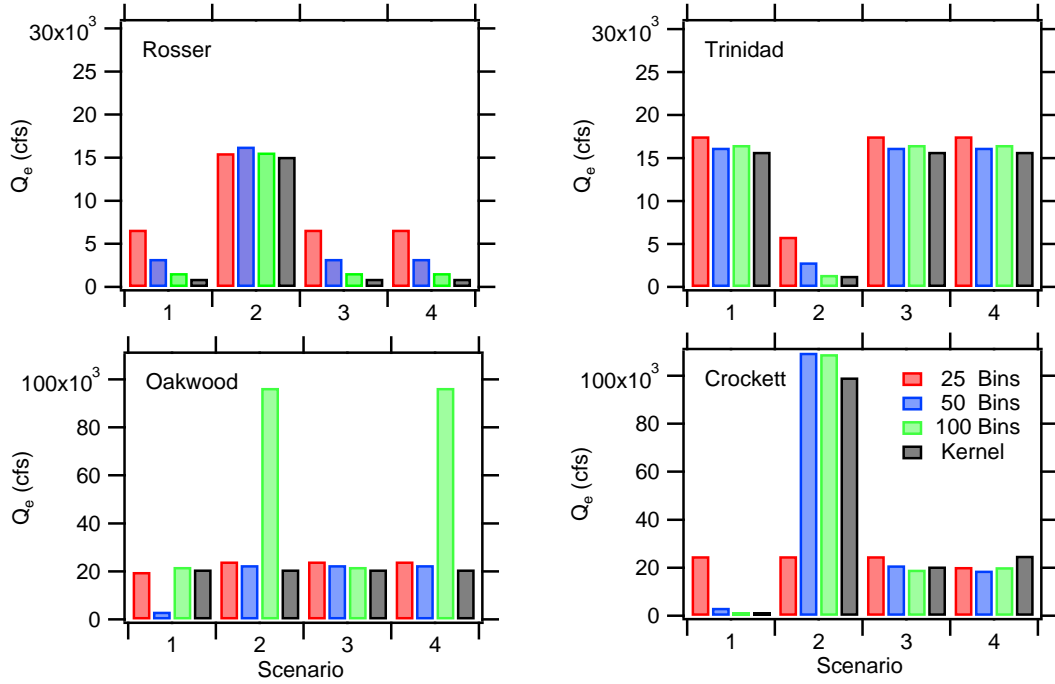


Figure 5.1: Effective discharge calculations for each for the four scenarios using each of the four different methods for generating the flow PDF on the Trinity River.

Comparing the kernel density estimate and the standard frequency analysis with 100 bins shows that the two methods can produce different results even though the number of the bins in each method are equal. For instance at Highbank on the Brazos, the kernel density estimate results in an effective discharge of 32,000 cfs. At the same station, the manual frequency analysis with 100 bins results in an effective discharge of 1,000 cfs. The reason for the large discrepancy is related to the presence of a double peak in the sediment effectiveness histogram. The first of the two peaks occurs at very low flows with high reoccurrence frequencies. The second peak is more aligned with high flow (figure 5.2). In this way, even a very small change in flow frequency values will change the maximum of the sediment effectiveness from very low to very high flow and vice versa.

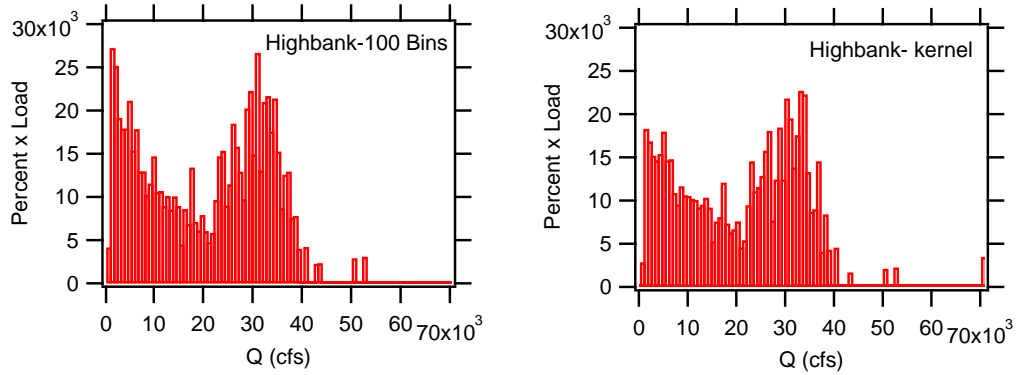


Figure 5.2: Comparison of the sediment effectiveness histograms of the Highbank station calculated by 100 bins and kernel density estimate.

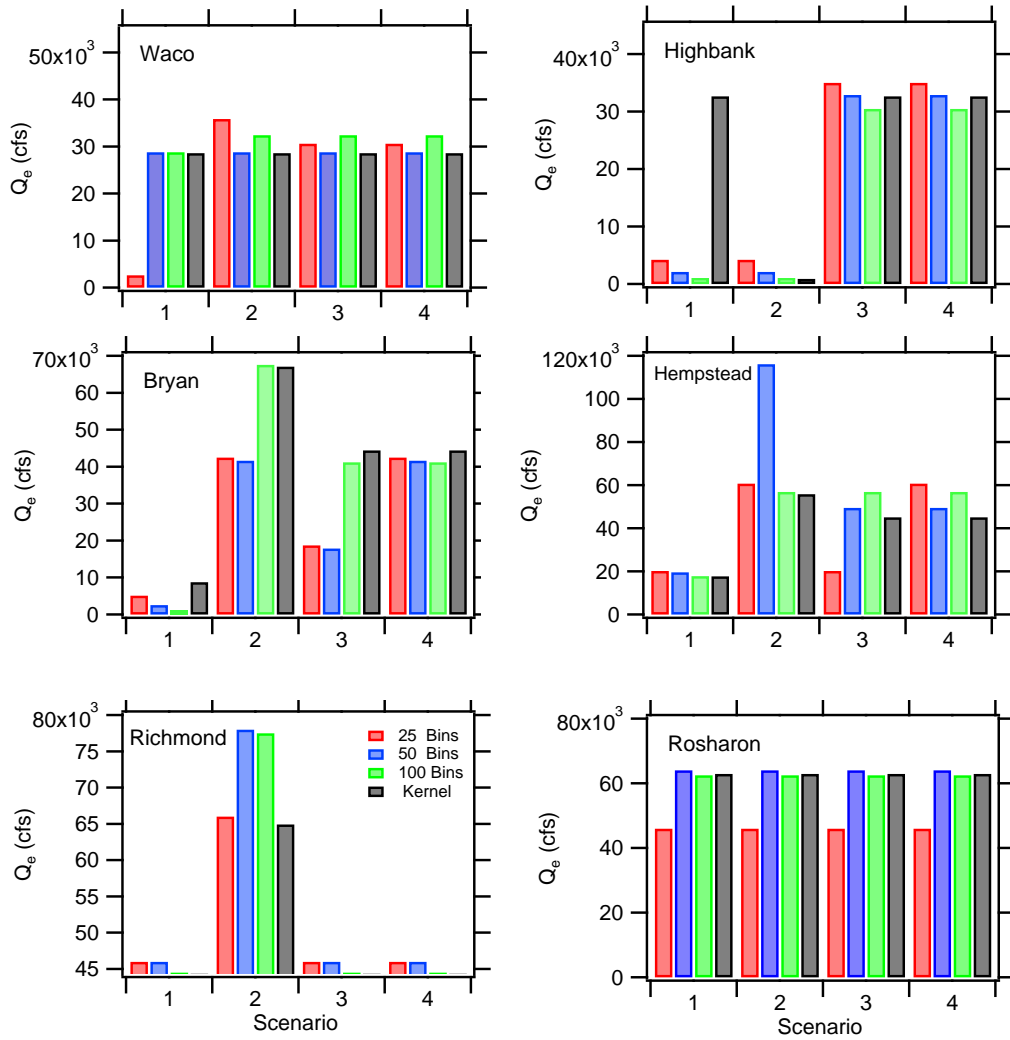


Figure 5.3: Variability of the effective discharge of the Brazos River due to different flow-frequency analysis and amount of measured data used in calculations.

Figures 5.1 and 5.3 indicate that even within a particular scenario, change in flow frequency analysis may change the calculated effective discharge dramatically. The reason for these spikes is related to the definition of the effective discharge as the discharge in which the sediment effectiveness histogram is maximum. By this definition, wherever the maximum of S_h happens, regardless to any trend in histogram, that corresponded discharge is designated as the effective discharge even if the discharges one bin down or up may have a substantially lower S_h value. In fact, for many stations there are spikes in the initial bins (figure 5.4) because of the approach taken for binning flow data. These spikes are primarily considered as the effective discharge since they are maximum of S_h .

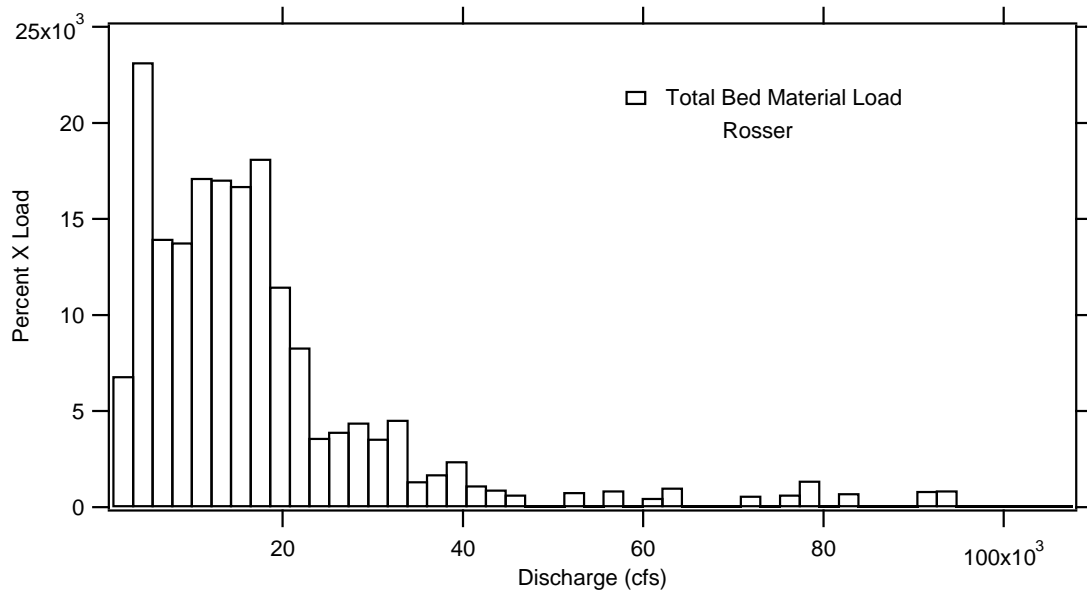


Figure 5.4: Spike in initial bin of sediment effectiveness histogram for Rosser gauge station at Trinity.

Also one can easily find that scenario 2 results in the largest fluctuations in calculated Q_e as a function of scenario and flow frequency analysis. The reason for the discrepancy is related to the computed steepness of the sediment transport rating curves. Since the power law function is used for the sediment load (equation 1.3), the magnitude of the power, β , plays a strong role in determining what discharge carries

the largest fraction of sediment in the analysis.

Table 5.1: Slope of the sediment transport rating curves of Trinity River for different scenarios. **Bold** and *Italic* numbers show the maximum and minimum values respectively.

Scenario	Rating Curve Slope, β			
	Rosser	Trinidad	Oakwood	Crockett
1	1.3	1.7	1.4	1.0
2	2.1	<i>1.2</i>	2.4	2.5
3	1.2	1.6	2.0	1.8
4	1.3	1.8	2.3	2.0

Table 5.1 along with figure 5.1 shows the importance of β and its effect on the effective discharge calculations. Scenario 2 ends up with either minimum or maximum β values. When the β gets large values, Q_s exponentially increases and though forces the effective discharge to happen toward the very high discharges and vice versa.

Smoothing Technique

Much of the variability in the calculated effective discharge in the preceding section can be attributed to the “lone peak” problem in S_h (see for example figures 4.3 and 5.4 for Rosser or 4.4 for Crockett). Often times, this lone peak occurs in one of the first few bins, and selection of such a discrete peak would lead to effective discharges associated with the lowest flows in the river. Additionally, the problem of an isolated peak can come and go depending on the exact number of bins and bin widths used; making the selection of effective discharge vary dependent on the method used for generating the discharge pdf.

The lone-peak problem can be avoided by making use of the suggestion of Bieden-harn et al. (2000) by fitting a smooth and continuous line through the entire S_h distribution by eye. Figure 5.5 shows the smoothing technique applied to the total bed material load in Trinity River. The effective discharge is then chosen as the peak of this smooth distribution.

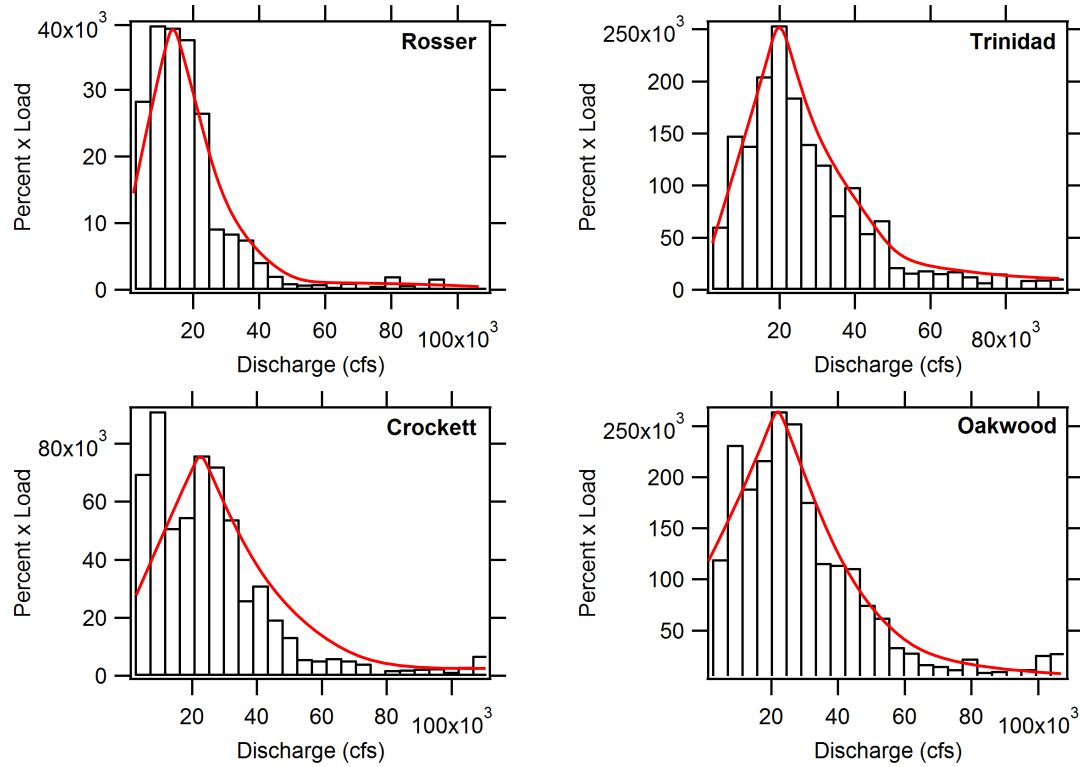


Figure 5.5: Smoothed curves fit to total bed material load of Trinity River.

While this method does retain a measure of user subjectiveness, the method does produce more consistent results for the effective discharge, and it keeps high frequency, but very low magnitude flows (or low frequency but high magnitude flows), from being assigned as the effective discharge.

Figures 5.6 and 5.7 indicate that effective discharge is not sensitive to the amount of the measured data used in calculations if the smoothing technique is applied. However, this is not true across the board as scenario 2 (using measured flow velocity along with SAMwin to calculate sediment transport) still results in different effective discharges between methods. These differences are mostly due to the change β values (table 5.1). These results indicate that measurements of cross sectionally averaged flow properties and suspended sediment concentration are not essential for calculating the effective discharge. By this way, data required for calculating the effective

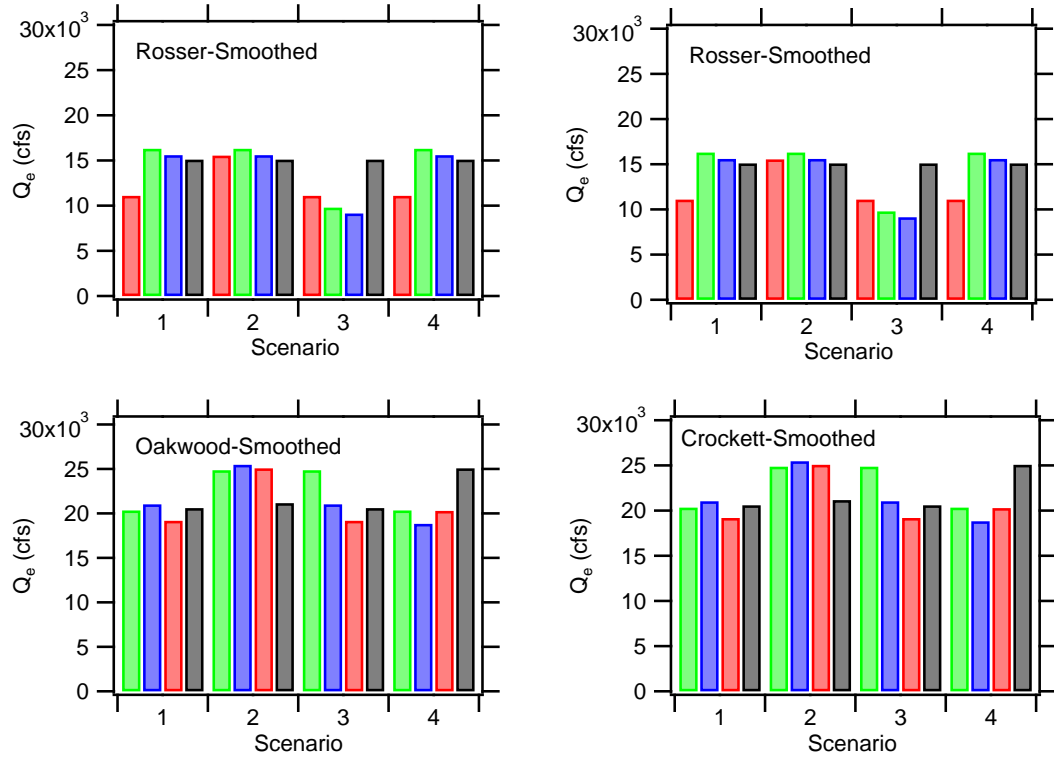


Figure 5.6: Variability of the effective discharge of the Trinity River after applying smoothing technique due to different flow-frequency analysis and amount of measured data used in calculations.

discharge includes (1) historic flow discharges, and (2) bed sediment grain size distribution (river slope assumed as known parameter). However the necessity of having a measured bed GSD is analyzed in the following section.

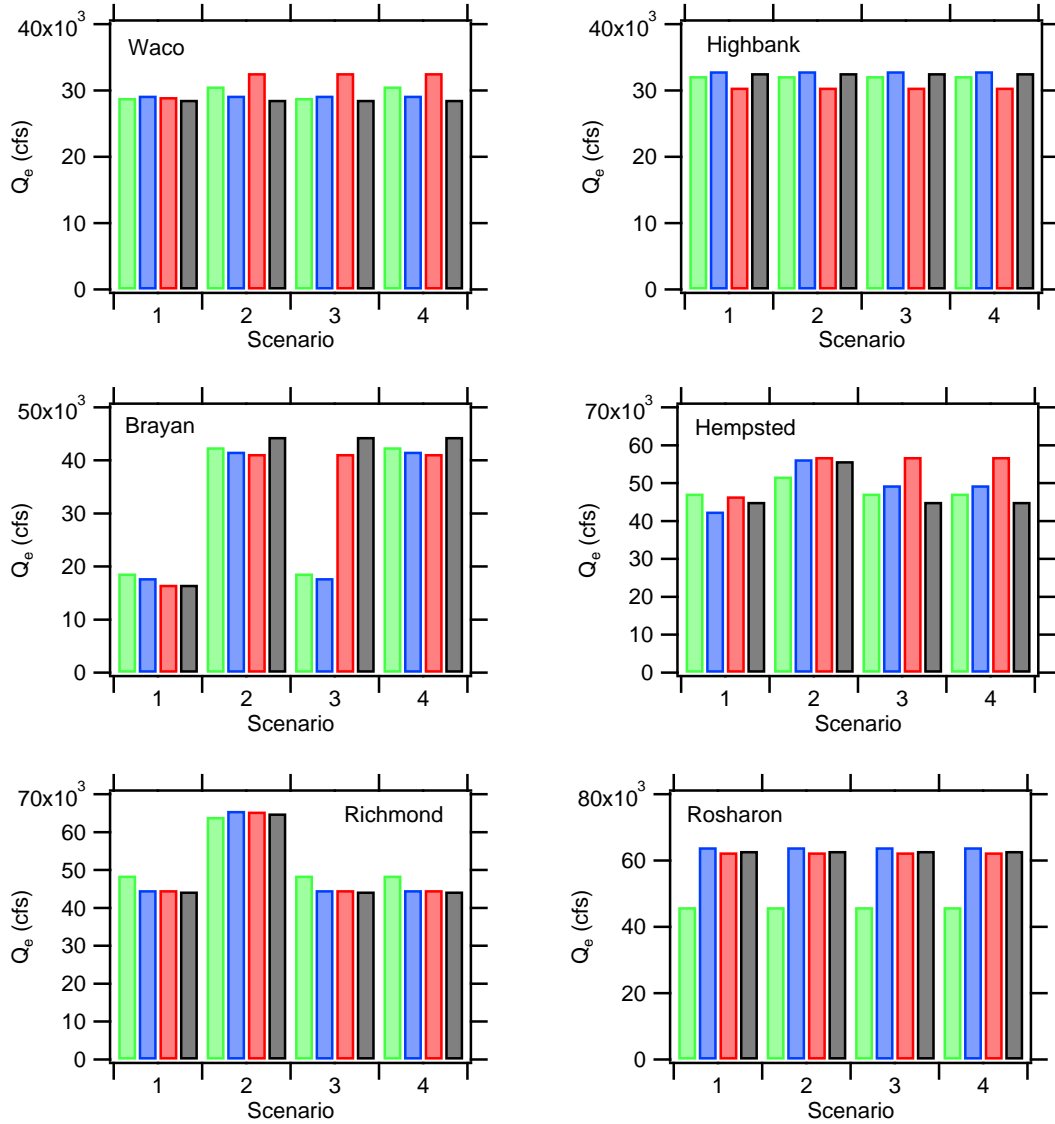


Figure 5.7: Variability of the effective discharge of the Brazos River after applying smoothing technique due to different flow-frequency analysis and amount of measured data used in calculations.

5.3 SENSITIVITY OF EFFECTIVE DISCHARGE CALCULATIONS

Table 5.1, along with figure 5.1, indicate that a change in the β value may cause a substantial change in the effective discharge value. There are two potential sources that could produce variation in β when sediment transport rate is calculated. The first is the choice of transport equation. The second is the input parameters used for the transport equation. Therefore, it would be a matter of interest to analyze the effect of different sediment transport equations and their inputs on β and Q_e .

SAMwin was used to perform the analysis. All sediment transport equations examined are tabulated in table 5.2, and all equations can calculate load by size fraction. The inputs to these equations include channel geometry, slope, and the bed sediment grain size distribution. The Manning roughness coefficient was assumed to be constant and equal to 0.033 for all discharges, which ranged from 1,000 to 18,000 cfs. In the following section, the impact of the choice of different sediment transport equations and the change in input parameters on the final effective discharge are discussed. The first parameter examined is the impact of the channel side slope. Following this, the impacts of grain size distribution and channel slope are explored.

Table 5.2: Summary of sediment transport equations used in analysis.

Equation	Calculates	Type of bed	Concept	Verified by
Meyer-Peter and Müller (1948)	Q_b	Gravel	Excess shear	Lab data
Parker (1990)	Q_b	Gravel	Shear stress	Field data
Einstein (1950)	Q_{tl}	Sand	Shear stress	-
Ackers and White (1973)	Q_{tl}	Sand and gravel	Stream power	Field data
Yang (1979)	Q_{tl}	Sand and gravel	Stream power	Lab and Field

5.3.1 Channel Geometry

Measured sections from Trinity River indicate that the cross sectional shape can be reasonably approximated as being trapezoidal. Therefore 4 trapezoidal cross sections with bottom width of 200 ft and side slopes of $(1_V : Z_h)$ $Z_h = 0, 1, 2,$ and

3 were defined. Two general grain size distributions were defined for the bed; one was a typical sand size distribution and the other a typical gravel size distribution (Figure 5.8). The equations of Einstein (1950), Meyer-Peter and Müller (1948), Yang (1979), Parker (1990) are used within SAMwin to calculate sediment transport load needed for the development of the rating curves. The Meyer-Peter and Müller (1948), and Parker (1990) equations are designed to yield estimates of the bedload transport rate, while the Einstein (1950), Ackers and White (1973), and Yang (1979) method calculate total bed material load.

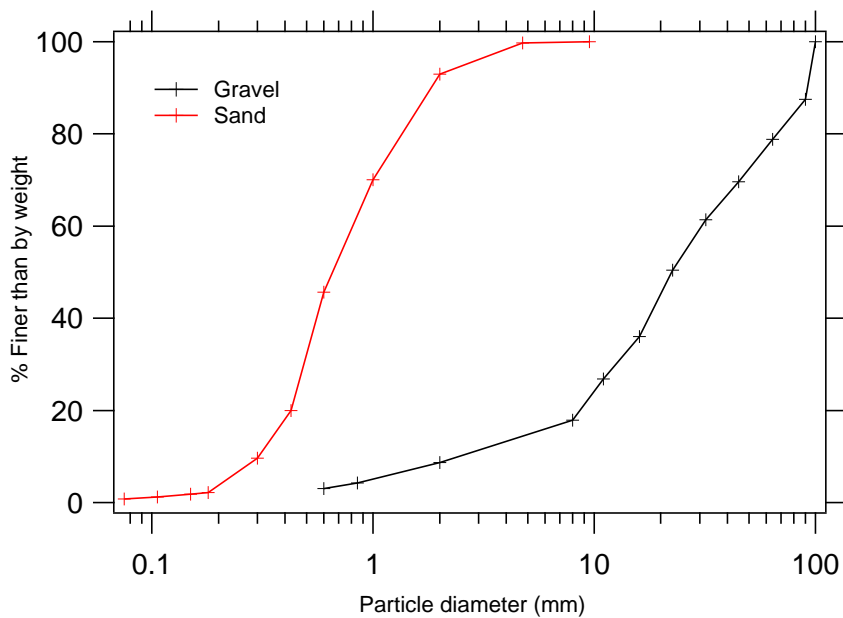


Figure 5.8: Gravel and sand grain size distribution used in analysis of geometry effect on β value.

The equations of Meyer-Peter and Müller (1948), Yang (1979), Parker (1990) were all used to calculate β as a function of side slope using the gravel grain size distribution; the method of Einstein (1950) was used for sand. Table 5.3 indicates that changes in the channel side slope did not translate to a substantial change in either α or β for any of the cases. The Parker equation resulted in the largest β value, and the value was quite different from those produced with the others equations. The reason for this is that the Parker equation calculates that no transport will occur for

flows less than $\approx 16,000$ cfs. After this value, there is a sharp increase in the sediment discharge. Therefore the slope of the total bed material load is very high, 9.9, and this caused the effective discharge to correspond to the largest flood. The variability of the effective discharge in accordance with table 5.3 is accomplished by using the discharge data of the Trinidad station. Results show the effective discharge for all the formulas except Parker is constant and equal to 17,535 cfs regardless of the side slope used. However using the Parker formula in calculations forces the effective discharge to happen at largest flood which is equal to 95,000 cfs.

Table 5.3: Variability of the α and β values by change in side slope of trapezoidal cross sections in different sediment transport formulas

Side Slope	Gravel						Sand	
	Yang		MPM		Parker		Einstein	
	α	β	α	β	α	β	α	β
Z=0	5.0E-05	1.828	0.0042	1.309	5.0E-42	9.998	3.0E-05	2.036
Z=1	5.0E-05	1.809	0.0048	1.291	5.0E-42	9.990	6.0E-05	1.946
Z=2	5.0E-05	1.806	0.0050	1.286	5.0E-41	9.620	5.0E-05	1.966
Z=3	6.0E-05	1.791	0.0052	1.281	1.0E-40	9.460	6.0E-05	1.949

Table 5.3 indicates that by lowering the rise over run of the channel banks (or increasing Z_h), the α and β will tend to decrease slightly. The reason for this is that the depth associated with each discharge grows more slowly as Z_h goes up. The lower rate of depth increase results in a lower rate of bed shear stress increase with discharge, and, therefore, a lower rate of increase in sediment transport rate with increases in discharge. While change Z_h did produce a change in the slope of the rating curve, this change was not significant enough to change the calculated effective discharge. A second outcome of this analysis is α and β value can vary strongly between different sediment transport equations (table 5.3).

5.3.2 Sediment Grain Size Distribution

Eight synthetic grain-size distributions were developed to analyze the variability of β and Q_e due to changes in the grain size distribution of the bed. These distributions were developed to reflect both a change in the D_{50} and σ_g of the distributions since the transport equations used all calculate load by size fraction. As shown in figure 5.9, grain size distributions 1, 2, and 3 have a D_{50} of 1 mm with varying σ_g , while the other distributions have present of variation in D_{50} from 2 to 87 mm with a constant standard deviation.

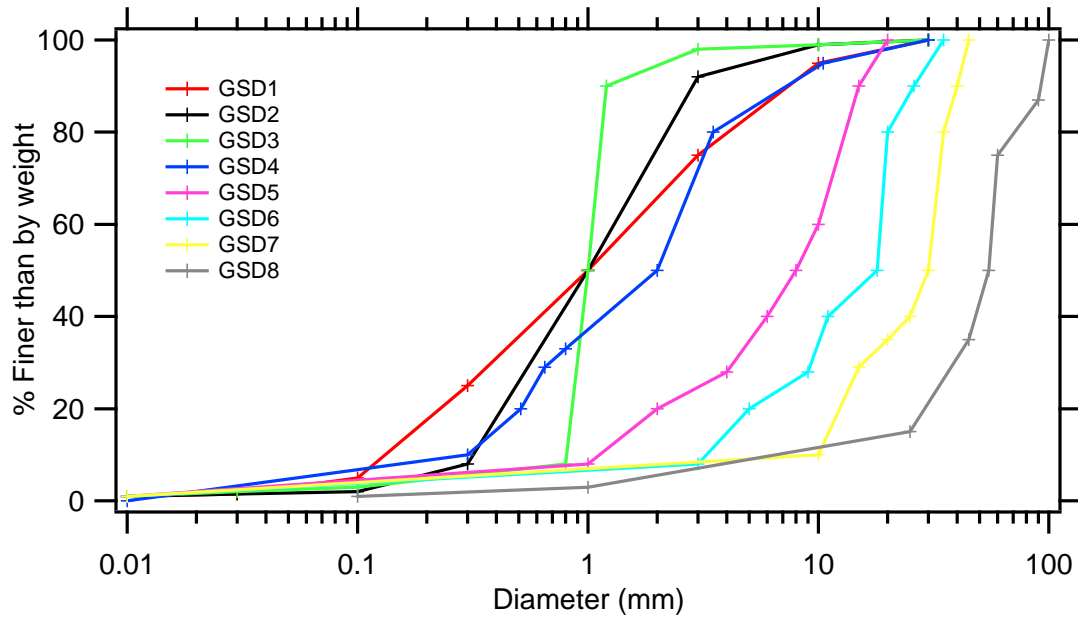


Figure 5.9: Synthetic grain size distributions used in analysis of the variability of the β due to change in grain size distribution.

Only two total load equations are used for the grain size distribution analysis. These equations are the stream-power based equations of Yang (1979) and Ackers and White (1973). These two equations were chosen for their general good historic performance when it comes to predicting total load over a range of sediment sizes and transport rates.

Two primary observations resulted from this analysis. The first is that the slope of the sediment rating curve is specific to the sediment transport equation chosen

Table 5.4: Variability of α and β due to change in grain size distribution using Ackers-White and Yang sediment transport equation

GSD Number	D_{50} [mm]	σ_g [mm]	Ackers-White		Yang	
			α	β	α	β
1	1	5.4	7.0E-06	2.34	0.0003	1.79
2	1	2.5	5.0E-06	2.28	0.0002	1.82
3	1	1.2	3.0E-06	2.33	0.0002	1.85
4	2	3.5	2.0E-06	2.33	0.0001	1.82
5	8	2.9	6.0E-07	2.43	4.0E-05	1.86
6	18	2.3	5.0E-07	2.41	2.0E-05	1.82
7	30	1.8	5.0E-07	2.41	2.0E-05	1.82
8	55	1.8	3.0E-07	2.32	2.0E-05	1.83

for the development of the rating curve. This is to be expected, and it could have a substantial impact on the effective discharge since rating curves with higher slopes will produce larger effective discharges. The second observation is intuitive but less expected. The analysis showed that changing D_{50} and/or σ_g had little impact on the slope of the rating curve, β , for a given transport equation (table 5.4). This means that while the actual predicted transport rates are highly dependent on grain size distribution, the functionality of the transport with discharge changes very little with grain size or gradation within a given transport equation. And, since changes in the effective discharge come from changes in β , the relatively constant β within each transport equation under variable grain size distributions shows that neither the D_{50} or σ_g influence the actual calculated effective discharge. This is a rather significant result, because it means that when transport is calculated, the actual bed material size distribution is not important in defining the effective discharge.

The variability of the effective discharge due to different sediment transport equation is shown in table 5.5. At the Rosser station, changes in β resulted in changes to the effective discharge, while for other stations, the effective discharges did not change even though the bed grain size distribution changed substantially from sand to gravel.

Table 5.5: Variability of the effective discharge of the Trinity River due to different sediment transport equations

Site	Ackers-White		Yang	
	α	β	α	β
	6 E-07	2.4	2E-05	1.8
Rosser	17,000		13,300	
Trinidad	15,500		15,500	
Oakwood	22,600		22,600	
Crockett	22,000		22,000	

5.3.3 Slope

The slope of a river is a key component in setting the bed shear stress that derives sediment transport. In absence of measured slope, there are some approaches to calculate river slope such as using appropriate resistance equation or using the digital elevation models. These calculations leads to a variety of slope values that may affect the calculation of the effective discharge. To analyze the effect of slope on α and β values, as well as the effective discharge, the arbitrary grain size distribution number 1 in figure 5.9 is used along with SAMwin model to calculate sediment load in a trapezoidal channel with the side slope $Z_h = 1$ ($1_v : Z_h$) under different bed slopes. The transport equations of Yang and Einstein are chosen for calculation of sediment loads. Rating curve coefficients for sediment loads associated with discharges from 1,000 to 18,000 cfs and effective discharges for 4 stations are shown in table 5.6. Interestingly, by increasing the slope, α increases and β decreases in both equations. By using the Einstein equation the value of β at slope 0.0001 exceeds 3, forcing the effective discharges to happen at the largest historic flood. β from the Yang equation is smaller and produces a more reasonable effective discharge value. At a slope of 0.0005, the effective discharges are not sensitive at all to the transport equations, and both equations result in same effective discharge values. Increasing the slope 2 times to 0.001 causes a substantial change in α but only a slight change in β . The result of this is only a small change in the effective discharge calculations relative to

the $S = 0.0005$ case (table 5.6). This analysis indicates that the effective discharge estimates would be more sensitive to changes in slope for low gradient sand bed river comparatively to higher gradient streams. This presents somewhat of a problem since practically it becomes harder and harder to accurately measure slope the smaller it gets.

Table 5.6: Variability of effective discharge of total bed material load in a sand bed river due to change in calculated slope

Slope	Site	Einstein			Yang		
		α	β	Q_e [cfs]	α	β	Q_e [cfs]
0.0001		5.0E-09	3.02		4.0E-05	1.83	
	Rosser			106,000			13,300
	Trinidad			93,500			15,500
	Oakwood			101,000			17,500
	Crockett			108,500			22,500
0.0005		0.0014	1.93		0.006	1.59	
	Rosser			13,300			13,300
	Trinidad			15,500			15,500
	Oakwood			22,000			22,000
	Crockett			22,500			22,500
0.001		0.95	1.23		0.036	1.53	
	Rosser			13,300			13,300
	Trinidad			15,500			15,500
	Oakwood			22,000			17,500
	Crockett			18,000			18,000

In a similar approach the variability of the effective discharges due to change in slope was calculated for a characteristic gravel bed river by using an arbitrary gravel grain size distribution (GSD number 8 in figure 5.9) along with flow duration curves of 4 stations of the Trinity River. The slopes remained similar to slopes of table 5.6. To resemble natural gravel rivers more, and to ensure that low slopes are not biasing the results, one steep slope of 0.01 is added to gravel transport calculations. The equations of Parker and Yang were used in the analysis. Parker equation results in almost no sediment transport for these range of slopes except for $S = 0.01$. Parker equation results in high β values varying from 2.5 to 4.5 which unrealistically force

effective discharge to happen at the largest floods. Therefore, the Yang equation is chosen for the analysis. Table 5.7 shows a summary of results.

Table 5.7: Variability of effective discharge of total bed material load calculated by Yang transport equation in a gravel bed river due to change in calculated slope

Slope	Station	α	β	Q_e [cfs]
0.0001		8.0E-07	2.0	
	Rosser			22,500
	Trinidad			15,500
	Oakwood			22,500
	Crockett			22,000
0.0005		3.0E-04	1.6	
	Rosser			22,500
	Trinidad			15,500
	Oakwood			22,500
	Crockett			22,000
0.001		0.001	1.6	
	Rosser			13,000
	Trinidad			15,500
	Oakwood			22,500
	Crockett			22,000
0.01		0.168	1.45	
	Rosser			13,000
	Trinidad			15,500
	Oakwood			22,500
	Crockett			22,000

Similar to the result from the sand bed case, increases in calculated slope resulted in increases in α and decreases in β . Also lower slopes result in unrealistic higher effective discharge values. This means that in gravel bed rivers, similar to sand bed rivers, calculation of the effective discharge is more sensitive to lower calculated slopes.

Chapter 6. Discussion

6.1 COMPARISON OF EFFECTIVE DISCHARGE TO THE HALF-LOAD DISCHARGE AND PURE FLOW METRICS

The half-load discharge was introduced by Klonsky and Vogel (2011) as another potential index for the channel forming characteristic discharge. By definition, $Q_{1/2}$ is the discharge responsible for transporting half of the total sediment load over a long period of time. A reasonable question to ask is how the calculated effective discharges computed with the total load sediment histogram (equation 4.7) compare with (1) the effective discharge calculated using only the suspended bed material load histogram (equation 4.5), (2) the sediment half-load discharge calculated using total load, (3) the bankfull discharge, and (4) the 1.5 year return period flows at each of the sites. Calculation of the half-load discharges was done using the cumulative sediment loading curve as a function of discharge as described above.

A description of how each of these values was calculated has been given above for all discharges other than the bankfull discharge. The bankfull discharge, Q_{bf} is defined as the discharge that just fills the main channel up to the top of its banks with water. There are two primary methods for calculating the bankfull state. In the first, the bankfull cross section can be defined in the field using the geometric properties of the cross section and vegetation indicators. The discharge can then be calculated knowing the bankfull geometry, the channel slope, and the roughness coefficient (such as the Manning n value). It can also be defined using a measured range of discharges and geometric properties, e.g., stage or top width as a function of discharge. In this study, the bankfull discharge is calculated by using USGS stage discharge data at each site. With this second method, the bankfull state is defined as the discharge after which there is a change in the stage discharge functionality. The slope break can be viewed as the discharge at which water begins to spill out of the

main channel and onto the wider flood plain.

The estimated bankfull discharges for Trinity River are listed in Table 6.1 along with the other dominant discharge estimators. The bankfull discharge increased slightly in the downstream direction. However, this increase was more of a step change in discharge between Trinidad and Oakwood rather than a continuous change. Bankfull and 1.5 return period discharge are close in magnitude for all location.

In general, both the effective and half-load discharges of Trinity River are less than both the bankfull and 1.5 year flows. The effective discharge calculated using the total load histogram did not always aligned with those produced using the suspended bed material load only. The reason for this is that bedload makes up a very large fraction of the total load in our calculations (figures 4.3 and 4.4).

Table 6.1: Final effective discharge, Q_e , half-load discharges, $Q_{1/2}$, and bankfull discharges, Q_{bf} , at each of the four stations of Trinity River.

¹Effective and half-load discharges calculated from the total load histogram, $S_h = S_{h:sbm} + S_{h:b}$.

²Effective discharges calculated using the suspended bed material load histogram only, $S_{h:sbm}$.

Station	Total Load ¹		Suspended ²	Pure Flow Metrics		
	Q_e [cfs]	$Q_{1/2}$ [cfs]	Q_e [cfs]	Q_{bf} [cfs]	$Q_{1.5}$ (20 yrs) [cfs]	$Q_{1.5}$ (All yrs) [cfs]
Rosser	11,102	11,963	6,661	26,000	29,543	20,800
Trinidad	17,535	19,483	17,535	25,000	26,600	25,650
Oakwood	19,781	22,089	27,365	32,000	28,200	22,500
Crockett	20,345	18,084	34,031	33,300	30,100	25,700

A comparison of the effective discharge and half-load discharge data for Trinity River along with the fraction of time that flows exceeded the effective discharge, the fraction of sediment carried by flows less than the effective discharge, and the calculated return period of the effective discharge for both the manual and kernel density estimation methods are given in table 6.2. Effective discharge calculated using the two different methods for developing f_Q were fairly equivalent; especially when using the smoothed distribution method. Because the kernel density method

can be quite sensitive to loan peaks, it seems that the load histograms obtained with the manual developed daily flow pdfs are the best for estimating the effective discharge and half-load discharge for the four gauge stations.

Table 6.2: Effective discharge summary table for Trinity River. PT: percentage of time that the effective discharge, Q_e is exceeded. PS: percentage of sediment carried by flows less than the effective discharge. T_R : return period of the effective discharge.

Station	Manual $f_e(Q)$					Kernel Density Estimate of $f_e(Q)$				
	Q_e [cfs]	$Q_{1/2}$ [cfs]	PT Q_e exceeded	PS carried by $Q < Q_e$	T_R [yr]	Q_e [cfs]	$Q_{1/2}$ [cfs]	PT Q_e exceeded	PS carried by $Q < Q_e$	T_R [yr]
Rosser	11,102	11,963	11	32	1.0	15,099	12,924	4	57	1.0
Trinidad	17,535	19,483	7	32	1.0	15,742	20,559	10	29	1.0
Oakwood	19,781	22,089	10	35	1.2	20,820	23,002	8	42	1.2
Crockett	20,345	18,084	11	43	1.1	20,593	20,033	10	49	1.2

The half-load sediment discharge, $Q_{1/2}$ is calculated from cumulative distributions of the sediment moved as a function of discharge. These values and the cumulative curves for the amount of water and sediment moved during the analysis time period as a function of discharge are shown in figures 6.1 and 6.2. The plots shown in these figures are similar to the suggested summary plots of Klonsky and Vogel (2011). The plots can be used to easily see what the fraction of water moved by flows less than (or greater than) a particular discharge is and what percentage of sediment moved this corresponds to. For example, at Trinidad (figure 6.1), the figure can be used to see that about 50% of the water volume is moved by discharges less than approximately 10,000 cfs, but that discharges less than 10,000 cfs only transport about 25% of the sediment passing the station. The plots can also be used to show what the total fraction of sediment moved by flows equal to and less than the effective discharge. For example, at Trinidad, flows equal to and less than the effective discharge are responsible for transporting just under 50 % of the total sediment load.

Effective discharge for 6 gauge stations of Brazos River along with other descriptive discharge indexes are shown in table 6.1.

Effective discharge summary for Brazos River which is calculated by Strom and

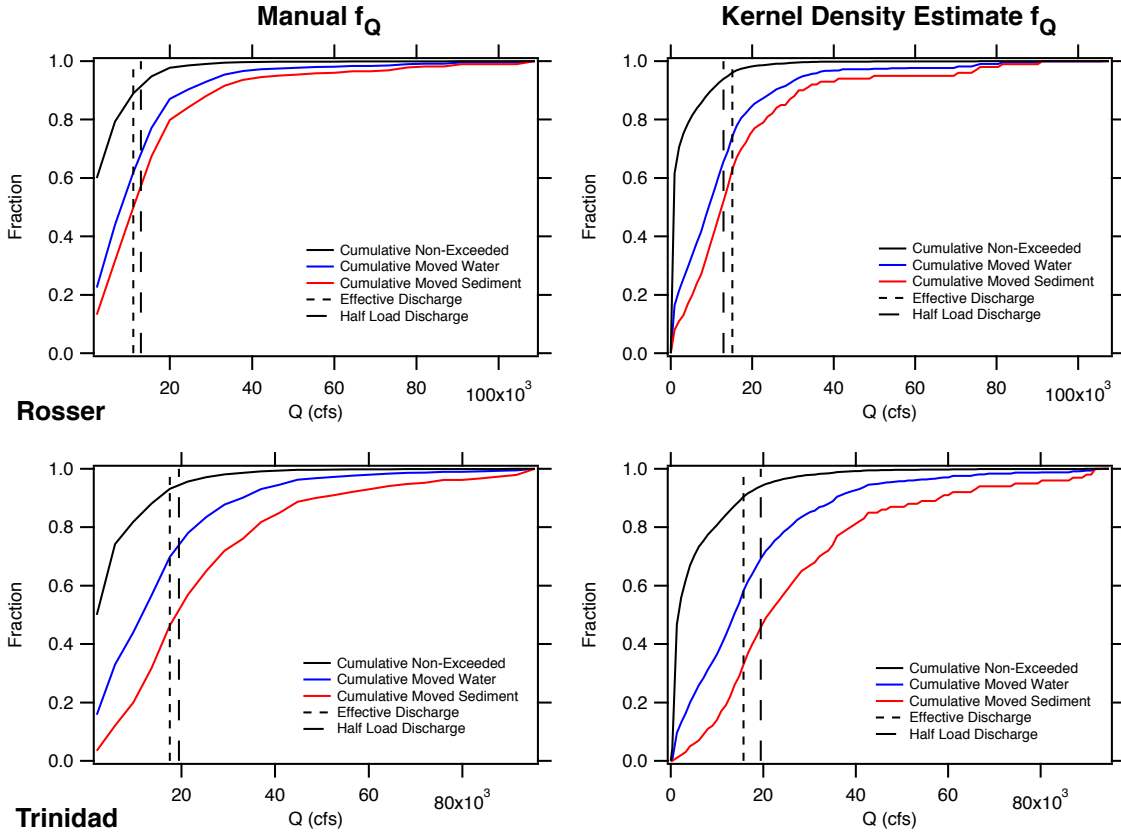


Figure 6.1: Summary plots showing the cumulative fraction of flow and sediment moved as a function of discharge, the flow non-exceedance curve, the sediment effective and half-load discharges for Rosser and Trinidad using the manual and kernel density estimate derived daily flow pdfs.

Rouhnia (2013) is shown in table 6.4.

The sediment and water discharge cumulative figures for Brazos River are depicted in Appendix A.

6.2 RECOMMENDATIONS FOR THE CALCULATION OF EFFECTIVE DISCHARGE

Effective discharge for the Trinity and Brazos Rivers differ (mostly smaller) from the pure flow metrics of $Q_{1.5}$ and bankfull discharges. Therefore, for the Trinity and Brazos Rivers, $Q_{1.5}$ and Q_{bf} can not be used as accurate estimators of the effective discharge. Half-load discharge is another descriptive index that helps one to get a

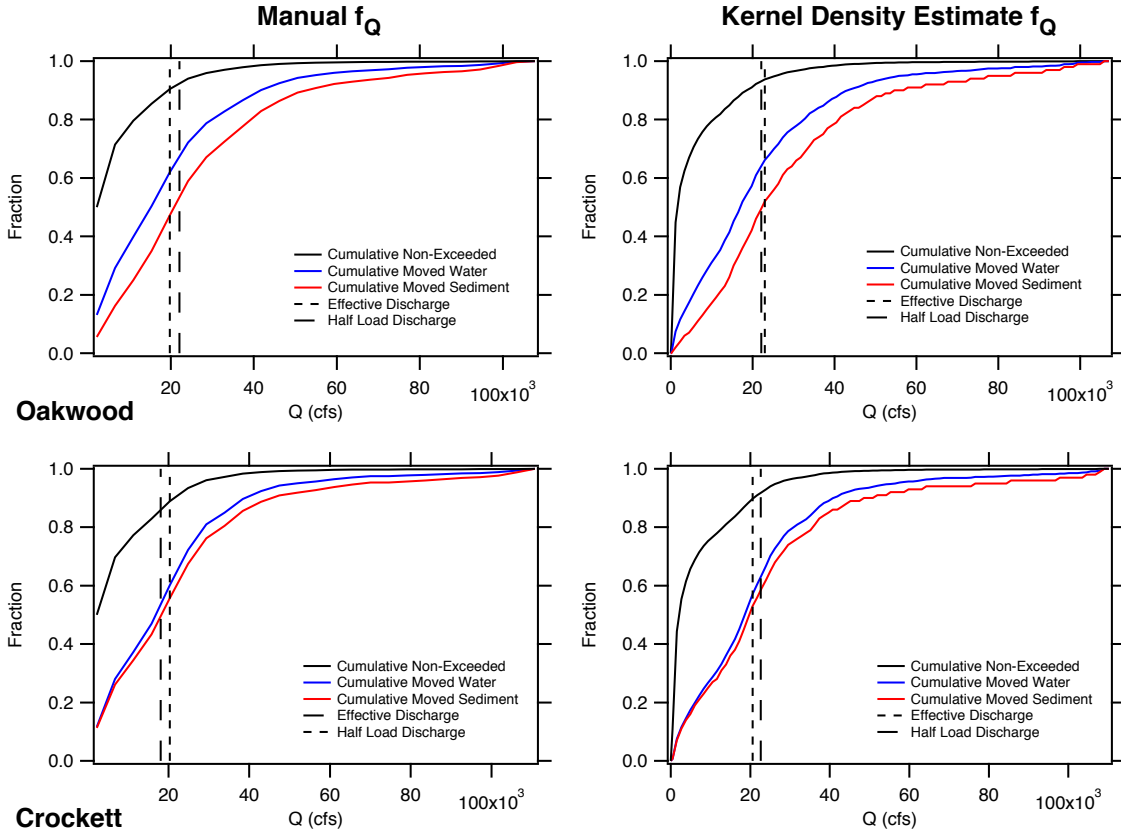


Figure 6.2: Summary plots showing the cumulative fraction of flow and sediment moved as a function of discharge, the flow non-exceedance curve, the sediment effective and half-load discharges for Oakwood and Crockett using the manual and kernel density estimate derived daily flow pdfs.

good feeling for the magnitude of the discharge above and below which 50 percent of the load is carried. One of the merits of the half-load discharge index is that, unlike the classic effective discharge definition, it is not sensitive to the so-called loan peak problem in the load histogram. This means that no graphic interpretation is needed for half-load discharge calculation. The half-load discharge in Trinity River is almost equal to effective discharge while in Brazos River they are different. However, by considering the concept that the most geomorphic work is proportionally related to the most sediment transport, (Wolman and Miller, 1960), it seems more reasonable to consider the effective discharge responsible for geomorphic work.

Calculation of the effective discharge is based on discharge and sediment load

Table 6.3: Final effective discharge, Q_e , half-load discharges, $Q_{1/2}$, and bankfull discharges, Q_{bf} , at each of the six stations of Brazos River. Table from Strom and Rouhnia (2013).

Station	Total Load ¹		Suspended ²	Pure Flow Metrics		
	Q_e [cfs]	$Q_{1/2}$ [cfs]	Q_e [cfs]	Q_{bf} [cfs]	$Q_{1.5}$ (20 yrs) [cfs]	$Q_{1.5}$ (All yrs) [cfs]
Waco	28,500	21,500	28,500	30,000 ³	16,300	24,800
Highbank	30,500	22,000	30,500	20,000	20,000	21,200
Bryan	17,000	23,000	17,000	25,000	28,800	28,800
Hempstead	18,000	34,000	18,000	32,000	45,900	40,700
Richmond	45,000	43,000	45,000	40,000	51,400	44,500
Rosharon	46,000	38,000	46,000	50,000	46,300	44,000

Table 6.4: Effective discharge summary table for Brazos River. PT: percentage of time that the effective discharge, Q_e is exceeded. PS: percentage of sediment carried by flows less than the effective discharge. T_R : return period of the effective discharge. Table from Strom and Rouhnia (2013).

Station	Manual $f_e(Q)$					Kernel Density Estimate of $f_e(Q)$				
	Q_e [cfs]	$Q_{1/2}$ [cfs]	PT Q_e exceeded	PS carried by $Q < Q_e$	T_R [yr]	Q_e [cfs]	$Q_{1/2}$ [cfs]	PT Q_e exceeded	PS carried by $Q < Q_e$	T_R [yr]
Waco	28,500	21,500	1	75	2.9	29,000	22,000	1	74	2.9
Highbank	30,500	22,000	1	77	2.3	33,000	22,000	1	85	2.6
Bryan	17,000	23,000	7	39	1.2	9,000	23,000	16	19	1
Hempstead	18,000	34,000	12	28	1.1	18,000	35,000	13	24	1.1
Richmond	45,000	43,000	3	52	1.4	44,000	44,000	3	50	1.4
Rosharon	46,000	38,000	3	60	1.5	63,000	41,500	1	80	2.3

quantification. Historic flow data are used for generating flow PDFs to account for flow frequencies while sediment loads produces the sediment rating curves. Flow-frequency calculations for Trinity River approved that binning flow data with 25 bins results in reasonable effective discharge values which is in agreement with Biedenharn et al. (2000). Analysis of the research questions approved that measuring the cross sectionally averaged properties of the flow, suspended sediment concentration, cross section, and bed sediment grain size, would not be necessary for calculation of the effective discharge. As a result and in case where measurements are not feasible at all, the following procedure is most likely to result in reasonable estimate of the effective discharge:

- Determination of the bed type of the river in terms of sand or gravel.
- Defining a synthetic GSD file based on the type of the bed.
- Estimating a possible range for slope by DEM, or back calculation by assuming Manning “n” values, or simply Google Earth images or etc.
- Assuming the largest slope (in the range calculated in previous step) in case of sand and gravel bed river as the slope of the river.
- Making flow PDFs by Binning the historic flow data into 25 bins.
- Determination of an appropriate sediment transport equation and generating rating curves.
- Generating sediment transport effectiveness histograms.
- Picking the effective discharge by considering smoothing technique.

Nevertheless it should be mentioned here that, for sand bed rivers, Einstein total load equation, and for gravel bed rivers, Yang equation seems reasonable for calculation of the effective discharge.

Chapter 7. Summary and Conclusions

Effective discharge is a descriptive index known as the flow discharge responsible for producing the most geomorphic work over a long period of time. The two objectives of these were, (1) to estimate the effective discharge for the middle Trinity River at USGS stations of Rosser, Trinidad, Oakwood, and Crockett; and (2) to use the collected data on the Trinity and Brazos rivers to explore general questions related to the calculation of the effective discharge. More specifically this work aimed to explore how different methods in developing flow PDFs changed the effective discharge, and what amounts and type of the field data were needed for reasonably accurate effective discharge calculations? Also, when the measurements are not feasible and though the effective discharge estimate is based off on pure calculations, how the choice of sediment transport relations and their inputs impact the final effective discharge.

To calculate effective discharge for the middle Trinity River, the following data were collected over a range of flows; suspended sediment concentration, bed sediment sample, cross section, and cross sectionally averaged flow properties. Quantification of the sediment load included measurements of the suspended bed material and calculation of the bedload by Brown (1950) formula. Effective discharge for total bed material load (measured suspended bed material added to calculated bedload) of the middle Trinity River follows downstream trend and varies from 11,000 cfs at Rosser to 20,000 cfs at Crockett. These values are significantly smaller than the bankfull and $Q_{1.5}$. The half-load discharges at Trinity River are fairly equal to effective discharges while in Brazos River, they are significantly different.

To analyze the impact of the method used in developing the flow PDFs on effective discharge, the historic flow data binned so that the number of the bins equaled to 25, 50, and 100. Added to this, the kernel density estimate proposed by Klonsky and Vogel (2011) was also used to generate the flow PDF. Four scenarios were

defined and used with decreasing amounts of measured data to address the second question pertaining to how much and what type of field data is needed for calculation of the effective discharge. The results showed that effective discharge may change significantly as a function of the method used in developing the flow PDFs. However, the flow PDF developed by 25 bins results in reasonable effective discharges. On the other hand, the calculated effective discharges were not sensitive to the amount or type of the measured data used in the calculations if the smoothing technique as proposed by Biedenharn et al. (2000) was applied. This means that measurement of the suspended sediment and flow properties is not necessary for calculation of the effective discharge. Also this analysis indicated that the slope of the sediment rating curve, β , has a deterministic role in effective discharge calculations. However, a summary of all the calculations indicated that a β value ranging from 1 to 2.4 is more likely to result in a reasonable effective discharge.

In case where the effective discharge is based on pure calculation, to analyze the impacts of different sediment transport equations and their input on effective discharge, sediment transport equations of Ackers and White (1973), Einstein (1942), Meyer-Peter and Müller (1948), Parker (1990), and Yang (1979) were used in SAMwin package along with change in input parameters including geometry, bed grain size distribution and river slope. The results showed that different sediment transport equations produces completely different total bed material rating curves with substantially different slope which may result in change in effective discharge. However, Einstein, Ackers and white, and Yang transport equations seem to be a reasonable choice for effective discharge calculations in sand and gravel bed rivers. On the other hand, results indicated that bed grain size distribution and river geometry do not substantially affect the total bed material load and effective discharge consequently. This means that measuring the bed sediment samples is not necessary for calculation of the effective discharges. In terms of slope calculations, effective discharges

may change substantially with river slope. In sand and gravel bed rivers, unrealistic change in effective discharge is more likely to happen by reducing the slope.

References

- Ackers, P. and White, W. R. (1973). "Sediment Transport: New Approach and Analysis." *Journal of the Hydraulics Division*, 99(hy11).
- Andrews, E. D. (1980). "Effective and Bankfull Discharges of Streams in the Yampa River Basin, Colorado and Wyoming." *Journal of Hydrology*, 46(3-4), 311–330.
- Ashmore, P. E. (1988). "Effective Discharge for Suspended Sediment Transport in Streams of Saskatchewan River Basin." *Water Resources Research*, 24, 864–870.
- Asquith, W. H. and Slade, R. M. (1997). "Regional equations for estimation of peak- streamflow frequency for natural basins in texas." *Report no.*, U.S. Geological Survey and U.S. Department of the Interior.
- ASTM (2007). "ASTM D3977 - 97(2007) Standard Test Methods for Determining Sediment Concentration in Water Samples." *American Society for Testing and Materials*, 11.02.
- Bedient, P. B., Huber, W. C., and Vieux, B. E. (2002). *Hydrology and Floodplain Analysis*. Upper Saddle River, NJ : Prentice Hall.
- Biedenharn, D. S., Copeland, R. R., Thorne, C. R., Soar, P. J., Hey, R. D., and Watson, C. C. (2000). "Effective Discharge Calculation: A Practical Guide." *ERD-C/CHL TR-00-15*, U.S. Army Engineer Research and Development Center, Coastal and Hydraulics Laboratory.
- Brown, C. B. (1950). *Sediment Transportation*. JohnWiley & Sons Ltd., New York.
- Bunte, K., Abt, S. R., Swingle, K. W., and Cenderelli, D. A. (2014). "Effective Discharge in Rocky Mountain Headwater Streams." *Journal of Hydrology*, 519, Part B(0), 2136 – 2147.

- Church, M. (2006). "Bed Material Transport and the Morphology of Alluvial River Channels." *Annual Review of Earth and Planetary Science*, 34, 325-54.
- Crowder, D. W. and Knapp, H. V. (2005). "Effective Discharge Recurrence Intervals of Illinois Streams." *Geomorphology*, 64(3-4), 167 – 184.
- Davis, B. E. (2005). "The US DH-2: A One-Liter Hand-Line Isokinetic Suspended-Sediment/Water-Quality Collapsible-Bag Sampler." *Report SS*, U.S. Geological Survey and the Federal Interagency Sedimentation Project, Vicksburg, MS.
- Diplas, P., Kuhnle, R., Gray, J., Glysson, D., and Edwards, T. (2008). *Sedimentation Engineering: Processes, Measurements, Modeling, and Practice - Sediment Transport Measurements*. ASCE Manuals and Reports on Engineering Practice No. 110, American Society of Civil Engineering, Chapter 5, 307–353.
- Doyle, M. W., Stanley, E. H., Strayer, D. L., Jacobson, R. B., and Schmidt, J. C. (2005). "Effective Discharge Analysis of Ecological Processes in Streams." *Water Resources Research*, 41, W11411.
- Eaton, B. C. and Church, M. (2011). "A Rational Sediment Transport Scaling Relation Based on Dimensionless Stream Power." *Earth Surface Processes and Landforms*, 36(7), 901–910.
- Edwards, T. K. and Glysson, G. D. (1999). "Field Methods for Measurement of Fluvial Sediment." *Techniques of Water-Resources Investigations Book 3, Chapter C2*, U.S. Geological Survey, Washington D.C.
- Einstein, H. A. (1942). "Formulas for the Transport of Bed Load." *Transactions ASCE*, 107, 561–573.
- Einstein, H. A. (1950). "The Bed-Load Function for Sediment Transportation in Open Channel Flow." *Report no.*, United States Department of Agriculture.

- Francalanci, S., Paris, E., and Solari, L. (2013). “A Combined Field Sampling-modeling Approach for Computing Sediment Transport During Flash Floods in a Gravel-bed Stream.” *Water Resources Research*, 49(10), 6642–6655.
- M. H. Garcia, ed. (2008). *ASCE Manual of Practice 110 - Sedimentation Engineering: Processes, Measurements, Modeling and Practice*. American Society of Civil Engineering.
- Goodwin, P. (2004). “Analytical Solutions for Estimating Effective Discharge.” *Journal of Hydraulic Engineering*, 130(8), 729–738.
- Hey, R. D. (1997). “Channel Response and Channel Forming Discharge: Literature Review and Interpretation.” *Final Report U.S. Army Contract Number R&D 6871-EN-01*.
- Klonsky, L. and Vogel, R. M. (2011). “Effective Measures of “Effective” Discharge.” *The Journal of Geology*, 119(1), 1–14.
- Lane, E. W. (1955). “The Importance of Fluvial Morphology in Hydraulic Engineering.” *Proc., ASCE*, 81(745), 1–17.
- Lenzi, M., Mao, L., and Comiti, F. (2006). “Effective Discharge for Sediment Transport in a Mountain River: Computational Approaches and Geomorphic Effectiveness.” *Journal of Hydrology*, 326(1-4), 257–276.
- Leopold, L. B., Wolman, M. G., and Miller, J. P. (1964). *Fluvial Processes in Geomorphology*. Freeman, Newyork, San Francisco.
- Ma, Y., Huang, H. Q., Xu, J., Brierley, G. J., and Yao, Z. (2010). “Variability of Effective Discharge for Suspended Sediment Transport in a Large Semi-arid River Basin.” *Journal of Hydrology*, 388(3-4), 357 – 369.

- Mackin, J. H. (1948). "Concept of the Graded River." *Geological Society of America*, 59, 463–512.
- Meyer-Peter, E. and Müller, R. (1948). "Formulas for Bed-load Transport." IAHR.
- Parker, G. (1990). "Surface-based Bedload Transport Relation for Gravel Rivers." *Journal of Hydraulic Research*, 28(4), 417–436.
- Philips, J. D., Slattery, M. C., and Musselman, Z. A. (2005). "Channel Adjustments of the Lower Trinity River, Texas, Downstream of Livingston Dam." *Earth Surface Processes and Landforms*, 30, 1419–1439.
- Phillips, J. D. (2008). "Geomorphic Processes, Controls, and Transition Zones in the Middle and Lower Trinity River." *Report no.*, Contract number 0704830781, Texas Water Development Board and Texas Instream Flow Program.
- Pickup, G. and Warner, R. (1976). "Effects of Hydrologic Regime on Magnitude and Frequency of Dominant Discharge." *Journal of Hydrology*, 29(1-2), 51–75.
- Roy, N. and Sinha, R. (2014). "Effective Discharge for Suspended Sediment Transport of the Ganga River and its Geomorphic Implication." *Geomorphology*, 227(0), 18 – 30 Tropical Rivers of South and South-east Asia: Landscape evolution, morphodynamics and hazards.
- Rubey, W. W. (1933). "Settling Velocity of Gravel, Sand, and Silt Particles." *American Journal of Science*, 25(148), 325–338.
- Shields, Jr., F., Copeland, R., Klingeman, P., Doyle, M., and Simon, A. (2003). "Design for Stream Restoration." *Journal of Hydraulic Engineering*, 129(8), 575–584.
- Sichingabula, H. M. (1999). "Magnitude-frequency Characteristics of Effective

- Discharge for Suspended Sediment Transport, Fraser River, British Columbia, Canada.” *Hydrological Processes*, 13(9), 1361–1380.
- Simon, A., Dickerson, W., and Heins, A. (2004). “Suspended-sediment Transport Rates at the 1.5-year Recurrence Interval for Ecoregions of the United States: Transport Conditions at the Bankfull and Effective Discharge?.” *Geomorphology*, 58(1-4), 243 – 262.
- Strom, K. and Rouhnia, M. (2013). “Suspended Sediment Sampling and Annual Sediment Yield on the Lower Brazos River.” *Report No. 1000011085, 1100011340*, University of Houston.
- Texas instream flow program and Brazos River authority (2010). “Instream Flow Study of the Middle and Lower Brazos River.” *Report no.*
- Vogel, R. M., Stedinger, J. R., and Hooper, R. P. (2003). “Discharge Indices for Water Quality Loads.” *Water Resources Research*, 39(10), 1273.
- Wolman, M. G. and Miller, J. C. (1960). “Magnitude and Frequency of Forces in Geomorphic Processes.” *Journal of Geology*, 68, 54–74.
- Wright, S. and Parker, G. (2004). “Flow Resistance and Suspended Load in Sand-bed Rivers: Simplified Stratification Model.” *Journal of Hydraulic Engineering*, 130(8), 796–805.
- Yang, C. T. (1979). “Unit Stream Power Equations for Total Load.” *Journal of Hydrology*, 40(1-2), 123 – 138.

Appendix A. Data for the Brazos River

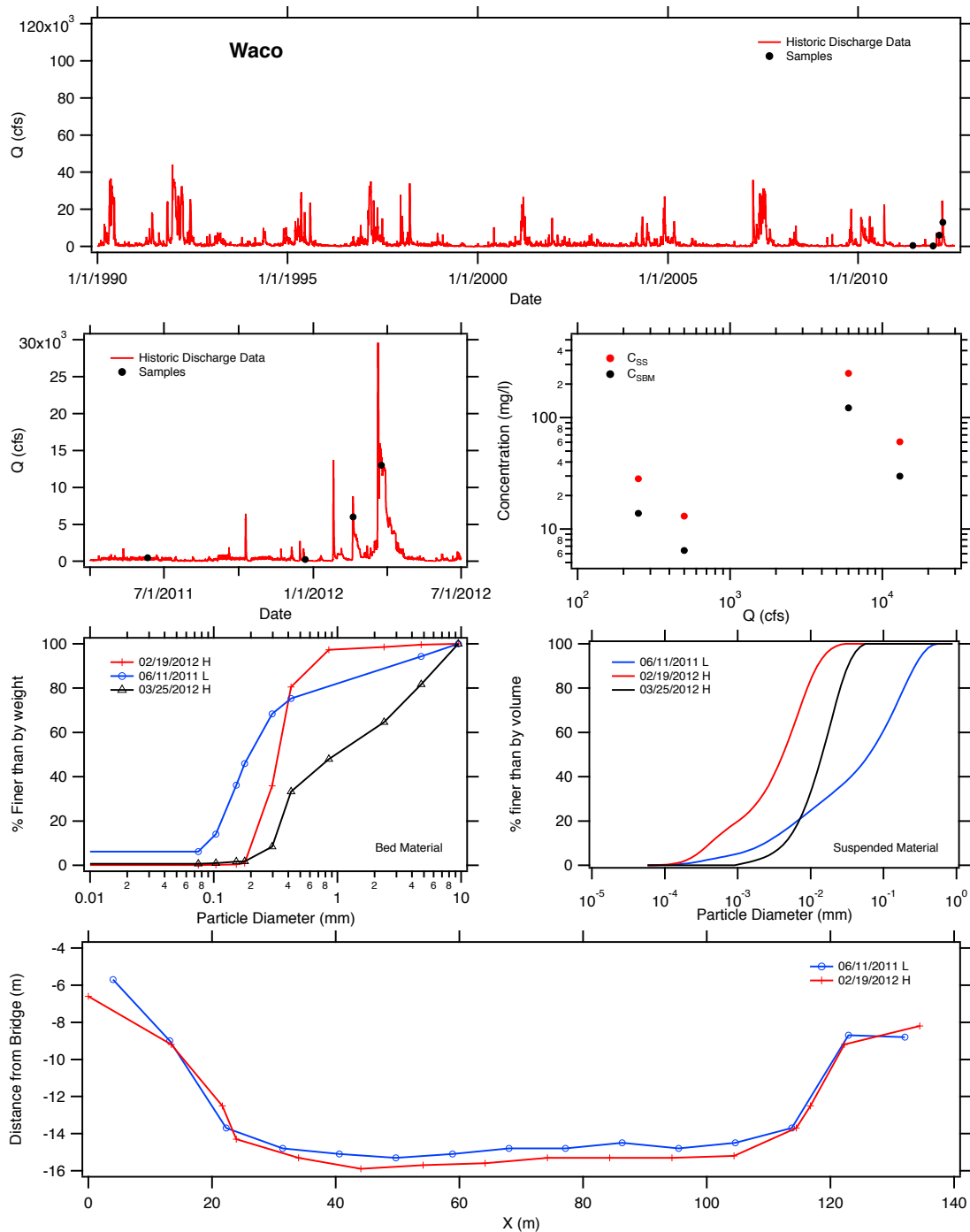


Figure A.1: Summary of collected data at Waco (USGS gage 0809650)- borrowed from Strom and Rouhnia (2013).

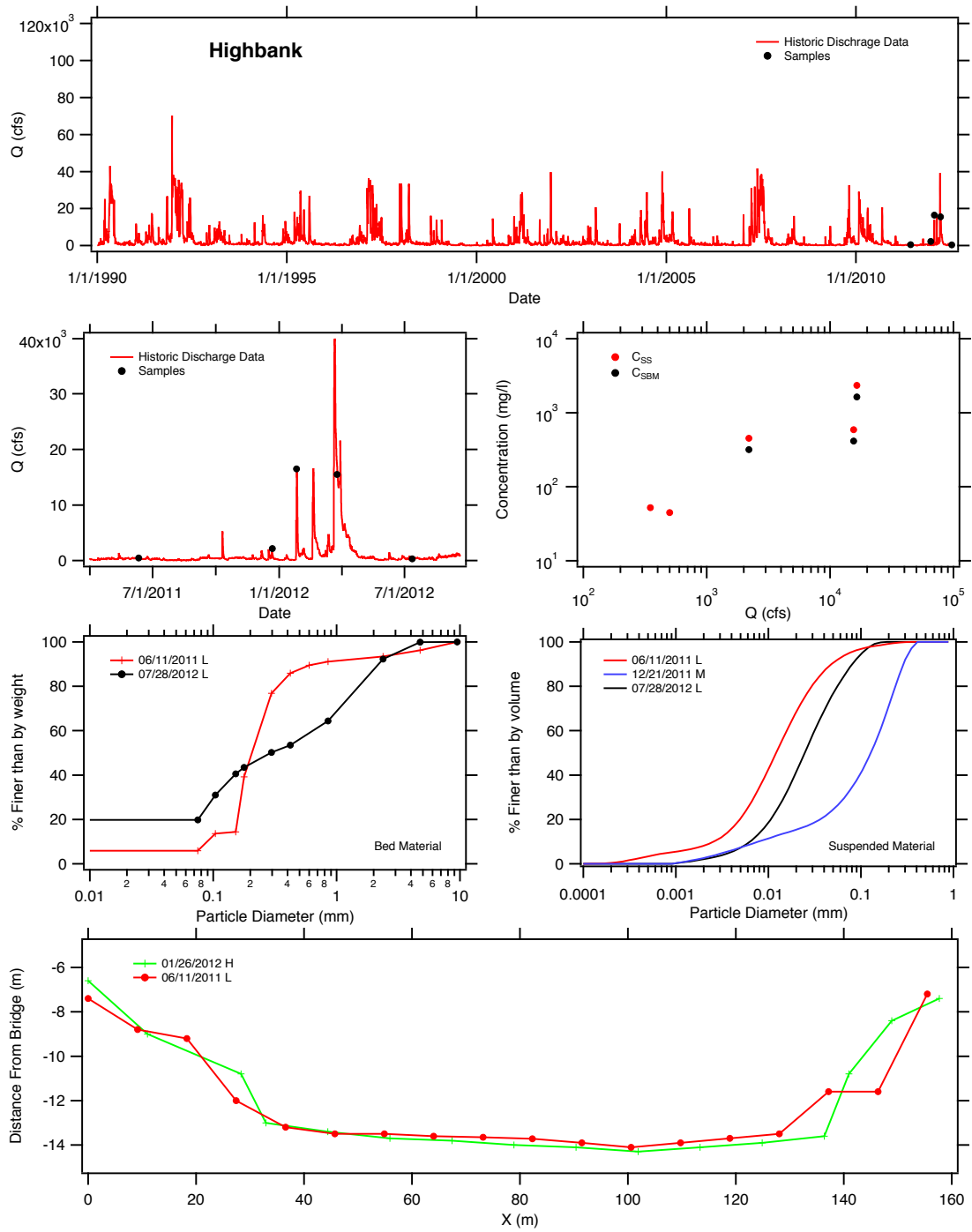


Figure A.2: Summary of collected data at Highbank (USGS gage 08098290).

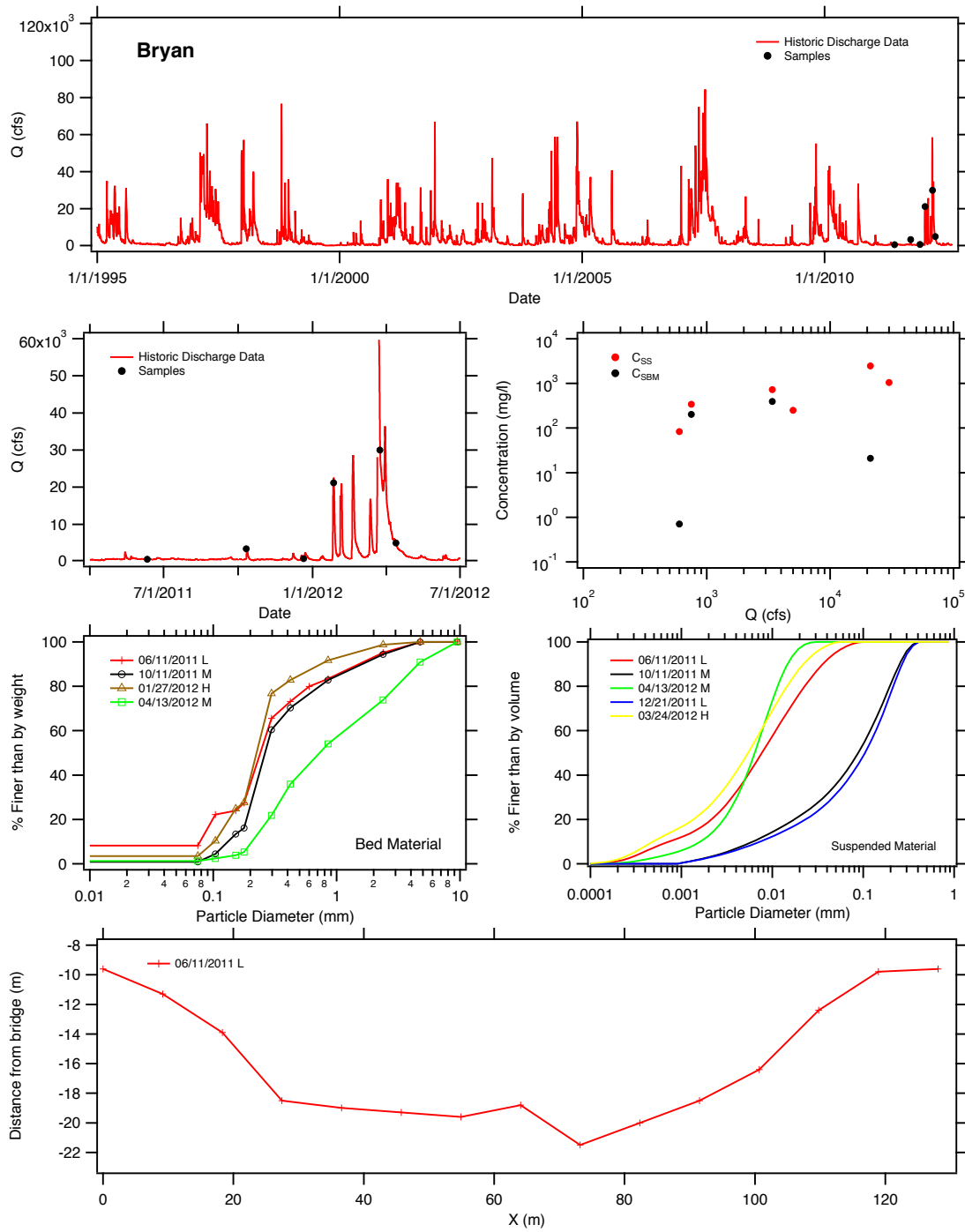


Figure A.3: Summary of collected data at Bryan (USGS gage 08108700).

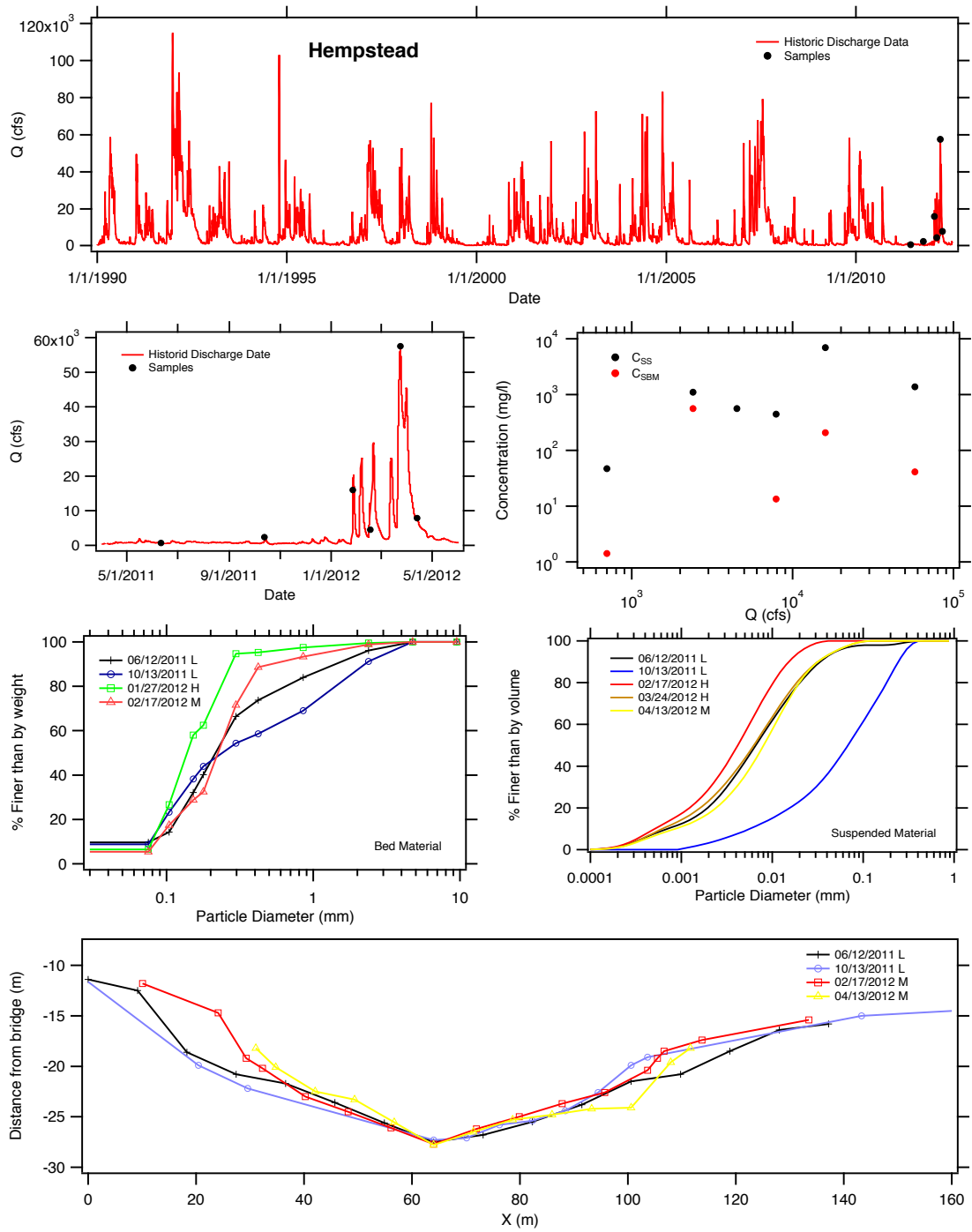


Figure A.4: Summary of collected data at Hempstead (USGS gage 08111500).

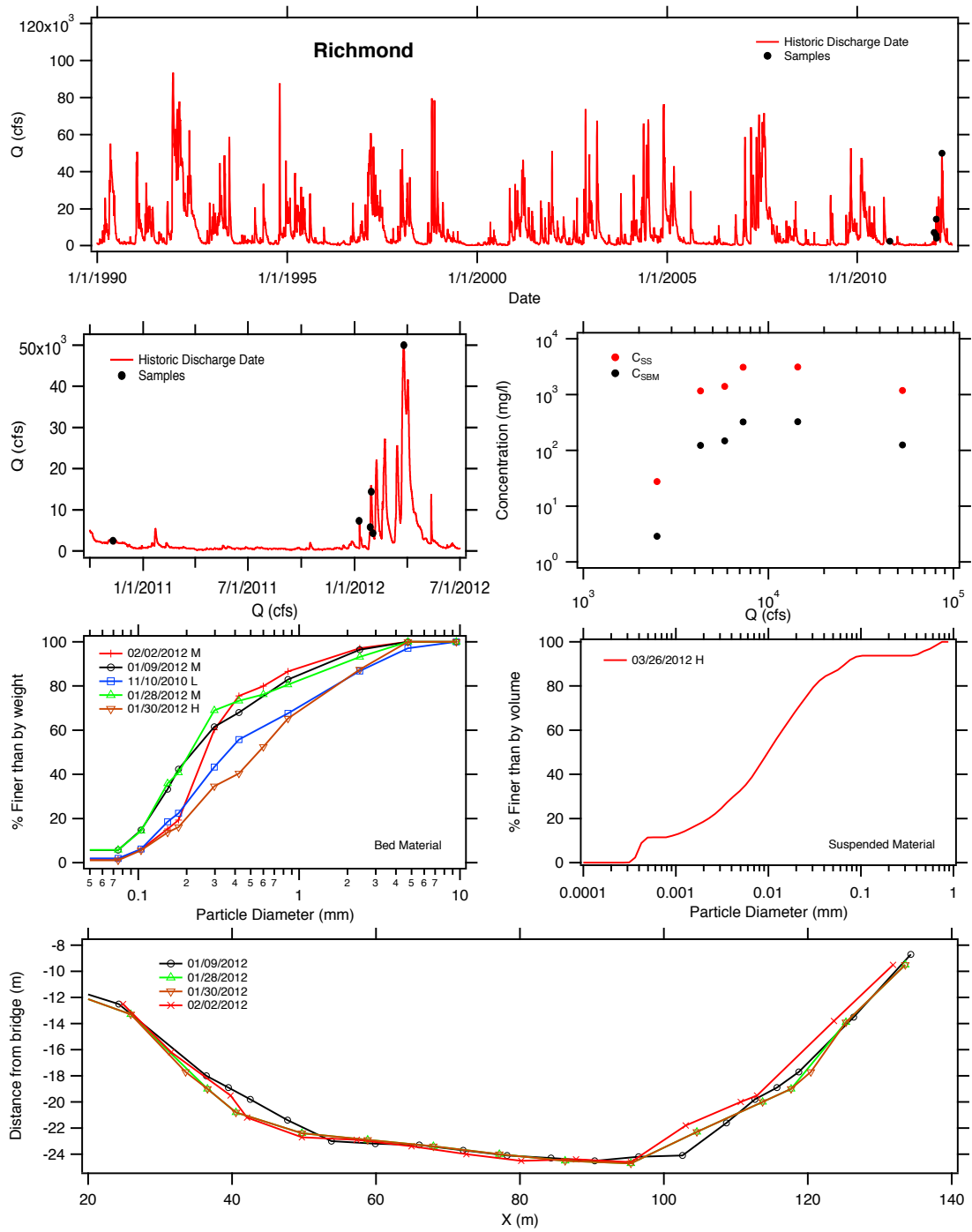


Figure A.5: Summary of collected data at Richmond (USGS gage 08114000).

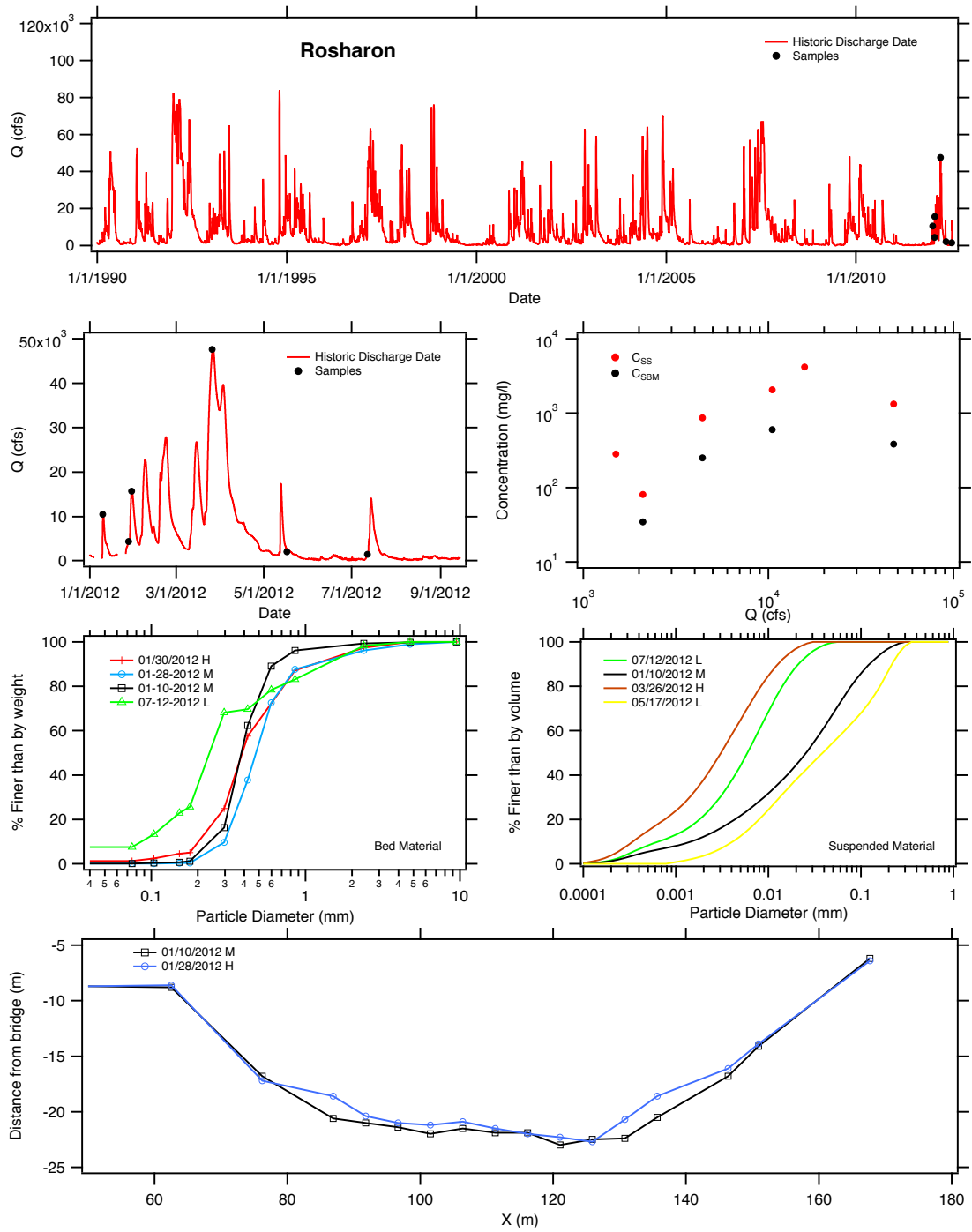


Figure A.6: Summary of collected data at Rosharon (USGS gage 08116650).

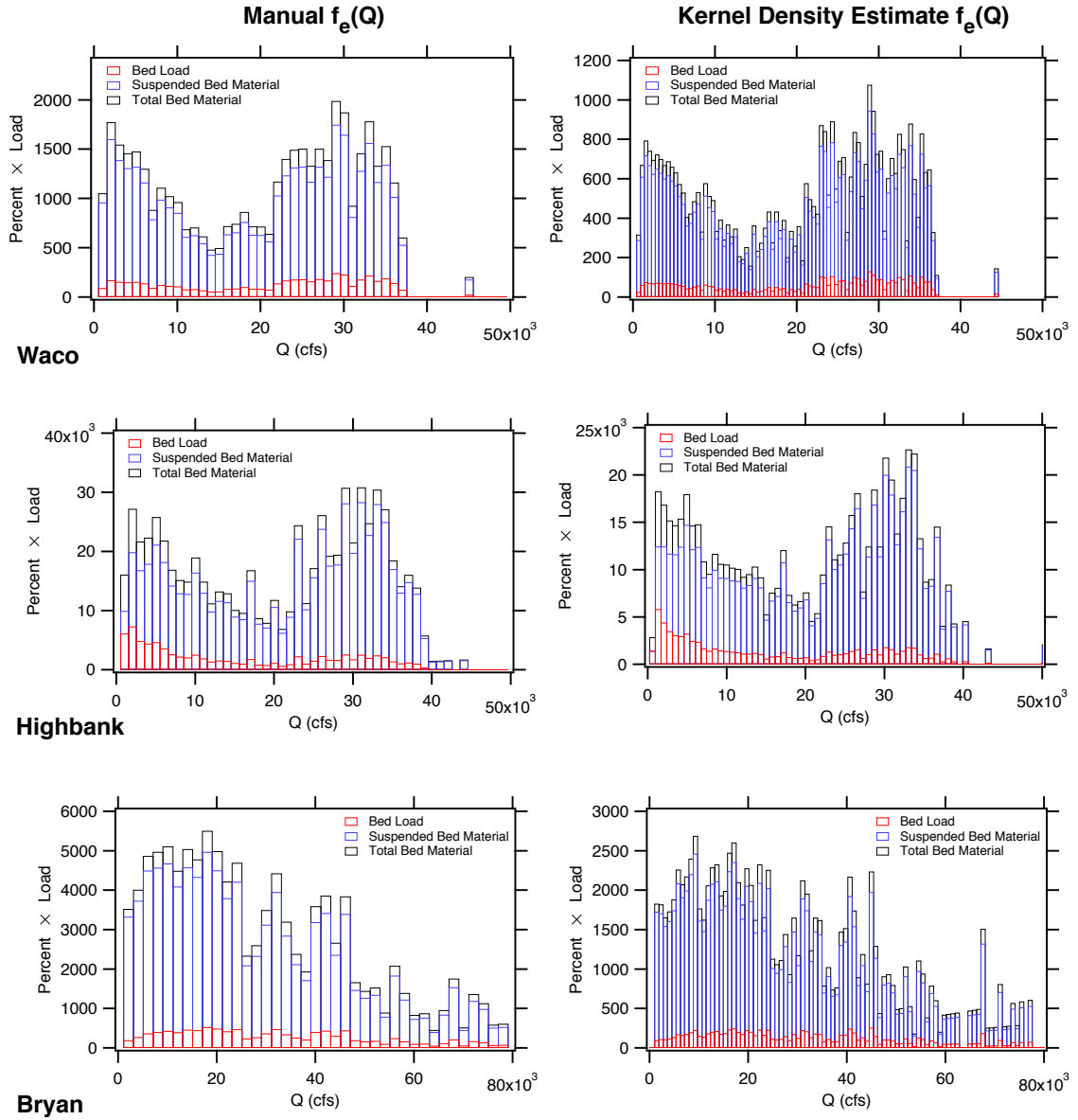


Figure A.7: Sediment transport effectiveness distributions for Waco, Highbank, and Bryan using both the manual and kernel density estimate derived daily flow pdfs.

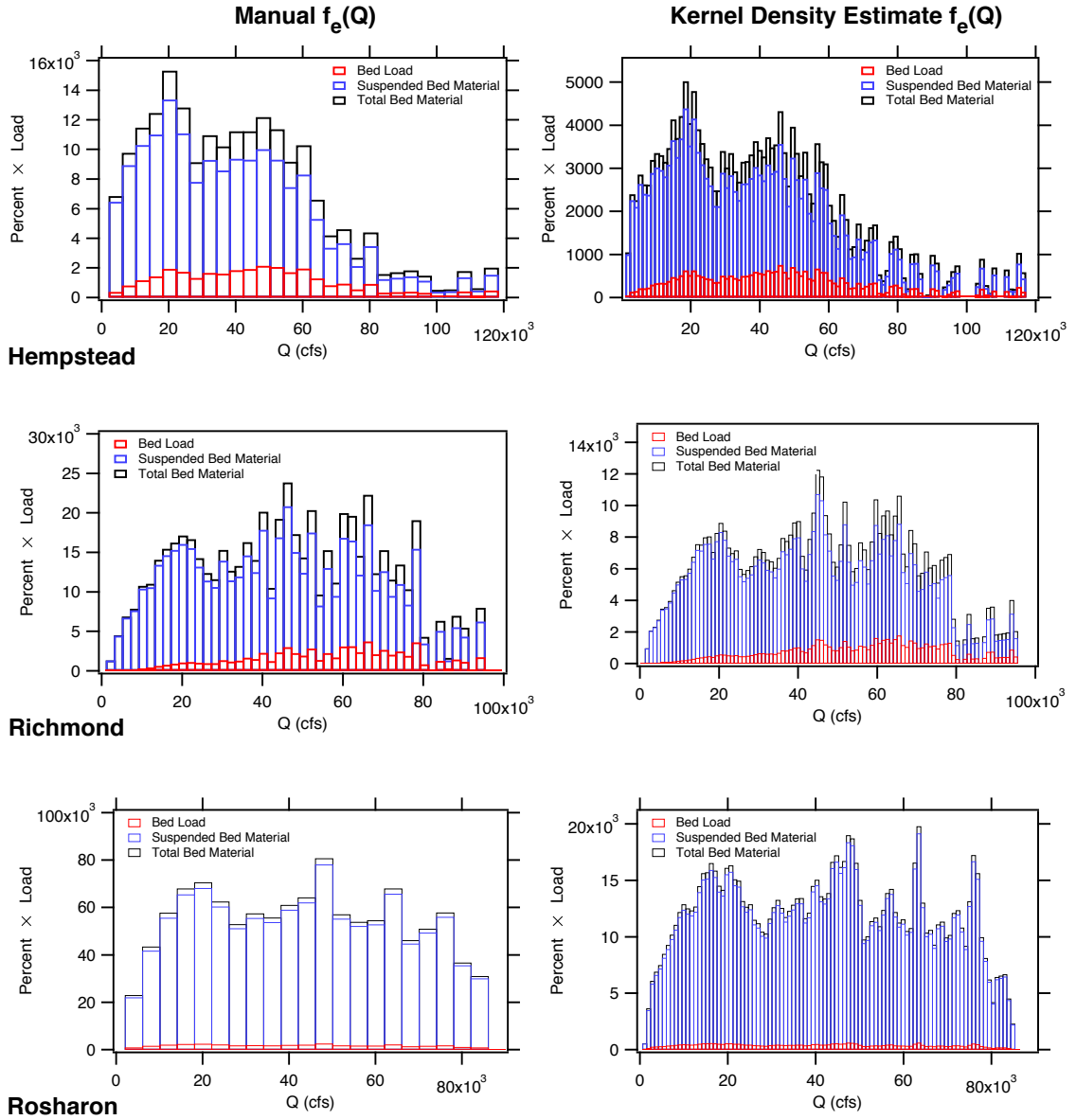


Figure A.8: Sediment transport effectiveness distributions for Hempstead, Richmond, and Rosharon using both the manual and kernel density estimate derived daily flow pdfs.

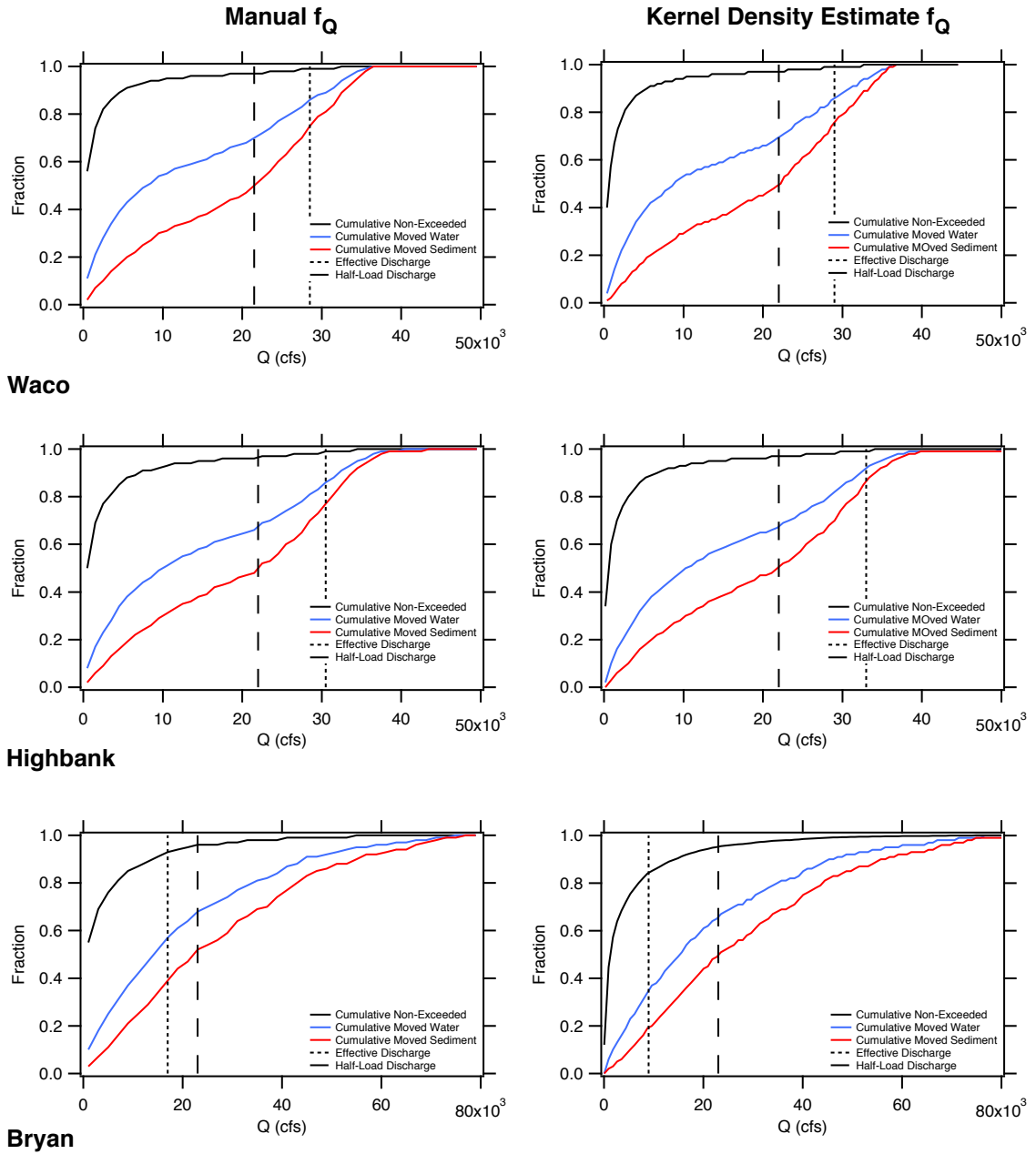


Figure A.9: Summary plots showing the cumulative fraction of flow and sediment moved as a function of discharge, the flow non-exceedance curve, the sediment effective and half-load discharges for Waco, Highbank, and Bryan using the manual and kernel density estimate derived daily flow pdfs.

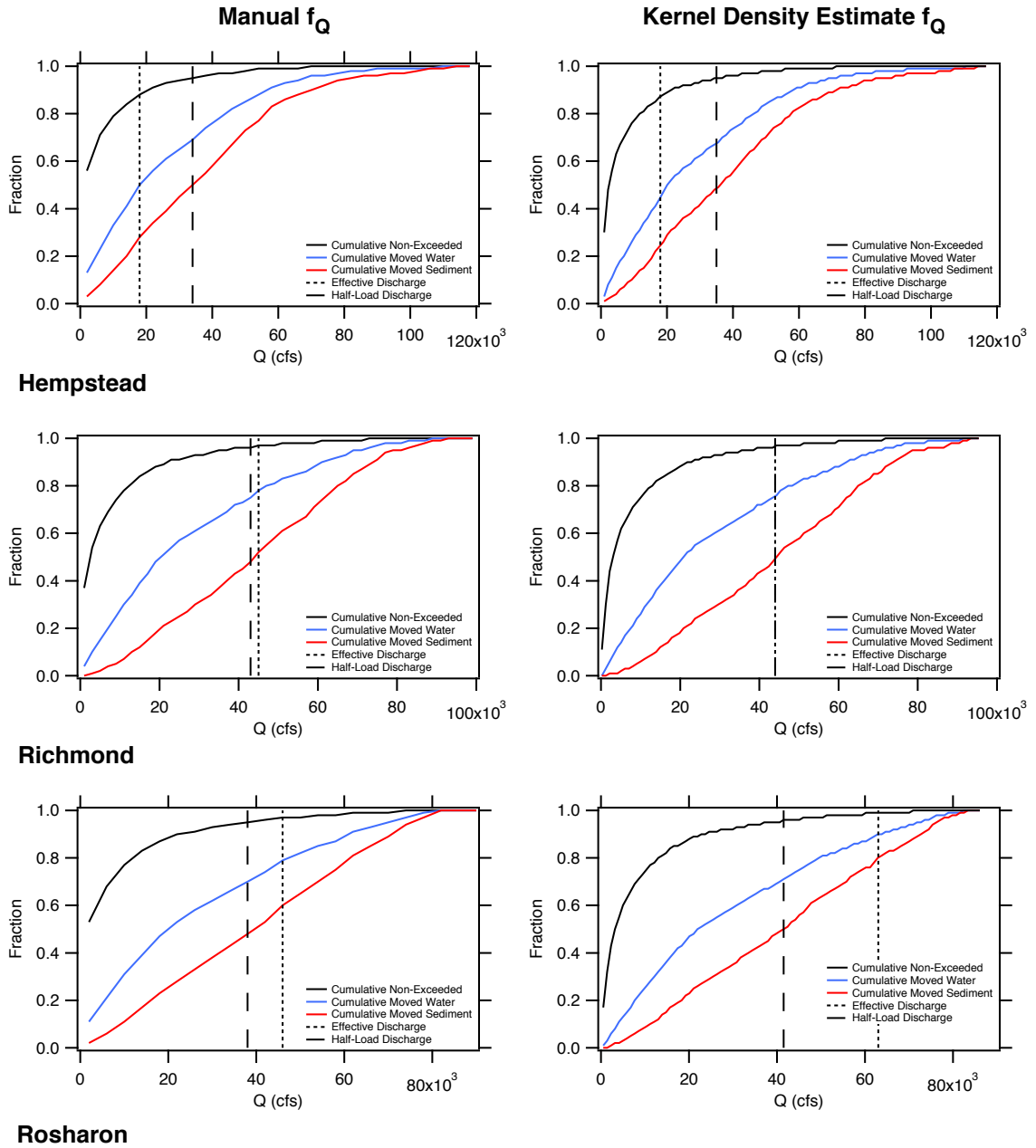


Figure A.10: Summary plots showing the cumulative fraction of flow and sediment moved as a function of discharge, the flow non-exceedance curve, the sediment effective and half-load discharges for Hempstead, Richmond, and Rosharon using the manual and kernel density estimate derived daily flow pdfs.